Turun yliopisto
University of Turku

DEVELOPING EXCHANGE-CORRELATION AND KINETIC ENERGY FUNCTIONAL APPROXIMATIONS FOR DENSITY FUNCTIONAL THEORY

Henrik Levämäki

TURUN YLIOPISTON JULKAISUJA - ANNALES UNIVERSITATIS TURKUENSIS
Sarja - ser. AI osa - tom. 572 | Astronomica - Chemica - Physica - Mathematica | Turku 2017

Turun yliopisto
University of Turku

DEVELOPING EXCHANGE-CORRELATION AND KINETIC ENERGY FUNCTIONAL APPROXIMATIONS FOR DENSITY FUNCTIONAL THEORY

Henrik Levämäki

TURUN YLIOPISTON JULKAISUJA – ANNALES UNIVERSITATIS TURKUENSIS
Sarja - ser. A I osa - tom. 572 | Astronomica - Chemica - Physica - Mathematica | Turku 2017

University of Turku

Faculty of Mathematics and Natural Sciences

Department of Physics and Astronomy

Supervised by

Docent Marko Punkkinen
Department of Physics and Astronomy
University of Turku
Turku, Finland

Professor Ágnes Nagy
Department of Theoretical Physics
University of Debrecen
Debrecen, Hungary

Professor Levente Vitos
Department of Materials Science and Engineering
Royal Institute of Technology
Stockholm, Sweden

Reviewed by

Ph.D Olga Lopez-Acevedo
Department of Applied Physics
Aalto University
Espoo, Finland

Professor Peter Blaha
Institute of Materials Chemistry
Vienna University of Technology
Vienna, Austria

Opponent

Ph.D. Ann E. Mattsson
Los Alamos National Laboratory
Los Alamos, New Mexico, United States

ISBN 978-951-29-7099-5 (PRINT)

ISBN 978-951-29-7100-8 (PDF)

ISSN 0082-7002 (Print)

ISSN 2343-3175 (Online)

Painosalama Oy - Turku, Finland 2017

. . . so yo then man what's *your* story?

— David Foster Wallace, Infinite Jest

Abstract

Henrik LEVÄMÄKI

Developing Exchange-Correlation and Kinetic Energy Functional Approximations for Density Functional Theory

A nearly endless amount of technology relies on the understanding of the properties of matter and materials. Because the properties emerge from the motion of the electrons within matter, deepest and most accurate understanding can only be achieved by measuring or simulating the electronic structure. This thesis considers the computational simulation aspect, and currently the most popular way of conducting these simulations on a computer is density functional theory (DFT). The accuracy of the DFT calculations mostly depends on a small, but very important, component of the total energy — the exchange-correlation (XC) energy. The exact form of the XC energy term is not known and therefore always has to be approximated. When calculating very big systems also the kinetic energy term has to approximated in an orbital-free manner, because computing the electronic orbitals is too expensive for the big systems.

Firstly, a new gradient-level XC approximation called QNA is presented, and it is designed for the calculation of metallic bulk alloys. QNA exploits the subsystem functional scheme to address the issue of inconsistent performance that current gradient-level approximations have with many alloys. QNA is shown to produce more accurate binary alloy formation energies, and the good accuracy of formation energies is very important in alloy theory.

Secondly, a new method of computing the kinetic energy without orbitals is presented and tested in practice. This method allows one, in principle, to perform orbital-free calculations for spherically symmetric systems at the high accuracy level of orbital DFT. A succesful orbital-free solution for the electronic structure of the Be atom is presented. One of the ultimate goals in DFT research is to combine the high accuracy of orbital DFT with the excellent computational speed of orbital-free DFT, and the proof-of-concept solution for the Be atom is a step in this direction.

Tiivistelmä

Henrik LEVÄMÄKI

Tiheysfunktionaaliteoriaa Varten Kehitetyt Vaihtokorrelaatio- ja Liike-energia -approksimaatiot

Lähes lukematon määrä teknologiaa nojautuu aineen ja materiaalien ominaisuuksien ymmärtämiseen. Koska nämä ominaisuudet kumpuavat aineen koossapitävästä elektronirakenteesta, syvällisin ja kaikista tarkin ymmärrys voidaan saavuttaa ainoastaan mittaamalla tai simuloimalla kyseistä elektronirakennetta. Tämä väitöskirja käsittelee jälkimmäistä vaihtoehtoa, eli elektronirakenteen mallintamista tietokoneella tehtävien laskujen avulla. Nykyään suosituin tällaisista laskentamenetelmistä on tiheysfunktionaalimenetelmä. Tiheysfunktionaaliteoriaan pohjautuvien laskujen tarkkuus riippuu pääasiassa yhdestä pienestä, mutta erittäin tärkeästä kokonaisenergian komponentista — vaihto-korrelaatioenergiasta. Vaihto-korrelaatioenergian tarkkaa matemaattista muotoa ei tunneta, joten sille on aina käytettävä jotakin approksimaatiota. Kun halutaan mallintaa erittäin kookkaita systeemejä, myös liike-energia on approksimoitava orbitaalivapaalla tavalla, sillä orbitaalien laskeminen kookkaille systeemeille on liian aikaavievää.

Ensimmäiseksi tässä tutkielmassa esitetään uusi gradientti-tason vaihto-korrelaatioapproksimaatio QNA, joka on suunniteltu metalliseosten laskemiseen. QNA hyödyntää alisysteemifunktionaaleja (subsystem functional scheme) parantamaan laskujen tarkkuutta metalliseoksille verrattuna nykyisiin gradienttitason funktionaaleihin. Nykyiset gradienttitason funktionaalit eivät useinkaan pysty mallintamaan kaikkia seoksen komponentteja (puhtaat alkuaineet) tarkasti, minkä tässä väitöskirjassa osoitetaan johtavan epätarkkoihin tuloksiin itse seokselle. QNA-approksimaatiossa kukin seoksen komponentti mallinnetaan erillisen alisysteemifunktionaalin avulla, jolloin kukin komponentti ja itse seos voidaan laskea tarkasti. Käytännön laskuilla osoitetaan, että QNA tuottaa erittäin tarkkoja muodostumisenergioita kaksikomponenttisille metalliseoksille, mikä on erittäin tärkeä seikka metalliseosten teoriassa.

Toiseksi tässä tutkielmassa esitetään uusi menetelmä, jolla liike-energia voidaan laskea ilman orbitaaleja. Menetelmä mahdollistaa pallosymmetristen systeemien orbitaalivapaan liike-energian laskemisen yhtä tarkasti kuin orbitaalien kanssa. Menetelmän käytännön pätevyyttä testataan laskemalla beryllium-atomin elektronirakenne. Yksi tiheysfunktionaaliteorian tutkimuksen suurimmista päämääristä on yhdistää orbitaalisen tiheysfunktionaaliteorian hyvä tarkkuus orbitaalivapaan tiheysfunktionaaliteorian nopeuteen. Beryllium-atomille suoritetut testilaskut ovat askel kohti edellämainittua päämäärää.

Acknowledgments

We write theses and when we write them we change them and are changed. For my thesis and my change I am most indebted to my research director Prof. Kalevi Kokko, whom I believe is the best boss anybody could have. This thesis would not be possible without him and his guidance. His door is always open and I never felt even a bit of nervousness, uneasiness, or insecurity when entering through that door.

I would like to thank my principal supervisor Doc. Marko Punkkinen and my co-supervisors Prof. Levente Vitos, and Prof. Ágnes Nagy. The role of Doc. Punkkinen was instrumental in the beginning. I am especially grateful to him for setting up a clandestine meeting between Prof. Vitos and myself in the depths of Harjoitustyöosasto 1 where I was given a modest assignment that eventually grew into my Master's thesis and the bulk of this work.

I am extremely grateful to Prof. Vitos for everything he has done for me. I thank him for sharing his EMTO density functional program, as well as his expert knowledge in density functional theory. He also made it possible for me to make many stimulating visits to the Royal Institute of Technology in Stockholm, and one to Uppsala university.

I owe a great deal to Prof. Nagy for her invaluable guidance in the orbital-free portion of this work. I would also like to thank her for her hospitality during my visits at the University of Debrecen in Hungary.

I thank Dr. Matti Ropo for guiding me in various projects. I appreciate all my colleagues at the Materials Physics group, as well as at the Materials Science and Engineering group at Royal Institute of Technology. Special thanks go to Wei, from whom I have learned a great deal about coding and computers, and to Liyun for teaching me badminton, alloy theory, minigolf, and Chinese. I also thank Dr. Mikael Kuisma for his considerable help in implementing QNA in GPAW.

I thank my parents and my sisters for their love and support. It was not always easy, but we made it. Many thanks are also owed to Antti Käki who kindly offered me about two weeks of shelter in Sweden for the low price of a bottle of tax-free cognag.

I gratefully acknowledge the Doctoral Programme in Physical and Chemical Sciences (PCS) and the University of Turku Graduate School (UTUGS) by whom this work was funded. The computational resources of the IT Center for Science (CSC), and the Finnish Grid and Cloud Infrastructure (FGCI) project are also acknowledged.

List of Papers

This thesis includes the following publications:

I **Levämäki, H.**, Punkkinen, M. P. J., Kokko, K., Vitos, L., "Quasi-non-uniform gradient-level exchange-correlation approximation for metals and alloys", Physical Review B **86**, 201104 (2012), DOI: 10.1103/PhysRevB.86.201104.

II **Levämäki, H.**, Punkkinen, M. P. J., Kokko, K., Vitos, L., "Flexibility of the quasi-non-uniform exchange-correlation approximation", Physical Review B **89**, 115107 (2014), DOI: 10.1103/PhysRevB.89.115107.

III **Levämäki, H.**, Nagy, Á., Kokko, K., Vitos, L., "Cusp relation for the Pauli potential", Physical Review A **90**, 062515 (2014), DOI: 10.1103/PhysRevA.90.062515.

IV **Levämäki, H.**, Nagy, Á., Kokko, K., Vitos, L., "Alternative to the Kohn-Sham equations: The Pauli potential differential equation", Physical Review A **92**, 062502 (2015), DOI: 10.1103/PhysRevA.92.062502.

V Tian, L.-Y., **Levämäki, H.**, Ropo, M., Kokko, K., Nagy, Á., Vitos, L., "Exchange-Correlation Catastrophe in Cu-Au: A Challenge for Semilocal Density Functional Approximations", Physical Review Letters **117**, 066401 (2016), DOI: 10.1103/PhysRevLett.117.066401.

Comment on my contributions to each thesis publication:

I All calculations and data analysis. The manuscript was written jointly.

II All calculations and data analysis. Principal author of the manuscript.

III All calculations. Data analysis was done jointly.

IV All calculations and data analysis. Principal author of the manuscript.

V Calculations and data analysis done jointly. Principal author of the manuscript.

Publications not included in this thesis:

I Laukkanen, P., Punkkinen, M. P. J., Puustinen, J., **Levämäki, H.**, Tuominen, M., Schulte, K., Dahl, J., Lång, J., Zhang, H. L., Kuzmin, M., Palotas, K., Johansson, B., Vitos, L., Guina, M., Kokko, K., "Formation and destabilization of Ga interstitials in GaAsN: Experiment and theory", Physical Review B **86**, 195205 (2012), DOI: 10.1103/PhysRevB.86.195205.

II Punkkinen, M. P. J., Kokko, K., **Levämäki, H.**, Ropo, M., Lu, S., Delczeg, L., Zhang, H. L., Delczeg-Czirjak, E. K., Johansson, B., Vitos, L., "Adhesion of the iron-chromium oxide interface from first-principles theory", Journal of Physics: Condensed Matter **25**, 495501 (2013), DOI: 10.1088/0953-8984/25/49/495501.

III Punkkinen, M. P. J., Laukkanen, P., Kuzmin, M., **Levämäki, H.**, Lång, J., Tuominen, M., Yasir, M., Dahl, J., Lu, S., Delczeg-Czirjak, E. K., Vitos, L., Kokko, K., "Does Bi form clusters in $GaAs_{1-x}Bi_x$ alloys?", Semiconductor Science and Technology **29**, 115007 (2014), DOI: 10.1088/0268-1242/29/11/115007.

IV Nurmi, E., Tuuli, E., **Levämäki, H.**, Kokko, K., Leiro, J., Vitos, L., "Directional Young's modulus of single-crystal and cold-rolled titanium from ab initio calculations: Preferred crystal orientation due to cold rolling", Philosophical Magazine **96**, 2736–2751 (2016), DOI: 10.1080/14786435.2016.1213443.

V Uusitalo, R.-R., Lahti, A., **Levämäki, H.**, Punkkinen, M. P. J., Vilja, I., Kokko, K., Vitos, L., "Order–disorder transition of $Pd_{0.5}Ag_{0.5}$ alloys", Philosophical Magazine **96**, 3697–3710 (2016), DOI: 10.1080/14786435.2016.1237055.

VI Lahti, A., **Levämäki, H.**, Mäkelä, J., Tuominen, M., Yasir, M., Dahl, J., Kuzmin, M., Laukkanen, P., Kokko, K., Punkkinen, M., "Electronic structure and relative stability of the coherent and semi-coherent HfO_2 /III-V interfaces", Applied Surface Science **427**, 243–252 (2018), DOI: 10.1016/j.apsusc.2017.08.185.

VII **Levämäki, H.**, Ropo, M., Tian, L.-Y., "Challenges in automated high-throughput *ab initio* thermodynamics of magnetic high-entropy alloys", Submitted (2017).

VIII **Levämäki, H.**, Nagy, Á., Kokko, K., Vitos, L., "Kullbach-Leibler and relative Fisher information as descriptors of locality", International Journal of Quantum Chemistry, Accepted (2017), DOI: 10.1002/qua.25557.

Contents

Abstract **v**

Tiivistelmä **vii**

Acknowledgments **ix**

List of Papers **xi**

1 Introduction **1**

2 Density Functional Theory **5**
2.1 Background 5
2.2 Hohenberg-Kohn Theorems 6
2.3 Kohn-Sham Scheme 8

3 Exchange and Correlation **11**
3.1 Properties 11
3.2 Local Density Approximation 13
3.3 Generalized Gradient Approximation 15
3.4 Perdew-Burke-Ernzerhof Approximation 18
3.5 Subsystem Functional Approach 21
3.6 Quasi-non-uniform Exchange-Correlation Approximation . 23

4 Orbital-Free Density Functional Theory **35**
4.1 Background 35
4.2 Pauli Potential 36
4.3 Pauli Potential Differential Equation 44

5 Practical Applications **51**
5.1 Quasi-non-uniform Exchange-Correlation Approximation . 51
5.2 Pauli Potential Differential Equation 59

6 Concluding remarks **65**

A Derivatives of GGA enhancement factor maps **67**

B Implementation of QNA in GPAW DFT code **71**
B.1 Energy expression 71
B.2 Forces 73
B.3 Stress tensor 75

Bibliography **79**

Original papers **95**

1 Introduction

The thesis at hand is part of a long line of theses seeking answers to two basic questions in materials science, which can be stated very simply:

i) What materials can exist?

ii) What are their properties?

Despite these two questions being ever so simple, ascertaining refined answers to them turns out to be anything but simple, or straightforward. This is because these answers we are looking for are ultimately encoded in the electronic structure of materials and matter, and the electronic structure itself is mathematically a so-called *many-body problem*. If characterized using two word phrases, we could say these many-body problems are "notoriously intractable" or "hopelessly difficult." This implies that the direct solution of the electronic structure is neither possible now nor will it become possible in the future within the confines of any conceivable future technology.

It is therefore necessary to probe the electronic structure using some less costly, indirect techniques. A lot of work has been carried out in an effort to define and develop practical methods of calculating the electronic structure. This work started roughly one hundred years ago and the most successful approach so far has been density functional theory (DFT). Following the rigorous theoretical inception of DFT by mainly Walter Kohn (1923-2016), DFT has become tremendously popular in many fields of science — a *de facto* technique. This is reflected in the Nobel Price in Chemistry awarded to Kohn (together with John Pople) [1, 2] "for his development of the density-functional theory." Recently, the dominance of DFT has also been distilled into a locution noting how now over 30,000 scientific papers utilizing DFT are published yearly [3–8]. By the time it takes to read this thesis around ten new DFT papers will have appeared.

The appeal of DFT lies in its ability to greatly simplify the intractable electronic many-body problem, making it solvable in the first place. In practical terms DFT can couple a low enough computational cost with a level of accuracy that is in many cases sufficient for useful predictions. Systems consisting of up to a few thousand atoms can be routinely handled.

However, the inevitable price to pay for the simplification is that a certain part of DFT, so-called *exchange* and *correlation* (XC) effects[1], have to be approximated. Furthermore, if one desires to make DFT calculations even faster, in order to treat millions of atoms, the so-called Kohn-Sham (KS) orbitals have to be dropped, and thereby also the (non-interacting) kinetic energy (KE), which is normally obtained from the KS orbitals, has to be approximated. This branch of DFT is called orbital-free DFT (OF-DFT). At the moment KS-DFT is the one that is in widespread use, because OF-DFT development has proven to be rather slow and difficult.

It is interesting to speculate what DFT will look like in the future and how many potential improvements there are to be made. When will OF-DFT become a viable tool for the masses? Or will DFT get phased out by more accurate wavefunction methods thanks to increasing computing power or some algorithmic breakthrough [10]? Tied to these speculations is not only the degree to which we are able to advance DFT theory, but also Moore's law and the evolution of numerical algorithms are very much involved.

The focus of this thesis is on the theory side of DFT, and there are two important avenues towards making DFT even better. The first avenue is the development of new XC approximations. In KS-DFT it is mostly the quality of the XC approximation that actually determines the accuracy of the calculations. Therefore XC development is a vitally important field, and one who is at the forefront of XC development certainly gets his/her fair share of citations [11]. Of course, citations are not everything that counts, but very often they are counted.

In this thesis I develop a new kind of approximation, a quasi-non-uniform gradient-level approximation (QNA), which uses the atomic number as an extra piece of information. The atomic number dependency can be used to extend the limits that are associated with the level of XC approximation we are considering. The QNA approach leads to improved accuracy, which would not be easily achieved by the more "conventional" approximations, because in certain terms the state-of-the-art conventional approximations are already quite close to the limits and cannot be improved much further. For practical calculations, the QNA approximation has been implemented in EMTO and GPAW DFT codes. An attractive application for QNA is found in the formation energies of metallic binary alloys.

The second avenue is the study and development of OF-DFT KE approximations. Of these two avenues, XC development is much more popular throughout the world, partly because it is simply easier to develop

[1] The term exchange-correlation originates from Feynman diagrams being applied to the Schrödinger equation [9].

a practically useful XC approximation than it is to develop a practically useful KE approximation. However, through collaboration with prof. Á. Nagy I have developed a fondness and great interest in OF-DFT and as a result of this collaboration I introduce a differential equation for the so-called Pauli potential, a quantity that represents the KE of the KS-DFT orbitals. In practical OF-DFT calculations, it is hence ultimately the effect of the Pauli potential that has to be approximated somehow. The Pauli potential differential equation (PPDE) is, in fact, no approximation, but rather produces the *exact* Pauli potential as the solution of the PPDE. However, it should be noted that solving the PPDE exactly is currently quite laborious. The hope, then, for the future is that the PPDE could be approximated or solved with such techniques that the accuracy of OF-DFT could be significantly improved, without significantly increasing the computational load. Spherically symmetric Be atom is used as a model system to test the PPDE concept. To my knowledge this is the first time self-consistent (non-trivial) atomic OF-DFT calculations at the KS-DFT level of accuracy have been performed without explicitly solving the KS orbital equations.

2 Density Functional Theory

2.1 Background

Chemical properties of a molecule and the specifics of a material stem from the quantum mechanical electronic structure of the system in question. Analogously to classical mechanics and optics, as Schrödinger showed in 1926 [12], the motion of electrons and atomic nuclei in the realm of quantum mechanics can also be described by a Hamiltomian $\hat{H}$. The resulting great leap forward was the Schrödinger equation, $\hat{H}\Psi = E\Psi$, where Ψ is the many-body wave function and E the accompanying energy eigenvalue. Our pursuit of understanding the behavior of molecules and performance of materials therefore requires us to find solutions to the Schrödinger equation, which after expanding the Hamiltonian and invoking the Born-Oppenheimer approximation (whereby atomic nuclei are considered fixed on the time-scale of the much lighter electrons) has the form

$$\left[-\frac{1}{2}\sum_i \nabla_i^2 + \frac{1}{2}\sum_{i\neq j} \frac{1}{|\mathbf{r}_i - \mathbf{r}_j|} - \sum_i \sum_j \frac{Z_j}{|\mathbf{r}_i - \mathbf{R}_j|} \right] \Psi(\mathbf{r}_1, \mathbf{r}_2, \dots, \mathbf{r}_i, \dots)$$
$$= (\hat{T} + \hat{V}_{\text{ee}} + \hat{V}_{\text{ext}})\Psi(\mathbf{r}_1, \mathbf{r}_2, \dots, \mathbf{r}_i, \dots) = E\Psi(\mathbf{r}_1, \mathbf{r}_2, \dots, \mathbf{r}_i, \dots), \quad (2.1)$$

where the first term of $\hat{H}$ is the kinetic energy of the electrons, the second is the electron-electron interactions, and the third is the Coulombic electron-nucleus interactions. Above, and throughout the rest of this thesis, Hartree atomic units will be used, so that $e^2 = \hbar = m = 1$, where e is the elementary charge, $\hbar$ is the reduced Planck's constant, and m is the electronic mass.

Being a notorious many-body problem, exact solutions of the Schrödinger equation are incredibly difficult to obtain. Roughly speaking, we only know how to solve it in just two very specific cases: one is the trivial one electron case and the other is the limit of infinitely many particles [5, 13–15]. The fundamental problem behind the difficulty lies behind the high dimensionality of Ψ, the so-called exponential wall [2]. Even Hartree, as early as 1957, knew that the wave function of a single iron atom has 78 dimensions (three spatial dimensions for each of the 26 electrons) and to

write down the wave function on a coarse grid of just 10 points per dimension would require 10^{78} numbers to be stored [16]. Given how 10^{78} vastly exceeds the number of atoms on Earth, it is difficult to imagine how the wave function could be stored on a computer, even if it was calculated. Employing and developing alternate approaches and approximate solutions to the Schrödinger equation is therefore vital.

Around the time Schrödinger equation was published Thomas [17], Fermi [18], and Dirac [19] experimented with the idea of using the electron density as the variable, rather that the many-body wave function. It should be noted that the Thomas-Fermi (TF) model was not developed as an approximation to the Schrödinger equation. In fact, it makes no reference to the Schrödinger equation and Thomas likely did not even know about it at the time he published his density-based model. Instead, based on statistical arguments they imagined that the kinetic energy and electron repulsion could be modeled locally as a uniform electron gas (UEG). In UEG, also known as jellium[1] and homogeneous electron gas (HEG), electrons occupy an infinite region of space with a uniform positive background charge, so that the electron density is also perfectly uniform.

Not only is the TF model the first DFT, it is a *true* DFT in the sense that every energy contribution is an explicit functional of the density. No orbitals are needed, which means the TF model is also the first OF-DFT. The work of Thomas and Fermi was ahead of its time, but due to the crudeness of its kinetic energy approximation it fails to reproduce atomic shell structure, a consequence of the Pauli exclusion principle, and at best the energies still have errors around $10\,\%$ [20], which is far too much to describe chemical bonding accurately.

2.2 Hohenberg-Kohn Theorems

The TF model is not accurate enough for practical calculations, but it shifted the focus to using the electron density $n(\mathbf{r})$ as the central variable. In 1964 Hohenberg, and Kohn, who had had an inkling that the density had a deeper meaning than just a sum of orbital amplitudes [1], established the foundations of modern DFT. In their 1964 paper Hohenberg and Kohn showed [21] that the density can be regarded as the "basic variable" [22, 23], and the resulting DFT is an *exact* many-body theory. This was accomplished by presenting and proving two important theorems [5, 21, 23–26]:

I For any system of interacting particles moving in an external potential V_{ext}, this external potential V_{ext} is uniquely determined, up to an

[1] The word "jellium" was invented by Conyers Herring, a late American physicist.

arbitrary constant, by the ground state density n_{GS}. There exists a one-to-one mapping between V_{ext} and the density. Therefore all properties of the system are determined by its ground state density. Especially the total energy E can now be expressed as a functional of the density as $E[n]$.

II There will be a so-called *universal* functional $F[n]$ associated with the total energy $E[n]$. More specifically, part of the total energy is given by this universal functional, and its universality means its mathematical form remains unchanged with *any* choice of external potential V_{ext}. Additionally, for any given V_{ext} the total energy $E[n]$ has a global minimum, called the ground state energy E_{GS}, and the density that achieves this minimun has to be the exact ground state density n_{GS}.

By thinking in terms of density, the exponential wall can be circumvented because the density is always a function of just three spatial variables. This is a tremendous simplification compared to solving the Schrödinger equation. The theorems above guarantee that any property of the system can be obtained by applying functionals to the density. The most important functional, the total energy, is written (for simplicity, spin-unpolarized notation is used) as

$$E[n] = F[n] + E_{\text{ext}}[n], \quad E_{\text{ext}}[n] = \int V_{\text{ext}}(\mathbf{r}) n(\mathbf{r})\, d\mathbf{r}, \tag{2.2}$$

where the universal functional F has the form [23]

$$F[n] = \langle \Psi[n] | \hat{T} | \Psi[n] \rangle + \langle \Psi[n] | \hat{V}_{\text{ee}} | \Psi[n] \rangle = T[n] + E_{\text{ee}}[n]. \tag{2.3}$$

The term $T[n]$ is the kinetic energy functional and $E_{\text{ee}}[n]$ is the energy of electron-electron interactions. The wave function $\Psi[n]$ is the minimizing wave function that yields the density n. Both T and E_{ee} are functionals of n without reference to the external potential, because the many-body wave function Ψ itself is a functional of n. The second theorem guarantees that the ground state energy comes from the DFT variational principle as

$$E_{\text{GS}} = \min_{\Psi} \langle \Psi[n] | \hat{H} | \Psi[n] \rangle = \min_{n} (F[n] + E_{\text{ext}}[n]). \tag{2.4}$$

The Hohenberg-Kohn theorems are classic existence theorems. Quite literally, they guarantee that the universal functional F exists, but cannot answer the obvious follow-up question of what F is actually supposed to look like. The discovery of the exact expression of F will likely not happen any time soon, if ever, so some kind of approximation for it is needed

before any practical density functional calculations can take place. Indeed, this is precisely what Thomas, Fermi, and Dirac did. They wrote an approximate total energy functional, which has the form

$$E_{\text{TF}}[n] = C_{\text{F}} \int n(\mathbf{r})^{5/3}\, d\mathbf{r} + \frac{1}{2} \int \frac{n(\mathbf{r})n(\mathbf{r}')}{|\mathbf{r}-\mathbf{r}'|}\, d\mathbf{r}d\mathbf{r}' + A_{\text{X}} \int n(\mathbf{r})^{4/3}\, d\mathbf{r} + \int V_{\text{ext}}(\mathbf{r})n(\mathbf{r})\, d\mathbf{r}, \tag{2.5}$$

where $C_{\text{F}} = (3/10)(3\pi^2)^{2/3} \approx 2.871$ and $A_{\text{X}} = -(3/4)(3/\pi)^{1/3} \approx -0.738$. The first term in Eq. (2.5) is an approximation for the kinetic energy, the second term is the classical electrostatic Hartree energy, and the third term is the exchange energy of UEG developed by Dirac. The exchange approximation of Dirac is today best known as the exchange part of the so-called local density approximation (LDA) and it is still very much in widespread use (see section 3.2). The crudeness of the Thomas-Fermi model already shows that expressing different energy contributions accurately as density functionals, especially the kinetic energy, is a highly difficult task. In fact, the whole problem of extracting properties out the density alone is extremely difficult [23, p. 131].

2.3 Kohn-Sham Scheme

The Hohenberg-Kohn theorems show that density is the variable of choice, but so far no method has been provided for actually calculating the density and its functionals. Help for this conundrum arrived quite quickly. A year after the Hohenberg-Kohn theorems, in 1965, Kohn and Sham published a paper containing an *ansatz* that makes practical calculations possible [27]. The idea is to replace the interacting many-body problem by a fictitious system of non-interacting particles. Kohn and Sham assumed that a set of non-interacting particles can be chosen in such a way that its density is the same as the ground state density of the original interacting many-body system. No general proof for this *ansatz* exists, so in practice its validity is simply assumed. It should be noted that even though the general proof eludes DFT theorists there has nevertheless been a discussion about the validity of the "true system" $\leftrightarrow$ KS-system equivalence known as the *N-representability problem*. N-representability of a density n means that n can be represented as the density of some antisymmetric N-particle wavefunction Ψ. The universal functional F is defined for all densities n which are N-representable, and it can at least be shown that all non-negative n normalized to N are N-representable [25].

Having assumed non-interacting particles, their Hamiltonian is simply $\hat{H} = -1/2 \sum_i \nabla_i^2 + V_{\text{KS}}$, with some central effective potential V_{KS} that is yet to be determined. For non-interacting particles the many-body wave function Ψ is a product of the single-electron orbitals ψ_i, and applying variational principle to the total energy $\langle \Psi | \hat{H} | \Psi \rangle$ leads to a set of single-electron equations

$$\left[-\frac{1}{2}\nabla^2 + V_{\text{KS}}(\mathbf{r}) \right] \psi_i(\mathbf{r}) = \epsilon_i \psi_i(\mathbf{r}). \tag{2.6}$$

These are the celebrated Kohn-Sham equations for non-interacting electrons moving in an effective potential V_{KS}, which will produce the correct interacting many-body density

$$n(\mathbf{r}) = \sum_i |\psi_i(\mathbf{r})|^2. \tag{2.7}$$

Kohn and Sham derived V_{KS} by writing the universal functional in a new form, in terms of the non-interacting kinetic energy T_{S}:

$$F[n] = T_{\text{S}}[n] + E_{\text{H}}[n] + E_{\text{XC}}[n], \quad E_{\text{H}}[n] = \frac{1}{2} \int \frac{n(\mathbf{r}) n(\mathbf{r}')}{|\mathbf{r} - \mathbf{r}'|} \, d\mathbf{r} d\mathbf{r}' \tag{2.8}$$

where the subscript "s" in T_{S} refers to "single-electron" and E_{H} is the classical Coulomb repulsion energy of the electron density interacting with itself, known as the Hartree energy. E_{XC} is the so-called exchange-correlation (XC) term, which is responsible for capturing the many-body effects. It is edifying to rewrite Eq. (2.8) in terms of E_{XC} as a grouping

$$\begin{aligned} E_{\text{XC}}[n] &= F[n] - T_{\text{S}}[n] - E_{\text{H}}[n] \\ &= (T[n] - T_{\text{S}}[n]) + (E_{\text{ee}}[n] - E_{\text{H}}[n]), \end{aligned} \tag{2.9}$$

which reveals that XC energy is the difference between the kinetic energies of the true interacting system and the non-interacting one, as well as the difference between the true electron-electron interaction energies and the approximate classical Hartree energy.

By inserting the new F into Eq. (2.2), forming the Euler-Lagrange equation, and then comparing that to the Euler-Lagrange equation of the non-interacting system [24], it is found that

$$V_{\text{KS}} = V_{\text{ext}} + V_{\text{H}} + V_{\text{XC}}, \quad V_{\text{H}} = \int \frac{n(\mathbf{r}')}{|\mathbf{r} - \mathbf{r}'|} \, d\mathbf{r}'. \tag{2.10}$$

The second term V_{H} is the classical Hartree potential and V_{XC} is defined to

be the functional derivative of the XC energy: $V_{\text{XC}} \equiv \delta E_{\text{XC}}/\delta n$. Clearly V_{KS} depends on the density, which means that the correct density is needed in order to compute V_{KS}. But the correct density can only be calculated from the KS equations, which themselves depend on V_{KS}. Luckily this vicious circle does not stop us from performing practical calculations because the variational principle of Eq. (2.4) guarantees that the proper ground state n and V_{KS} can always be found *self-consistently* with the use of an iterative solution scheme [28]. We start with some initial guess for V_{KS} and solve the KS equations to obtain a new density. In the second iteration this new density is then used to compute a new guess for V_{KS} and the KS equations are solved once again. When this self-consistent loop is iterated with care, n and V_{KS} approach such values that they change no more from iteration to iteration. The density n of Eqs. (2.6) and (2.7) is then said to be consistent with V_{KS} of Eq. (2.10), and that defines self-consistency.

The key behind the success of the KS approach is that the non-interacting kinetic energy can be calculated *exactly* from the KS orbitals as

$$T_{\text{S}} = -\frac{1}{2}\sum_i \langle\psi_i|\nabla^2|\psi_i\rangle = \frac{1}{2}\sum_i \int |\nabla\psi_i(\mathbf{r})|^2 \, d\mathbf{r}. \tag{2.11}$$

This conceptual shift creates a significant increase in accuracy compared to the TF model because, as it turns out, the non-interacting kinetic energy is very close to the exact interacting many-body kinetic energy. Getting the kinetic energy right is crucial, because it is a big part of the total energy; it is of the same order of magnitude as the total energy itself.

Main reason behind the "downfall" of the TF model is its *local*, explicit density functional approximation for the kinetic energy. In other words, Thomas and Fermi used an orbital-free approximation for the kinetic energy. But the kinetic energy is by nature a heavily non-local quantity, which means its essence is much more easily captured in terms of orbitals than the density. To this day no one has been able to create an acceptably accurate general purpose orbital-free approximation for the kinetic energy; local, semi-local or otherwise. Due to this non-locality issue of the kinetic energy, Kohn and Sham essentially separated out the non-interacting kinetic energy and the long-range Hartree terms, which is revealed by Eq. (2.9). The remaining unknown part of the total energy, the XC contribution, can be approximated surprisingly accurately even by simple local schemes.

3 Exchange and Correlation

It is often claimed that the KS scheme works because the approximate part, the XC term, is small. This is a somewhat inaccurate statement, because it seems to imply that neglecting the XC term altogether should be a reasonable option. However, setting $V_{\text{XC}} = 0$, i.e. the Hartree approximation[1] [29–31], leads to much too weak bonds, which is why XC has been given the nickname "Nature's glue" [32].

As a theory DFT is exact, meaning that if the exact XC term was known, we would be calculating the total energy *almost* exactly correctly. The reason why the total energy would still be only almost exact and not exact[2] is due to the finite accuracy of computers, and choices and compromises made in the implementations of DFT codes[3]. In any case, recently it was shown that for a fixed XC approximation all popular modern DFT codes are well-honed enough to give practically identical answers [33]. Therefore the accuracy of a DFT calculation depends only on the choice of the XC approximation. In this light, it is no wonder that hundreds of XC approximations have been developed, taking us little by little closer to the "Divine functional" [9] — an approximation that might not be the exact one, but is accurate enough for all intents and purposes, both in physics and chemistry. Out of the considerable richness of XC theory, the concepts and approximation most relevant to this thesis are presented in the following sections.

3.1 Properties

Although the form of the exact XC functional is not known, the exact properties and features of XC can be studied, which is helpful in developing XC approximations and understanding why, and how, these approximations

[1] Hartree also defined a different electrostatic potential for each electron by removing self-interaction, so that the potential for electron i becomes $V_{\text{H}}^{i}(\mathbf{r}) = \sum_{j \neq i} \int |\psi_j(\mathbf{r}')|^2 / |\mathbf{r} - \mathbf{r}'| \, d\mathbf{r}'$.

[2] In practice, exact science is not exactly exact.

[3] In practical DFT codes many simplifications are made in order to achieve reasonable running times.

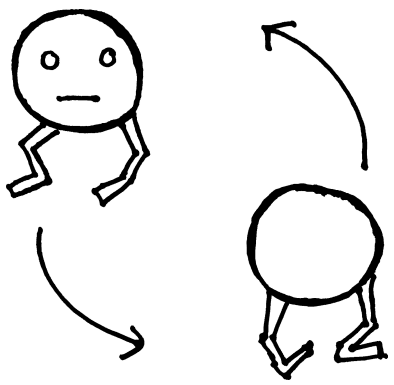

FIGURE 3.1: A sketch of two electrons avoiding each other because of exchange and correlation effects. Reprinted with permission from J. Chem. Theory Comput., 2009, 5 (4). Copyright 2009 American Chemical Society.

work. A physically relevant definition for the XC energy can be derived using the coupling-constant integration technique [22–24, 34]. A coupling-constant λ is introduced, which connects the imaginary Kohn-Sham system to the real, interacting physical system through a continuum of Hamiltonians

$$\hat{H}^{\lambda} = \hat{T} + V_{\mathrm{KS}} + \lambda(\hat{V}_{\mathrm{ee}} + V_{\mathrm{ext}} - V_{\mathrm{KS}}). \tag{3.1}$$

For each λ the minimizing wave function is denoted by $\Psi^{\lambda}[n]$. The case $\lambda = 0$ represents the non-interacting Kohn-Sham case and $\lambda = 1$ gives the Hamiltonian of the real physical system. This leads the XC energy to be written in the form

$$\begin{aligned} E_{\mathrm{xc}}[n] &= \langle \hat{T} \rangle + \langle \hat{V}_{\mathrm{ee}} \rangle - T_{\mathrm{S}} - E_{\mathrm{H}} \\ &= \langle \Psi^{\lambda}[n] | \hat{T} + \lambda \hat{V}_{\mathrm{ee}} | \Psi^{\lambda}[n] \rangle_{\lambda=1} - \langle \Psi^{\lambda}[n] | \hat{T} + \lambda \hat{V}_{\mathrm{ee}} | \Psi^{\lambda}[n] \rangle_{\lambda=0} - E_{\mathrm{H}} \end{aligned} \tag{3.2}$$

Equation (3.2) can be turned into an integral about λ, and with the help of the Hellmann-Feynman theorem the XC energy can be expressed as a Coulomb type integral

$$E_{\mathrm{XC}}[n] = \frac{1}{2} \iint \frac{n(\mathbf{r}) \bar{n}_{\mathrm{XC}}(\mathbf{r}, \mathbf{r}')}{|\mathbf{r} - \mathbf{r}'|} \, d\mathbf{r} d\mathbf{r}', \tag{3.3}$$

where the so-called exchange-correlation hole $\bar{n}_{\mathrm{XC}}(\mathbf{r}, \mathbf{r}')$ is introduced. The physical meaning of the XC hole is that an electron at point $\mathbf{r}$ reduces the

probability of finding another electron at point $\mathbf{r}'$, due to electrons repelling one another. From Eq. (3.3) it follows that the XC energy can be seen as the interaction energy between an electron and its corresponding XC hole. One important property of the XC hole is a sum-rule

$$\int \bar{n}_{\mathrm{XC}}(\mathbf{r}, \mathbf{r}')\, d\mathbf{r}' = -1, \tag{3.4}$$

which means that if an electron is found at point $\mathbf{r}$, then it must be missing from the rest of the system.

It is quite customary to write the XC energy as a sum of separate exchange (X) and correlation (C) contributions

$$E_{\mathrm{XC}}[n] = E_{\mathrm{X}}[n] + E_{\mathrm{C}}[n]. \tag{3.5}$$

The XC hole can be decomposed similarly into

$$\bar{n}_{\mathrm{XC}}(\mathbf{r}, \mathbf{r}') = \bar{n}_{\mathrm{X}}(\mathbf{r}, \mathbf{r}') + \bar{n}_{\mathrm{C}}(\mathbf{r}, \mathbf{r}'). \tag{3.6}$$

It can be shown that the X and C holes respect the following sum rules:

$$\int \bar{n}_{\mathrm{X}}(\mathbf{r}, \mathbf{r}')\, d\mathbf{r}' = -1, \quad \int \bar{n}_{\mathrm{C}}(\mathbf{r}, \mathbf{r}')\, d\mathbf{r}' = 0. \tag{3.7}$$

These sum rules — and other such exact constraints — are very important in the field of XC approximation development. Logically, if the approximate functional fulfills the same constraints as the exact XC functional, it will likely behave like the exact functional. Consequently, approximations are often designed in a way that they respect as many of the physically relevant constraints as possible.

3.2 Local Density Approximation

Local density approximation (LDA) was introduced by Kohn and Sham [27], and in some sense it is the most important XC approximation. This view is supported by the following observations:

- It is the earliest and the simplest[4] XC approximation.
- It is rigorously constructed and exact for a perfectly homogeneous density, the UEG model.

[4] Excluding the Hartree type $V_{\mathrm{XC}} = 0$ approximation.

- It fulfills a number of important physical constraints, such as the sum rule of Eq (3.4).
- It represents a universal limit of all quantum systems [5, 13–15].
- It is, at the end of the day, a surprisingly accurate approximation.

Historically, LDA was almost exclusively adopted by the physics community, because for solid state systems the important regions are relatively slowly varying, and so e.g. solid state geometries are quite accurate with LDA. Chemists, however, who mostly deal with atoms and molecules, were not impressed by LDA. Atomic tails, which decay exponentially, are far from being slowly varying, which causes big problems for LDA, e.g. massive overbinding.

Locality implies that the XC energy per particle at point $\mathbf{r}$ depends only on the density at that same point, so the XC energy of LDA can be written as a simple integral

$$E_{\mathrm{XC}}^{\mathrm{LDA}}[n] = \int n(\mathbf{r})\varepsilon_{\mathrm{X}}^{\mathrm{LDA}}([n],\mathbf{r})\,d\mathbf{r} + \int n(\mathbf{r})\varepsilon_{\mathrm{C}}^{\mathrm{LDA}}([n],\mathbf{r})\,d\mathbf{r}, \tag{3.8}$$

where $\varepsilon_{\mathrm{X}}^{\mathrm{LDA}}([n],\mathbf{r})$ [$\varepsilon_{\mathrm{C}}^{\mathrm{LDA}}([n],\mathbf{r})$] is the exchange [correlation] energy per particle of the UEG.

The exact formula for $\varepsilon_{\mathrm{X}}^{\mathrm{LDA}}([n],\mathbf{r})$ is obtained quite easily, and it was first derived by Dirac [19] in 1930 as a correction to the TF model, which at that time lacked any treatment for exchange and correlation. First it should be noted that in UEG the electrons occupy an infinite region of space in a uniform external potential, so the solutions of the KS equations are simply plane waves and the energy is given by the momentum or the wavevector $\mathbf{k}$ of the plane wave. Dimensional analysis reveals that $\varepsilon_{\mathrm{X}}^{\mathrm{LDA}}$ must be proportional to the Fermi wavevector

$$k_{\mathrm{F}} = \left(3\pi^2 n\right)^{1/3}, \tag{3.9}$$

which is the radius of the sphere in momentum space that contains all occupied plane wave states. Evaluating the exact exchange integral of the Hartree-Fock theory [23, 35]

$$E_{\mathrm{X}} = -\frac{1}{2}\sum_{i,j}\iint \frac{\psi_i^*(\mathbf{r})\psi_j^*(\mathbf{r}')\psi_i(\mathbf{r}')\psi_j(\mathbf{r})}{|\mathbf{r}-\mathbf{r}'|}\,d\mathbf{r}d\mathbf{r}' \tag{3.10}$$

with the plane waves yields

$$\varepsilon_{\mathrm{X}}^{\mathrm{LDA}}([n],\mathbf{r}) = A_{\mathrm{X}} n^{1/3}, \quad A_{\mathrm{X}} = -(3/4)(3/\pi)^{1/3} \approx -0.738. \tag{3.11}$$

Expression for the correlation energy is quite a bit more difficult to obtain. When working with correlation, it is customary to define the Wigner radius

$$r_s = \left(\frac{3}{4\pi n}\right)^{1/3}, \tag{3.12}$$

the radius of a sphere which on average contains one electron. Whereas the exchange formula of Eq. (3.11) is simple and valid for any density, correlation is known analytically only in two limiting cases:

- Low-density limit ($r_s \to \infty$):

$$\varepsilon_{\text{C}}(r_s) \to \frac{a_1}{r_s} + \frac{a_2}{r_s^{3/2}} + \frac{a_3}{r_s^4} + \ldots, \tag{3.13}$$

  where $a_1 = 0.896$ and $a_2 = 1.325$.

- High-density limit ($r_s \to 0$):

$$\varepsilon_{\text{C}}(r_s) \to 0.0311 \ln r_s - 0.047 + 0.009 r_s \ln r_s - 0.010 r_s + \ldots \tag{3.14}$$

Intermediate values for ε_{C} between the two limits were produced by Ceperley and Alder in 1980 by using a highly accurate quantum Monte Carlo method [36]. These data are turned into practical approximations by producing an analytical function, whose parameters are determined by simultaneously requiring the function to respect the two known limits and having it fit the Monte Carlo data as closely as possible. The most popular LDA correlation approximations are Vosko-Wilk-Nusair [37], Perdew-Zunger [38], and Perdew-Wang [39].

3.3 Generalized Gradient Approximation

A straightforward attempt at improving over the LDA, which only uses the density as its information, is to include information about the gradient of the density. Since technically only an infinitesimally small region around point $\mathbf{r}$ is needed to compute the gradient at point $\mathbf{r}$, gradient-level approximations are often called *semilocal* approximations. A gradient correction for LDA was already proposed by Kohn and Sham [27] who wrote a power series expansion for the LDA XC energy in terms of the gradients of the density:

$$E_{\text{X}}^{\text{GEA}}[n] = \int n(\mathbf{r}) \varepsilon_{\text{X}}^{\text{LDA}}([n], \mathbf{r}) \left[1 + A_{\text{X}}([n], \mathbf{r}) s_1^2 + B_{\text{X}}([n], \mathbf{r}) s_2^2 + \ldots\right] d\mathbf{r}, \tag{3.15}$$

$$E_{\mathrm{C}}^{\mathrm{GEA}}[n] = \int n(\mathbf{r}) \left[\varepsilon_{\mathrm{C}}^{\mathrm{LDA}}([n],\mathbf{r}) + A_{\mathrm{C}}([n],\mathbf{r})s_1^2 + B_{\mathrm{C}}([n],\mathbf{r})s_2^2 + \dots\right] d\mathbf{r}, \tag{3.16}$$

where s_m is the natural, dimensionless expansion coefficient of any functional with power law scaling[5], and it is defined [23] by

$$s_m = \frac{|\nabla^m n|}{(2k_{\mathrm{F}})^m n}. \tag{3.17}$$

This approach is known as the gradient expansion approximation (GEA), and since it is an expansion for LDA, it is only valid in the slowly varying density limit. This is an important notion, because densities in real systems are not slowly varying, and indeed it turned out that GEA is not a universal improvement over LDA in real systems, but actually makes things worse in many cases. One of the most notable failures of GEA is that it does not satisfy the sum rules of Eq. (3.7).

By studying the failures of GEA, in particular the GEA hole problem, a much more practically useful approach was developed, the generalized gradient approximation (GGA) [22, 41–44]. The basic premise of GGA is the observation that the poor performance of GEA at large s_m can be remedied by fixing the sum rule violation, and this can be achieved by a method called real-space cutoff technique [22, 45–47]. The XC hole of GEA shows oscillations as a function of distance $u = |\mathbf{r} - \mathbf{r}'|$ from the reference electron at point $\mathbf{r}$, making the hole oscillatory and unphysically positive for large values of u [24]. The solution is to use a step function to cut off the the X and C holes at point $\mathbf{r}'$, which is chosen in such a way that the sum rules of Eq. (3.7) are satisfied. Using the step function, the GEA hole can be integrated, which produces a *numerical* GGA; a set of data that can be subsequently parametrized to produce an analytical GGA. One of the most popular XC functionals constructed with the help of the real-space cutoff technique is the Perdew-Wang PW91 functional [48].

GGA represents the first step beyond LDA [49], and as such only the lowest order gradient s_1 is used in a GGA, and for convenience we define $s \equiv s_1$. Inclusion of higher order gradients, as well as the kinetic energy density, is of course possible, which happens in so-called meta-GGA functionals [50]. GGA might seem like an *ad hoc* truncation of the GEA, but the aim really is to construct a framework, where s is used in such a way that

[5] Scaling conditions are very important in understanding the many aspects of density functionals, such as the degree of their density dependence; see Eq. (3.18) and Refs. [22, 24, 25, 40].

a GGA can be practical and useful for all values of s, unlike the "feckless" GEA.

In order to yield the GGA framework, the expansions of Eqs. (3.15-3.16) are studied for exchange and correlation parts separately. By using the exchange scaling relation [22, 24, 40]

$$E_{\mathrm{X}}[n_\gamma] = \gamma E_{\mathrm{X}}[n], \quad n_\gamma = \gamma^3 n(\gamma \mathbf{r}) \tag{3.18}$$

it becomes easy to show that for exchange the coefficients $A_{\mathrm{X}}([n], \mathbf{r}) = 10/81$, $B_{\mathrm{X}}([n], \mathbf{r}) = 146/2025$ etc. cannot contain γ dependence, and so they have to be rational numbers. The important observation here is that $\varepsilon_{\mathrm{X}}^{\mathrm{LDA}}$ takes care of the density dependence and the gradient correction only depends on s, in a dimensionless manner. In DFT parlance Eq. (3.18) says that the exchange energy scales linearly (in terms of γ), and it is easy to show that LDA exchange fulfills this condition. Therefore, the standard way of writing any GGA exchange functional, which uses LDA as its "starting point", is

$$E_{\mathrm{X}}^{\mathrm{GGA}}[n] = \int n(\mathbf{r}) \varepsilon_{\mathrm{X}}^{\mathrm{LDA}}([n], \mathbf{r}) F_{\mathrm{X}}(s)\, d\mathbf{r}, \tag{3.19}$$

where an exchange *enhancement factor* $F_{\mathrm{X}}(s)$ is defined.

As per usual, the "recalcitrant" [51] nature of correlation poses a bigger challenge, because there is no scaling condition similar to Eq. (3.18) for correlation. Often another reduced gradient

$$t = \left(\frac{\pi}{4}\right)^{1/2} \left(\frac{9\pi}{4}\right)^{1/6} \frac{s}{r_s^{1/2}} \tag{3.20}$$

is defined when working with correlation[6]. The coefficients in the correlation gradient expansion of Eq. (3.16) are not as simple as they are for exchange. It has been shown [52] that A_{C} approaches a constant value of 0.066725, when approaching the limit $n \to \infty$. Also the weak density and spin dependencies of A_{C} are known [22]. Using the aforementioned known properties of A_{C} a correlation enhancement factor $F_{\mathrm{C}}(r_s, t)$ can be defined and different approximations for it developed. With $F_{\mathrm{C}}(r_s, t)$ the correlation functional of a GGA can be written in terms of $\varepsilon_{\mathrm{X}}^{\mathrm{LDA}}$ as

$$E_{\mathrm{C}}^{\mathrm{GGA}}[n] = \int n(\mathbf{r}) \varepsilon_{\mathrm{X}}^{\mathrm{LDA}}([n], \mathbf{r}) F_{\mathrm{C}}(r_s, t)\, d\mathbf{r}, \tag{3.21}$$

[6] In practice t is spin dependent, but here, for simplicity, the spin dependency is suppressed.

so that the total GGA XC functional could be expressed as a sum

$$\begin{aligned} E_{\mathrm{XC}}^{\mathrm{GGA}}[n] =& E_{\mathrm{X}}^{\mathrm{GGA}}[n] + E_{\mathrm{C}}^{\mathrm{GGA}}[n] \\ =& \int n(\mathbf{r})\varepsilon_{\mathrm{X}}^{\mathrm{LDA}}([n],\mathbf{r})F_{\mathrm{X}}(s)\,d\mathbf{r} + \int n(\mathbf{r})\varepsilon_{\mathrm{X}}^{\mathrm{LDA}}([n],\mathbf{r})F_{\mathrm{C}}(r_s,t)\,d\mathbf{r} \\ =& \int n(\mathbf{r})\varepsilon_{\mathrm{X}}^{\mathrm{LDA}}([n],\mathbf{r})[F_{\mathrm{X}}(s) + F_{\mathrm{C}}(r_s,t)]\,d\mathbf{r} \\ =& \int n(\mathbf{r})\varepsilon_{\mathrm{X}}^{\mathrm{LDA}}([n],\mathbf{r})F_{\mathrm{XC}}(r_s,s,t)\,d\mathbf{r}, \end{aligned} \tag{3.22}$$

where $F_{\mathrm{C}}(r_s,t)$ is expressed in a form

$$F_{\mathrm{C}}(r_s,t) = \frac{\varepsilon_{\mathrm{C}}^{\mathrm{GGA}}}{\varepsilon_{\mathrm{X}}^{\mathrm{LDA}}}. \tag{3.23}$$

The function $\varepsilon_{\mathrm{C}}^{\mathrm{GGA}}$ is a gradient corrected correlation energy per particle, most often based on and building up from LDA correlation. It is seen that building a practical GGA involves developing some approximations for the exchange and correlation enhancement factors F_{X} and F_{C}. A large number of different GGAs have been developed over the years [53]. Some are aimed towards the needs of chemistry [20] and others are meant to be accurate in solid state physics [54]. The fact that so many different approximations have been developed is a manifestation of two core challenges of DFT [34, 43, 55, 56]:

- There is (yet) no really systematic way of developing new XC functionals or improving existing ones. Some functionals are *non-empirical*, derived from physical constraints. Others are *empirical*, which are created by fitting them to some experimental data sets.
- It has proven very difficult to develop an XC approximation that would be simultaneously accurate both in chemistry and solid state physics. For best accuracy, one regime or the other has to be focused on.

One very popular GGA, which plays a central role in this thesis, is introduced next.

3.4 Perdew-Burke-Ernzerhof Approximation

The highly popular Perdew-Burke-Ernzerhof (PBE) GGA [57] has earned its place as a standard functional in solid state physics. It is non-empirical

and turns out to be very similar in its performance to the older PW91 functional. Unlike PW91, however, it fulfills more physical constraints and in doing so manages to avoid the need to use the real-space cutoff data.

In order to resemble the second order gradient expansion, PBE correlation energy particle $\varepsilon_{\mathrm{C}}^{\mathrm{PBE}}$ of Eq. (3.23) has the form

$$\varepsilon_{\mathrm{C}}^{\mathrm{PBE}} = \varepsilon_{\mathrm{C}}^{\mathrm{LDA}} + H(r_s, t) = \frac{F_{\mathrm{C}}(r_s, t)}{\varepsilon_{\mathrm{X}}^{\mathrm{LDA}}}. \tag{3.24}$$

The gradient dependent term H itself has the form

$$H(r_s, t) = \gamma \ln \left\{ 1 + \frac{\beta}{\gamma} t^2 \left[\frac{1 + At^2}{1 + At^2 + A^2 t^4} \right] \right\}, \tag{3.25}$$

where $\gamma = (1 - \ln 2)/\pi^2$, $\beta = 0.066725$, and

$$A = \frac{\beta}{\gamma} \left[\exp\left\{ -\varepsilon_{\mathrm{c}}^{\mathrm{LDA}} / \gamma \right\} - 1 \right]^{-1}. \tag{3.26}$$

This expression for H appeared already as a part of the PW91 correlation energy and is derived based on three conditions [57]:

- In the slowly varying limit $t \to 0$, H recovers the second order GEA. This condition fixes the value of β to 0.066725.
- In the rapidly varying limit $t \to \infty$, $H \to -\varepsilon_{\mathrm{C}}^{\mathrm{LDA}}$ to make correlation vanish. This condition is connected to the correlation sum rule of Eq. (3.7): when t grows, $\bar{n}_{\mathrm{C}}(\mathbf{r}, \mathbf{r}')$ has to be cut off closer and closer to $\mathbf{r}$, until at the limit $t \to \infty$ the only way to satisfy the sum rule is to make the correlation hole density vanish [24].
- In the high-density limit of uniform scaling of Eq. (3.18), correlation energy must scale to a constant.

The exchange enhancement factor in PBE is given by

$$F_{\mathrm{X}}^{\mathrm{PBE}}(s) = 1 + \kappa - \frac{\kappa}{1 + \mu s^2 / \kappa}. \tag{3.27}$$

This form is simple[7], but it satisfies several important physical boundary conditions:

- In order to recover LDA in the homogeneous limit, $F_{\mathrm{X}}^{\mathrm{PBE}}(s) \to 1$, when $s \to 0$.

[7] It is actually the same expression that was already proposed by Becke in 1986.

- For small s the form of the second order GEA, $1 + \mu s^2$, is recovered[8].
- κ is chosen to be 0.804, which is a limit determined by the Lieb-Oxford bound [22, 58]

$$E_{\mathrm{X}}[n] \geq E_{\mathrm{XC}}[n] \geq E_{\mathrm{XC}}^{\lambda=1}[n] \geq 2.273 E_{\mathrm{X}}^{\mathrm{LDA}}. \tag{3.28}$$

  The limiting value 0.804 can be derived by utilizing the spin-scaling relation of exchange[9] and considering the case of fully spin-polarized density in the $r_s \to 0,\ s \to \infty$ limit (implying $t \to \infty$), where $F_{\mathrm{C}} \to 0$ and exchange dominates [22].
- The parameter μ is chosen to be $(\pi^2/3)\beta = 0.21951$. The condition $\mu = (\pi^2/3)\beta$ arises naturally, when the coefficient of the GEA are calculated using linear response technique [22]. Therefore, in order to recover the linear response of LDA, the condition $\mu = (\pi^2/3)\beta$ should be respected. It should be noted that $\mu = 0.21951$ is not the correct coefficient of the second order GEA, which is $\mu^{\mathrm{GEA}} = 10/81 = 0.123\ldots$. This higher value than μ^{GEA} was chosen because it gives accurate exchange energies for neutral atoms.

In practice, results calculated with PBE are most of the time almost identical to the old PW91 functional, but not always [59]. The great victory of PBE over the "more Byzantine" [57] PW91 is its simpler form and physically more robust, elegant, and easier derivation, and these qualities have made PBE one of the most popular functionals of all time.

The two parameters, μ and β, control the behavior of PBE by controlling the strength of the gradient corrections. In PBE μ and β were fixed in such a way that atomization and cohesion energies would be accurate, because they are very important in chemistry. As noted previously, what is accurate in chemistry, is often not as accurate in solid state physics. One of the most notable problems of PBE is its tendency to overestimate volumes in solid state calculations. While LDA ($\mu^{\mathrm{LDA}} \equiv 0$) tends to underestimate volumes by some amount, PBE tends to overestimate them by a comparable amount. Too large PBE volumes are a direct consequence of violating the second order GEA of exchange by making $\mu^{\mathrm{PBE}} \approx 2\mu^{\mathrm{GEA}}$. This observation suggests that fixing μ to μ^{GEA} would lead to more accurate volumes than those of either LDA or PBE.

The deficiency of PBE in solid state calculations was addressed by some of the authors of the original PBE functional [60]. They created a "solid

[8] $1 + \mu s^2 - F_{\mathrm{X}}^{\mathrm{PBE}}(s) = \mu s^4/(\kappa + \mu s^2)$, so that for small values of s the error w.r.t. the second order GEA is very small, in the fourth order.

[9] $E_{\mathrm{X}}[n_\uparrow, n_\downarrow] = 1/2 E_{\mathrm{X}}[2n_\uparrow] + 1/2 E_{\mathrm{X}}[2n_\downarrow]$

state version" of PBE, called PBEsol, by re-parametrizing μ and β, the two important coefficients in the PBE functional form. In PBEsol the exchange gradient expansion is restored, and so $\mu^{\text{PBEsol}} = \mu^{\text{GEA}}$. Correlation parameter β^{PBEsol} is determined by a requirement of good surface energies, and its value was chosen to be 0.046, which is a fit to TPSS meta-GGA [61] jellium XC surface energies.

In a series of benchmarks that followed the release of PBEsol [62–65], it was found that the idea of adjusting μ and β indeed leads to improved solid state performance. Some other notable solid-state oriented GGAs are AM05 [66–68], WC [54], HTBS [69], and SG4 [70].

3.5 Subsystem Functional Approach

The PBE functional was developed following the principle of fulfilling as many of the constraints of the exact XC functional as possible. The cornerstone of the constraint-based XC ideology is the Jacob's ladder model of functional development, as proposed by Perdew et al. [49, 61, 71–73]. The Jacob's ladder model is a classification system of functionals, in which functionals at each higher rung of the ladder include more and more useful information. Thereby, functionals at a higher rung are able to satisfy a greater number of constraints than the ones below, presumably leading to an improvement in accuracy. This scheme has progenated many famous functionals, such as PBE and TPSS meta-GGA [61].

An alternate, and more or less competing, scheme to the Jacob's ladder was put forward and further developed by Kohn, Mattsson, and Armiento [74–78]. Named subsystem functional approach (SFA), its viewpoint is fundamentally different from that of the Jacob's ladder. This difference stems from the fact that it is derived from a very dissimilar physical argument: the "nearsightedness" principle of electrons [79]. The crux of the subsystem functional scheme is the observation that in different regions of a physical system (e.g. deep interior vs. surface), different kinds of physics might occur. It is therefore sensible to divide the system into *subsystems* by these regions and assign an appropriate *subsystem functional* (SF) to each of the subsystems. These subsystem functionals are specially designed to accurately describe the physics occuring within the particular subsystem. A functional designed in this way can therefore offer extended accuracy compared to Jacob's ladder functionals, which conventionally apply one and same "rigid" mathematical form to all regions of space.

The basic principle behind SFA is the use of model systems: mathematical expressions for the subsystem functionals are developed by studying

the properties of tractable model systems, such as LDA, Airy gas [74, 75, 80], or Mathieu gas [76], where similar physics are happening as in some particular region of the real system. LDA can be very naturally seen as a model system because, after all, it is exact for the UEG, which is a model.

In order to actually calculate the XC energy within SFA, it is observed that any integral over the total system volume V can be broken into a sum of integrals over smaller volumes V_i, where $V = V_1 + V_2 + \cdots + V_i + \cdots + V_N$. For a system, which is divided into N subsystems, the total XC energy thus becomes

$$E_{\text{XC}} = \sum_{i=1}^{N} \int_{V_i} n(\mathbf{r}) \varepsilon_{\text{XC}}^{\text{SF}_i}([n], \mathbf{r})\, d\mathbf{r}, \tag{3.29}$$

where $\varepsilon_{\text{XC}}^{\text{SF}_i}$ is the subsystem functional specific to subsystem i and the integration domains V_i are those regions of space, which are occupied by subsystem i. It should be noted that breaking down the integral will create surface terms at the boundaries of V_i, and this should be taken into account in the design of the subsystem functionals, so that these surface terms either vanish or are negligibly small in actual calculations.

In addition to model systems, one of the most important aspects of the design of SFs is determining the criteria governing the division of space into subsystems. The SF should be able to determine which point in space belongs to which subsystem, based somehow on available information, such as the density at that particular point (LDA) and its gradients (GGA). For an SF to be of use in practical calculations, this process of categorizing the space should happen automatically, hidden from the end-user of a DFT code. This automation is achieved by way of interpolation: different subsystems should be connected by some kind of interpolation function. For example, the first subsystem functional, AM05, utilizes two model systems, LDA for interior regions and Airy gas for edge and surface regions:

$$\varepsilon_{\text{XC}}^{\text{AM05}}([n, s], \mathbf{r}) = X(s)\varepsilon_{\text{XC}}^{\text{interior}}([n], \mathbf{r}) + [1 - X(s)]\, \varepsilon_{\text{XC}}^{\text{edge}}([n, s], \mathbf{r}), \tag{3.30}$$

where $0 \leq X(s) \leq 1$ is a gradient dependent interpolation function, whose job is to decide whether a point $\mathbf{r}$ in space is purely part of the interior ($X(s) \approx 1$) or the surface ($X(s) \approx 0$), or in the boundary between the two subsystems ($X(s) \approx 1/2$).

3.6 Quasi-non-uniform Exchange-Correlation Approximation

The popularity, elegance, and simplicity of PBE have encouraged many to study it and design a myriad of improvements. The best-known effort down this line is the PBEsol functional, where μ and β were assigned new values. Another interesting strategy is to make μ and/or β more general, for example by making μ depend on s [54]. For a list of different attempts the reader is referred to Ref. [81] and references therein.

To a large extent PBEsol fixes the issue of overestimated lattice constants (LCs) of PBE, but not completely. Nevertheless, the unsolved problem of inconsistent accuracy of LCs of solids on GGA level still stands. This is unfortunate because volume is one of the most fundamental and important properties of solids. It is well-known that PBE tends to give accurate LCs for light $3d$ elements, but overestimates those of heavy $5d$ elements, and LDA tends to be accurate for $5d$ elements, but underestimates LCs of light elements. There is no GGA functional that has consistent accuracy at both ends. This is a dilemma, similar to the dilemma of trying to have simultaneously accurate GGA atomic exchange energies and solid state properties. To wit: "At the GGA level, one must choose" [60]. Ultimately, GGA level is only one rung above LDA in the Jacob's ladder and therefore its accuracy can be expected to be limited in various ways.

One of the questions this thesis wants to answer is whether the limits of GGA level can be overcome in some fashion. The most obvious option is to climb the Jacob's ladder and use more sophisticated approximations. There is, however, good reasons to remain on the GGA level, if possible. For example, self-consistent meta-GGA calculations are not yet commonplace, because they require modifying KS equations, because meta-GGA XC potential is KS orbital dependent. Also, it appears that self-consistent meta-GGA calculations demand more careful attention to numerical details than GGA calculations [82]. Methods even more sophisticated than meta-GGAs could of course be utilized, but their biggest drawback is the fact that they are computationally orders of magnitude heavier than GGAs. We therefore focus on the GGA level and think of strategies that could be used to design a functional that is still a GGA, but with an extended range of applicability and accuracy. Our work down this line started in papers I and II (see page xi), which set out to investigate

- if there are some global $\{\mu, \beta\}$ pairs that would yield even more accurate LCs than PBEsol (on average);

- what kind of $\{\mu, \beta\}$ pairs would be needed to reproduce the experimental LC for several different bulk metals; and
- how to possibly overcome the GGA level LC "accuracy limitation" described above.

In paper I, the goodness of $\{\mu, \beta\}$ pairs were judged by performing a two-dimensional $\{\mu, \beta\}$ scan for seven bulk metals and monitoring the relative error between the calculated equilibrium LCs and the experimental ones. Mathematically, finding $\{\mu, \beta\}$ pairs of lowest error can be cast into a form of a minimization problem by defining some $\{\mu, \beta\}$ dependent cost function, which is to be minimized. In paper I the cost function was

$$C(\mu, \beta) = \sum_i \left[\frac{w_i(\mu, \beta)}{w_i(\text{expt})} - 1 \right]^2, \tag{3.31}$$

where i is an index running over the seven selected metals and $w = (3V/4\pi)^{1/3}$ is the Wigner-Seitz radius, the radius of a sphere with the same volume as the unit cell V.

In line with the anticipated limitations of the GGA level, it was found that no global $\{\mu, \beta\}$ pair exists, which would yield accurate LCs across the periodic table. However, it was noticed that each element has "local" $\{\mu, \beta\}$ pairs, which exactly reproduce the experimental LC. In fact, each element has an infinite amount of such pairs and they form continuous lines in $\{\mu, \beta\}$ space. The best performing global $\{\mu, \beta\}$ pair of paper I was found by minimizing the cost function using BOBYQA [83], a derivative-free black-box[10] optimization algorithm. The best $\{\mu, \beta\}$ pair, $\{0.151990, 0.230019\}$, is not a significant improvement over PBEsol.

A similar two-dimensional $\{\mu, \kappa\}$ scan with β fixed to the LDA linear response value $3\mu/\pi^2$ was performed by Fabiano et al. [81]. They observed that PBEsol is nearly the global minimum in average LC error for a test set of six solids. In paper II we arrived at the same conclusion through a different route. Similarly to paper I the "best local" (henceforth "optimal") $\{\mu, \beta\}$ pairs were sought for 25 elemental bulk metals, but this time also the goodness of the calculated bulk modulus (w.r.t. experimental bulk modulus) was taken into account in the cost function. Volume and bulk modulus together provide two constraints, which means a unique optimal $\{\mu, \beta\}$ pair can be found for each element. The result of Fabiano et al. is

[10] The calculation of $C(\mu, \beta)$ for given μ and β involved calculating the total energy for several w using EMTO Green's function DFT code and then extracting the equilibrium w using an equation of state fit. Direct information about the $\partial C/\partial\mu$ and $\partial C/\partial\beta$ is thus not available.

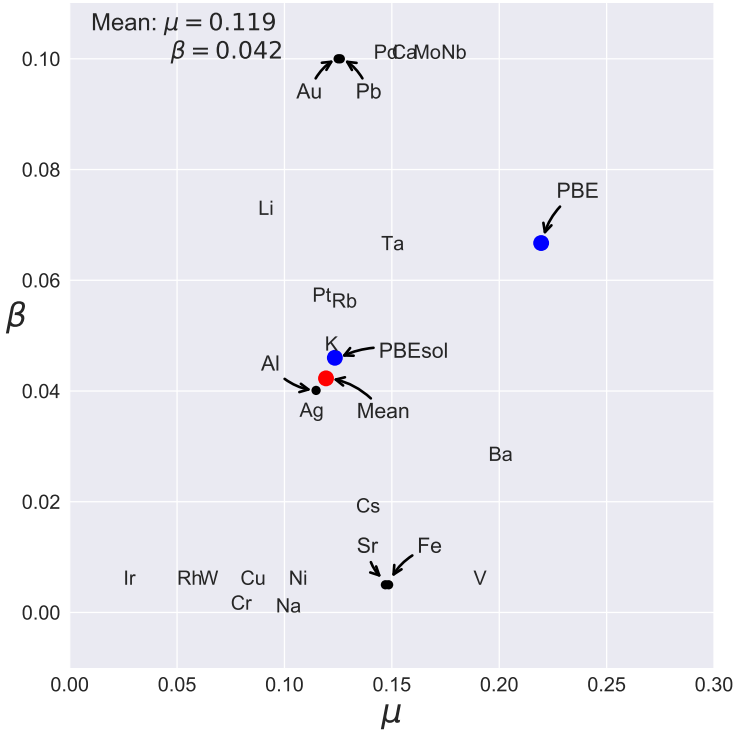

FIGURE 3.2: The average of optimal μ and β values.

now recovered, if one is to compute the average of the calculated optimal μ and β to find that these average values are very close to PBEsol μ and β. The optimal $\{\mu, \beta\}$ pairs and their average are presented in Fig. 3.2 and listed in a table in paper II.

The mechanism by which a GGA yields a particular equilibrium volume for a given solid has been investigated in earlier papers. One might expect the equilibrium volume of solids to be determined by the density in the region between the atoms, which region is called the interstitial region. But earlier studies have shown that equilibrium volume is determined in a deeper region, located between the core of the atom and the interstitial region, where core electrons interact with the valence electrons [64, 84–87]. We call this important region the core-valence overlap region (CVOR).

So, in order to analyze the question of why one functional yields better LCs than another, we focus on the CVOR. With the aid of non self-consistent treatment to remove all effects except those of XC, it can be shown that

the equilibrium LC is determined by the steepness of the XC energy volume derivative curve $\partial E_{\text{XC}}/\partial V$ [87]. Non self-consistency means that the electron density is first converged using some XC functional A, and the total energy is then evaluated with the target functional B using the "wrong" density to yield equilibrium quantities for functional B. For LCs self-consistency effects are very small and the non self-consistent treatment does not introduce additional errors.

The study of $\partial E_{\text{XC}}/\partial V$ leads to the identification of CVOR as the crucial area w.r.t. LCs. On one hand, most of the XC energy comes from near the atomic core, where the electron density is the highest. However, the core density hardly changes when the lattice is squeezed or expanded, so the effect of the core region on the $\partial E_{\text{XC}}/\partial V$ curve vanishes. On the other hand, in the interstitial region s is close to zero and GGAs are reduced to LDA. The effect from the interstitial region $\partial E_{\text{XC}}/\partial V$ is thus the same for all GGAs and therefore does not contribute to differences in LCs between functionals. What remains as the "active" region is the CVOR. For bulk metals the CVOR is typically located within $0.5 \leq s \leq 2$ and $0.5 \leq r_s \leq 3$. Figure 3.3 shows the approximate locations of V and Cu CVORs in s vs. r_s space. One technique for finding the CVOR is by defining a subsystem functional $E_{\text{XC}} = (1-\theta(r))E_{\text{XC}}^{\text{LDA}} + \theta(r)E_{\text{XC}}^{\text{PBE}}$, where $\theta(r)$ is a Heavyside step-function and r is atomic site centered radius parameter. By calculating the volume with increasing values of r, it is possible to chart the part of space where LDA volume starts turning into PBE volume.

The identity of a GGA is completely characterized by its total XC enhancement factor F_{XC} defined by Eq. (3.22). Since on the GGA level F_{XC} only depends on two variables, r_s and s, it is very useful to draw the F_{XC} as a two-dimensional map in s vs. r_s space. The shape of such a map then contains all the information about a particular GGA, at a glance. The F_{XC} maps of LDA and eleven GGAs are drawn in Fig. 3.4.

We can analyze the F_{XC} maps in greater detail in order to understand why the optimal $\{\mu, \beta\}$ pairs of a given element in Fig 3.2 lead to a good LC and bulk modulus for that particular element. After all, the "map" picture provides a very useful connection between a GGA and the kind of LCs the GGA will yield. Papers II and V, and Ref. [87] consider the different contributions to $\partial E_{\text{XC}}/\partial V$, when the volume derivation is carried out in Eq. (3.22):

$$\frac{\partial E_{\text{XC}}}{\partial V} = A\left(\int_{\text{CVOR}} \frac{4}{r_s^5}\frac{dr_s}{dV}F_{\text{XC}}\,d\mathbf{r} - \int_{\text{CVOR}} \frac{1}{r_s^4}\frac{dF_{\text{XC}}}{dr_s}\frac{dr_s}{dV}\,d\mathbf{r} - \int_{\text{CVOR}} \frac{1}{r_s^4}\frac{dF_{\text{XC}}}{ds}\frac{ds}{dV}\,d\mathbf{r}\right), \tag{3.32}$$

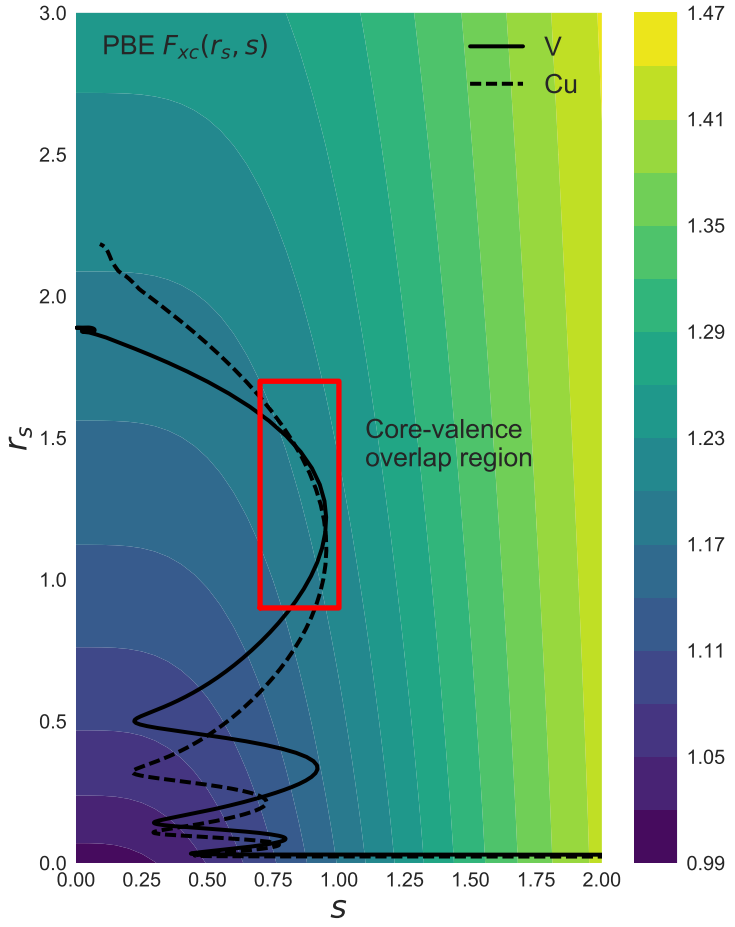

FIGURE 3.3: The s vs. r_s of V and Cu overlaying the PBE XC enhancement factor. The location of the core-valence overlap region (CVOR) is roughly sketched using a red rectangle.

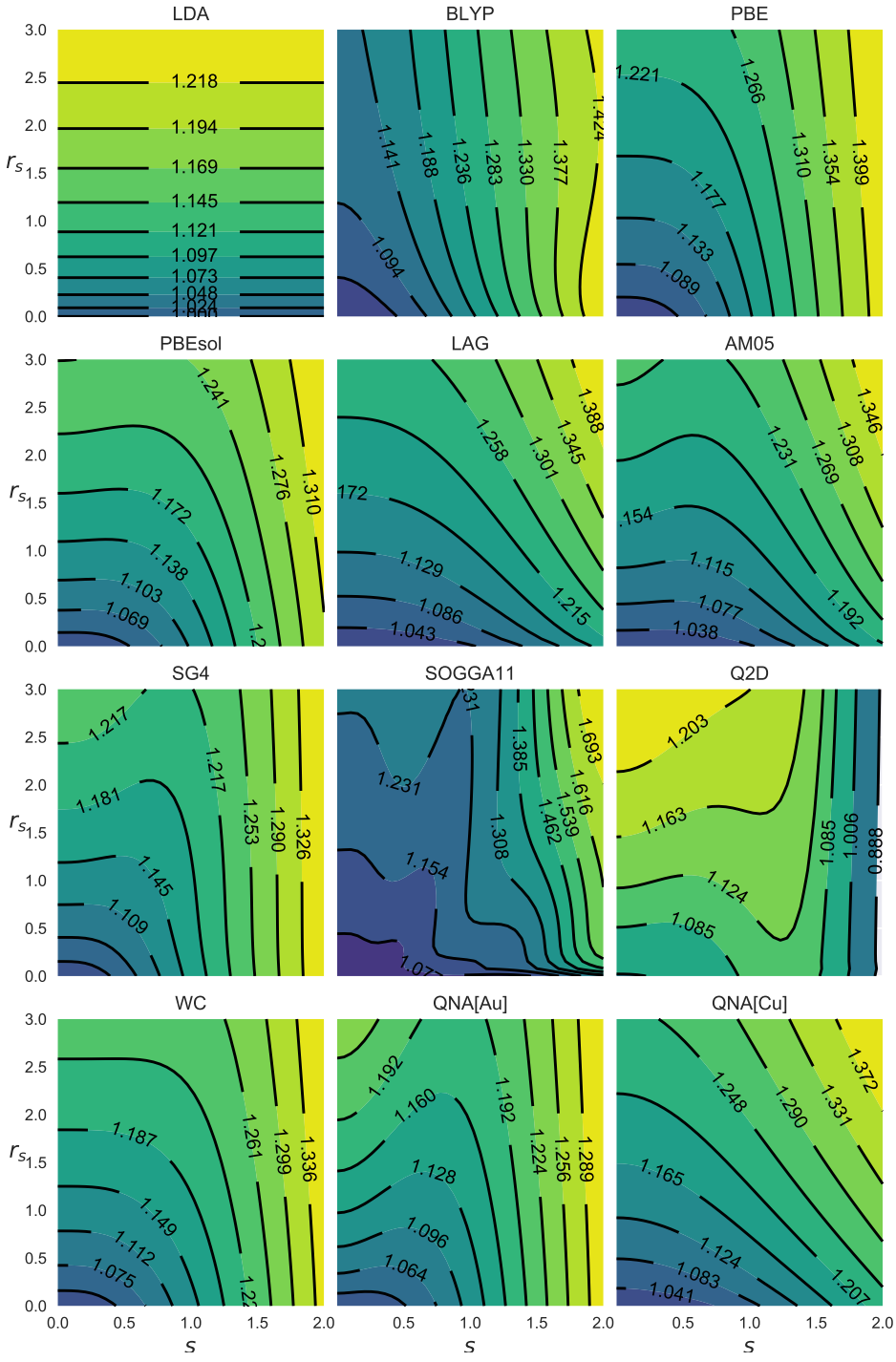

FIGURE 3.4: F_{XC} maps of various functionals.

where $A = (3/4)(3/\pi)^{1/3}[3/(4\pi)]^{4/3}$. If non self-consistent treatment is used in the evaluation of the integrals of Eq. (3.32), then r_s, s, and their derivatives dr_s/dV and ds/dV are fixed and differences between functionals only come from the three remaining components F_{XC} (see Fig. 3.4), dF_{XC}/ds (Fig. A.1 in Appendix A), and dF_{XC}/dr_s (Fig. A.2 in Appendix A).

The "competition" of the three integral terms in Eq. (3.32) determines what kind of LCs a given functional yields. The first integral creates the largest contribution and it is positive in sign. The second and third integrals are negative and generally one to two orders of magnitude weaker than the first one. It turns out [87] that the values of the first two integrals are relatively similar between different functionals, which means that differences mostly arise from the last integral, which contains the dF_{XC}/ds term.

To illustrate this competition we shall consider the well-known trend of LDA vs. PBE LCs. For LDA, by definition, $dF_{\text{XC}}/ds \equiv 0$, meaning the first integral will dominate, leading to a steep $\partial E_{\text{XC}}/\partial V$ curve and small lattice constants. For PBE dF_{XC}/ds is significant, as can be seen from Fig. A.1. As a result, PBE volumes will be large because a considerable portion of the first term in Eq. (3.32) is canceled by the third term.

The above analysis was expanded in paper II to explain the differences in bulk moduli between different functionals. We studied how calculating the bulk modulus using different $\{\mu, \beta\}$ pairs changes its value. The biggest effect comes from the volume effect, which means that XC functionals that predict small LCs automatically tend to predict large bulk moduli and vice versa.

It should be noted that LCs can be analyzed from other viewpoints as well. One can construct a deeper analysis for the LDA/PBE example using the XC holes of LDA and PBE [24]. The LDA hole is too shallow and widespread, leading to underestimated XC energy and overbinding. PBE hole, however, is much deeper, which makes PBE LCs larger in comparison. Yet another way of thinking about underestimated LDA LCs is the fact that LDA is exact for UEG and therefore favors ground states whose densities are more homogeneous than not. Since s tends to increase as a function of volume, small volumes lead to more homogeneous densities. PBE has a tendency to overcorrect with the gradients, so PBE favors inhomogeneous ground states, which have larger volumes.

Analysing the CVOR for several transition metals makes it clear why GGA level has to have a certain lower limit to the average error in LCs. The only information a GGA functional has about the system in question are r_s and s, and this is not enough to "distinguish" all elements from one

another. Figure 3.3 displays spherically averaged s vs. r_s curves of V and Cu for their respective PBE equilibrium LC. These curves were obtained by outputting r_s and s as a function of atomic radius from a DFT code and then plotting them by using the radius as a common index. It can be seen that within the important CVOR the curves have an extreme overlap. So, in the eyes of a GGA functional these two elements seem more or less identical; the GGA cannot really tell if it is calculating V or Cu. This is a problem because the LCs of V and Cu tend to show qualitatively different trends w.r.t. experimental data. For example, PBE underestimates the LC of V, but overestimates it for Cu. The harsh reality is that it is practically impossible to design a GGA F_{XC} map that would be able to yield accurate volumes for both elements simultaneously.

To summarize the section up to this point, accurate volumes and LCs are very important in solid state physics and one who needs accurate LCs in his/her studies might hit a dead end at the GGA level. To proceed, one option is always to move up in the Jacob's ladder and try some of the more sophisticated, beyond-GGA approaches. Fourth rung "hybrid" and "hyper" functionals, which use the Hartree-Fock exchange expression to describe exchange effects much more accurately, have been shown to be able to rectify some of the pressing volume issues of the GGA level [88]. Be that as it may, employing hybrid functionals is not always a valid option. Firstly, hybrids have some acute shortcomings in metallic solid state calculations [89]. Secondly, the biggest issue with hybrids is that they are computationally much heavier that GGAs, and so their use in large-scale projects is currently not very feasible[11]. We would prefer staying on the GGA level and in order to accomplish that we propose a new SF approximation in this thesis (see paper I).

We call it the *quasi-non-uniform* gradient-level approximation (QNA) and to our knowledge it is the only way of reconciling the GGA level volume dilemma whilst still remaining on the GGA level. Since no one "uniform" GGA can accurately describe volumes across the periodic table, we construct a "quasi-non-uniform" GGA by splitting the insurmountable volume problem into tractable subproblems. The basic idea is to use a different SF for each element and every SF is designed to describe accurately the solid bulk equation of state (EOS) solids of its associated element. The cornerstone of our approach is the fortuitous fact that the source of error in LCs is localized around the atomic cores inside the CVOR. This allows the space to be divided into atom-centered regions, like in Fig. 3.5, in such a

[11] This picture will of course change as a function of available processing power: General purpose graphical processing units (GPUs) can significantly speed up hybrid functional calculations [90, 91].

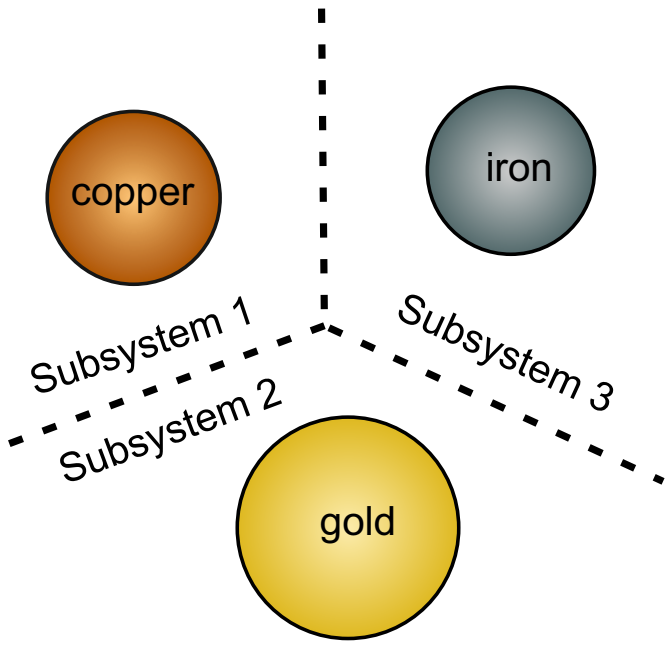

FIGURE 3.5: Division of space into subsystems in QNA.

way that every atomic site and its corresponding CVOR in the whole system is one subsystem. The individual SFs are connected by the interstitial region, where the electron density is quite homogeneous ($s \approx 0$). The interstitial region is therefore represented quite well by LDA and a relevant condition for the SFs is that they always reduce to LDA in the interstitial region. Using the PBE framework as a "template" for the SFs ensures that the interstitial condition is automatically fulfilled. Furthermore, the PBE form allows the SFs to be straightforwardly designed by modifying the values of μ and β.

For each element we can define an "optimal" subsystem functional, which is one that mimics the experimentally observed $0\,\mathrm{K}$ solid bulk EOS as closely as possible. These optimal SFs are constructed by finding optimal $\{\mu, \beta\}$ pairs, which yield the smallest possible error in the calculated LC and bulk modulus w.r.t. experiment. Paper II presents such optimal parameters for various transition metals, which were obtained by minimizing the combined error in LC and bulk modulus. Mathematically QNA can be

expressed as

$$E_{\mathrm{XC}}^{\mathrm{QNA}}[n] = \sum_q \int_{\Omega_q} \varepsilon_{\mathrm{X}}^{\mathrm{LDA}}([n], \mathbf{r}) F_{\mathrm{XC}}^{\mathrm{opt}_q}(r_s, s; \mu_q, \beta_q)\, d\mathbf{r}, \tag{3.33}$$

where $F_{\mathrm{XC}}^{\mathrm{opt}_q}$ is the PBE-like XC enhancement factor using the optimized μ_q and β_q of some element occupying atomic site q. Total system volume is divided into subdomains Ω_q that surround each atomic site q. One major practical challenge when implementing QNA lies in the choice of exactly how to divide the space into the Ω_q regions. In the GPAW [92, 93] implementation of QNA atom-centered Voronoi cells can be used (see Appendix B), whereas the EMTO [80] implementation is easier because densities at each atomic site are automatically separated from each other.

We will close this section with a list of pros and cons of the QNA approximation. The advantages of QNA are:

- 👍 Accurate description of elements' volumes in most cases improves the description of alloys. Especially interesting is the fact that formation energies of binary alloys are significantly improved compared to other GGAs.
- 👍 Empirical functionals, which often do not fulfill exact conditions, tend to have wildly oscillatory enhancement factors (for an example, see the F_{XC} map of SOGGA11 in Fig. 3.4). The oscillatory behavior make empirical functionals unreliable outside of the range of systems they were designed for. By relying on the PBE form QNA eschews problematic oscillations, because all the exact conditions of PBE (that make PBE so accurate and reliable) are retained, despite fitting the optimal parameters. In this sense QNA can be seen as a *semiempirical* functional, which aim to combine the desirable features of constraint-based and empirical functionals into one approach. It should also be noted that the level of empiricism can be lowered by employing known XC functionals, such as LDA, PBE, PBEsol, and AM05, instead of the empirically LC-optimized ones.

The disadvantages of QNA are:

- 👎 Some other properties, such as surface energies and elastic constants, are not improved.
- 👎 The guidelines of SFA are not strictly followed because no theoretically sound model systems are used to derive the optimal parameters for each element. Currently the optimal parameters are determined by empirical fitting, which is intellectually dissatisfying and disliked

by many in the DFT community. In future work it might be possible to obtain the optimal parameters from model systems. The most obvious choice for model systems would be isolated atoms, since the individual atoms that make up the system are the subsystems. Perhaps an approach similar to the way the SG4 functional was constructed [70, 94] would be a good starting point.

- 👎 Due to its construction it is more difficult to implement in existing DFT codes than a standard GGA. For example, the Hellman-Feynman force expression gains an extra term not present in forces of conventional GGAs (see Appendix B).

4 Orbital-Free Density Functional Theory

4.1 Background

In day-to-day speak "density functional theory" is synonymous with the Kohn-Sham formulation of DFT. In addition to KS-DFT there exists another branch of DFT, called *orbital-free DFT* (OF-DFT)[1], but Kohn-Sham is the engine with which nearly all practical DFT papers are published, and a far smaller group of people are reporting practically useful OF-DFT calculations, of which Ref. [96] is an example.

In fact, OF-DFT is the original and "pure" DFT and the idea was first published by Thomas and Fermi, decades before Hohenberg, Kohn, and Sham published their groundbreaking papers. Pureness here refers to the fact that every energy contribution in the TF model of Eq. (2.5) can be computed directly from the density; we recall from Chapter 2 that the TF model makes no use of orbitals of any kind. We also recall that the kinetic energy of the electrons is really difficult to approximate as an explicit functional of the density, which is why Kohn-Sham methodology introduces fictitious one-electron orbitals and a much more accurate implicit kinetic energy functional.

With orbitals KS-DFT elegantly solves the bottleneck of OF-DFT, which is its unimpressive accuracy in practical calculations. But the orbitals actually create another bottleneck, which is not an issue in OF-DFT since there is no orbitals. While KS-DFT has a very good speed to accuracy ratio, the orbitals still make it too slow for the simulation of systems bigger than hundreds of atoms. Due to the costly matrix diagonalization step needed when solving the KS orbital problem of Eq. (2.6), KS-DFT is slowed down by its $O(N^3)$ *scaling*, which means the computational time grows at least cubically[2] as a function of the number of atoms N in the system.

[1] Although a semantically more correct name for the approach would be *one-orbital* DFT [95].

[2] Linearly scaling KS-DFT approaches have been developed, but they have their own difficulties [97].

In contrast, OF-DFT scales only linearly and much bigger systems with millions of atoms can be simulated in a reasonable time [98]. But most of this vast speed benefit goes to waste for as long as the kinetic energy approximations of OF-DFT remain too crude for useful calculations. Consequently, much of the research effort in the OF-DFT field is directed towards developing more accurate kinetic energy functionals and improved numerical algorithms. In the meantime, while we wait for OF-DFT to mature, classical methods are often used to calculate very big systems, such as proteins. An efficient implementation of classical or "non ab initio" molecular dynamics (MD) method scales linearly, just like OF-DFT. One could therefore, in principle, replace the empirical, parameterized MD potentials by an OF-DFT solver for improved accuracy without a speed loss. But as of now OF-DFT is not, in general, ready to replace classical MD potentials, which have a long history and are highly tuned.

If the "divine" kinetic energy functional was found, OF-DFT might very well steal the title of *de facto* DFT, and DFT would have come full circle, returning back to its roots, which are in the orbital-free TF model. But of course only time can tell how much "market share" OF-DFT will be able to grab from KS-DFT and at which pace.

4.2 Pauli Potential

Total energy in OF-DFT is still given by Eq. (2.2):

$$E[n] = F[n] + E_{\text{ext}}[n] = T_{\text{S}}[n] + E_{\text{H}}[n] + E_{\text{XC}}[n] + E_{\text{ext}}[n]. \tag{4.1}$$

It is worth noting that not all familiar features of KS formalism are abrogated in OF-DFT; the non-interacting KE $T_{\text{S}}[n]$ is present and the XC term is used the same way as it is used in KS-DFT. There is nothing stopping one from trying other decompositions, but that would mean abandoning familiar XC functionals which are a result of decades of research; retaining known XC functionals and trying to approximate $T_{\text{S}}[n]$ seems much more viable than a complete overhaul of the way we think about DFT [95, 99].

Minimization of the total energy leads to the Euler equation

$$\frac{\delta T_{\text{S}}[n]}{\delta n} + V_{\text{KS}} = \mu, \tag{4.2}$$

where μ is a Lagrange multiplier and also the chemical potential. It can be shown that μ equals the eigenvalue of the highest-lying KS orbital ($\mu = \epsilon^{\text{KS}}_{\text{max}}$) and that it determines (or is determined by) the asymptotic decay of

the density [100]:

$$n(\mathbf{r} \to \infty) \sim e^{-2\sqrt{-2\mu}\mathbf{r}}. \tag{4.3}$$

Instead of expressing T_{S} and its functional derivative $\delta T_{\text{S}}/\delta n$ as functions of orbitals, OF-DFT aims to approximate it somehow. The earliest and simplest approximation comes from the TF model of Eq. (2.5):

$$T_{\text{S}} \approx T_{\text{TF}} = C_{\text{F}} \int n(\mathbf{r})^{5/3}\, d\mathbf{r}. \tag{4.4}$$

Since T_{TF} is really not a very good approximation, it is customary, instead, to decompose T_{S} into a sum of two terms:

$$T_{\text{S}} = T_{\text{W}} + T_{\text{P}} \geq 0. \tag{4.5}$$

The first term is known as the von Weizsäcker KE functional [101]

$$T_{\text{W}} = \frac{1}{8} \int \frac{|\nabla n|^2}{n}\, d\mathbf{r} \geq 0. \tag{4.6}$$

The von Weizsäcker term has the following important features: it gives the lower bound to the KS kinetic energy,

$$T_{\text{W}} \leq T_{\text{S}}, \tag{4.7}$$

and also gives the exact kinetic energy for one and two-electron systems [95]. The other term is called the Pauli kinetic energy and it is always non-negative, $T_{\text{P}} \geq 0$, which can be seen from Eqs. (4.5) and (4.7). Both kinetic energies can be calculated from their associated kinetic energy densities:

$$T_{\text{W}} = \int t_{\text{W}}(\mathbf{r})\, d\mathbf{r}, \quad T_{\text{P}} = \int t_{\text{P}}(\mathbf{r})\, d\mathbf{r}, \tag{4.8}$$

where

$$t_{\text{W}} = \frac{1}{8} \frac{|\nabla n|^2}{n}. \tag{4.9}$$

The composition of Eq. (4.5) leads to the well-known Schrödinger-like form of the Euler equation [100], which is what is often used in practical calculations. Another way of performing OF-DFT calculations is by direct minimization of Eq. (4.1). The first step is to compute the functional derivative $\delta T_{\text{S}}/\delta n$. After using the rules of functional derivation and some algebra we get

$$\frac{\delta T_{\text{W}}}{\delta n} = \frac{1}{\sqrt{n}} \left(-\frac{1}{2} \nabla^2 \right) \sqrt{n}. \tag{4.10}$$

The functional derivative of the Pauli kinetic energy is by definition just

$$V_{\mathrm{P}} \equiv \frac{\delta T_{\mathrm{P}}}{\delta n}, \tag{4.11}$$

because the exact form of it is unknown.

Inserting Eqs. (4.10) and (4.11) into Eq. (4.2) leads to

$$\left[-\frac{1}{2}\nabla^2 + V_{\mathrm{P}} + V_{\mathrm{KS}}\right]\sqrt{n(\mathbf{r})} = \mu\sqrt{n(\mathbf{r})}. \tag{4.12}$$

Equation (4.12) is the OF-DFT equivalent of KS equations in KS-DFT. Its form is identical to that of a KS equation except an additional potential term V_{P} has appeared. Instead of a one-electron wavefunction the solution is the square root of the total density. In OF-DFT the entire solution is thereby always obtained from a single equation rather than a set of one-electron equations, which is what makes OF-DFT much faster than KS-DFT at large electron numbers. The solution $\sqrt{n(\mathbf{r})}$ is positive for all $\mathbf{r}$ and so it is nodeless unlike KS orbitals. In practice the extra term V_{P} has to be approximated somehow and then n, V_{KS}, and μ in Eq. (4.12) are iterated into convergence. Thanks to its similarity with a KS equation Eq. (4.12) can be solved quite straightforwardly using existing KS solvers, but convergence issues and other numerical troubles have been reported in the literature [102]. Later work has revealed that some of these issues can be resolved by careful implementations [103]. In any case the best practices of solving Eq. (4.12) are not nearly as well understood as they are in the KS case. Also the currently existing OF-DFT KE approximations cannot compete with KS T_{S} in accuracy. For a comprehensive list of different OF-DFT KE approximations the reader is referred to Ref. [104].

The term V_{P} is called the Pauli potential, named after the Pauli exclusion principle [105]. Named so because if V_{P} was set to zero, the ground state solution would be a quasi-bosonic one where all the electrons were packed into a single orbital and the quasi-bosonic kinetic energy would be given exactly by T_{W}. It should be noted that the $V_{\mathrm{P}} = 0$ solution would not be exactly bosonic because there is some Pauli repulsion also in the exchange term. However, the quasi-bosonic solution can be expected to be very close to the fully bosonic one because the kinetic term after all is the dominant component of the total energy. The fact that electrons are fermions – and therefore have to obey the Pauli exclusion principle – is enforced by a non-zero V_{P}. In lieu of KS orbitals it is the responsibility of V_{P} to give rise to atomic shell structure. That is a heavy burden because one of the biggest challenges in OF-DFT is the difficulty of recreating KS-like shell structure

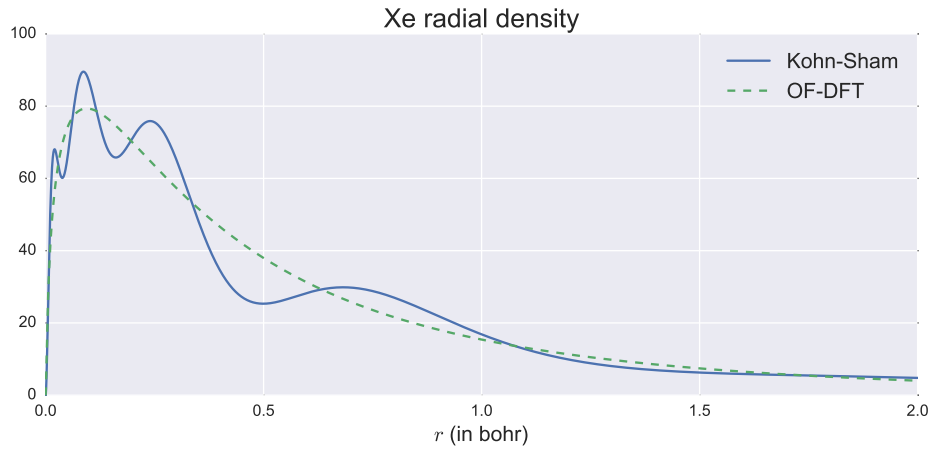

FIGURE 4.1: Self-consistently calculated KS and OF-DFT densities of Xe atom.

without using KS-orbitals. The kinetic energy and shell structure are very "orbital-like" by nature, which is why it has proven so difficult to approximate the kinetic energy accurately in OF-DFT. Figure 4.1, which compares KS and OF-DFT densities of the Xe atom, illustrates this difficulty. The OF-DFT density was calculated using a self-developed numerical atomic OF-DFT code with a kinetic energy approximation $T_{\mathrm{S}} = T_{\mathrm{TF}} + 1/5T_{\mathrm{W}}$ and LDA for XC effects. It can be seen that the realistic shell structure that KS-DFT produces with ease is completely missing in the OF-DFT solution. However, OF-DFT does produce an accurate average representation of the density and it has been shown that the "$T_{\mathrm{TF}} + 1/5T_{\mathrm{W}}$" approximation yields rather accurate total energies for atoms [106].

Figure 4.2 shows the V_{P} of spherically symmetric Be and Xe atoms calculated from converged LDA KS orbitals using Eq. (16)[3] of Ref. [107]. Note that for Xe a logarithmic scale is used. Close to the nucleus V_{P} is large and its effect is to push "extra" electrons to outer shells once an inner shell becomes fully occupied. One of the defining features of Pauli potential is its often oscillatory behavior, which correlates with the shell structure it is responsible for giving rise to. In the atomic tail region, where only the outermost orbital is left, $V_{\mathrm{P}} \equiv 0$ and T_{W} becomes exact. We also notice that V_{P}

[3] $V_{\mathrm{P}} = \sum_{i=1}^{M} \nabla(\psi_i n^{-1/2})^* \cdot \nabla(\psi_i n^{-1/2}) + \sum_{i=1}^{M}(\mu - \epsilon_i) 2\psi_i^* \psi_i n^{-1}$. Calculating V_{P} from this equation tends to be numerically more stable than inverting the Euler equation.

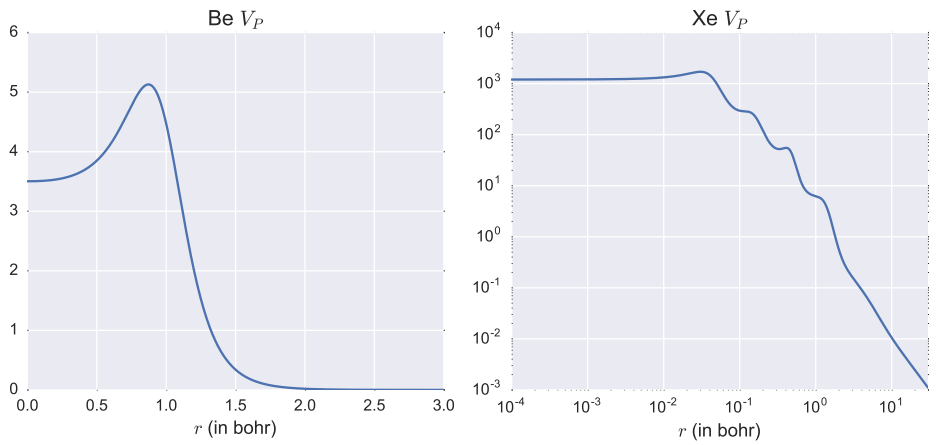

FIGURE 4.2: Pauli potentials of Be and Xe atoms.

is positive everywhere, and it can be shown [107] that

$$V_{\mathrm{P}}(\mathbf{r}) \geq 0 \;\; \forall \mathbf{r} \tag{4.13}$$

is a rigorous constraint for the exact V_{P}.

Beyond the characteristics listed above, the Pauli potential is not very well understood at the moment, and can be calculated exactly only for some simple model systems [108, 109] (in paper IV we compute self-consistently the exact Pauli potential of Be atom). In analogy to XC functional development it pays dividends to study and derive exact constraints for V_{P} to guide the approximation development process. For example, in Ref. [110] the $r \to \infty$ asymptotic expression of the Pauli KE density t_{P} has been studied and used to construct a new meta-GGA XC approximation. Especially the non-negativity constraints of T_{P} and V_{P} have proven to be very useful [102] (and references therein).

In paper III we derive a nuclear cusp conditions for the exact V_{P} of spherically symmetric Coulombic systems, such as noble gas atoms. These cusp conditions describe the asymptotic behavior of the exact V_{P} near an atomic nucleus ($r \to 0$). To summarize the derivation we start by solving Eq. (4.12) for V_{P}:

$$V_{\mathrm{P}} = \mu - V_{\mathrm{KS}} + \frac{1}{2}\frac{\nabla^2\sqrt{n}}{\sqrt{n}} \tag{4.14}$$

Since we are interested in the $r \to 0$ region we expand V_{KS} as [111–115]

$$V_{\text{KS}} = -\frac{Z}{r} + A + Br + Cr^2 + \dots, \tag{4.15}$$

where A, B, and C are constants. In order to obtain an expansion for $n(r \to 0)$ we first note that KS-orbitals of a spherically symmetric system in Eq. (4.46) can be expanded as

$$P_n = \sum_{lm} c_{nlm}^{(0)} r^{l+1} + c_{nlm}^{(1)} r^{l+2} + c_{nlm}^{(2)} r^{l+3} + \dots, \tag{4.16}$$

which follows from the fact that a KS-orbital ψ_n in general can be expanded as [112–114]

$$\psi_n = R_n Y_{lm} = \frac{P_n}{r} Y_{lm} = \sum_{lm} r^l (c_{nlm}^{(0)} + c_{nlm}^{(1)} r + c_{nlm}^{(2)} r^2 + \dots) Y_{lm}(\Omega), \tag{4.17}$$

where Y_{lm} are spherical harmonics. From Eq. (4.16) it follows that

$$\begin{aligned} P_n'' = \sum_{lm} & l(l+1) c_{nlm}^{(0)} r^{l-1} + (l+1)(l+2) c_{nlm}^{(1)} r^l \\ & + (l+2)(l+3) c_{nlm}^{(2)} r^{l+1} + \dots, \end{aligned} \tag{4.18}$$

where the $'$-notation refers to radial $\partial/\partial r$ derivatives. Inserting Eqs. (4.15), (4.16) and (4.18) into Eq. (4.46) and equating the coefficients of r^{l-1}, r^l, r^{l+1}, and r^{l+2} terms separately to zero we obtain the following set of equations:

$$Z c_{nlm}^{(0)} + (l+1) c_{nlm}^{(1)} = 0, \tag{4.19}$$

$$(\epsilon_n - A) c_{nlm}^{(0)} + Z c_{nlm}^{(1)} + (2l+3) c_{nlm}^{(2)} = 0, \tag{4.20}$$

$$-B c_{nlm}^{(0)} + (\epsilon_n - A) c_{nlm}^{(1)} + Z c_{nlm}^{(2)} + 3(l+2) c_{nlm}^{(3)} = 0. \tag{4.21}$$

Eqs. (4.19)–(4.21) can be solved to obtain the following relations between the $c_{nlm}^{(j)}$ parameters:

$$c_{nlm}^{(1)} = -\frac{Z}{l+1} c_{nlm}^{(0)}, \tag{4.22}$$

$$c_{nlm}^{(2)} = \frac{1}{2l+3} \left[\frac{Z^2}{l+1} - \epsilon_n + A \right] c_{nlm}^{(0)}, \tag{4.23}$$

$$c_{nlm}^{(3)} = -\frac{Z}{3(l+1)(l+2)} \left\{ (3l+4) c_{nlm}^{(2)} - \left[\frac{Z^2}{l+1} + \frac{(l+1)B}{Z} \right] c_{nlm}^{(0)} \right\}. \tag{4.24}$$

Assuming a spherically averaged density and using

$$\int_{\varphi}\int_{\theta} Y_{lm}Y^{*}_{l'm'}d\Omega = \delta_{ll'}\delta_{mm'} \tag{4.25}$$

together with substituting the parameters of Eqs. (4.22)–(4.24) into Eq. (4.17) and calculating the density $n = \sum_{n=1}^{N} |\psi_n|^2$ gives [114, 115]

$$n(r) = n(0)\left[(Zr-1)^2 + \frac{1}{3}\left(Z^3+B\right)r^3\right] + \zeta\left(r^2 - \frac{5}{3}Zr^3\right) + \xi\left(r^2 - Zr^3\right) + \mathcal{O}(r^4), \tag{4.26}$$

where

$$n(0) = \frac{1}{4\pi}\sum_{n}\left(c^{(0)}_{n00}\right)^2, \tag{4.27}$$

$$\zeta = \frac{1}{2\pi}\sum_{n} c^{(0)}_{n00}c^{(2)}_{n00}, \tag{4.28}$$

$$\xi = \frac{1}{4\pi}\sum_{n}\sum_{m=-1}^{m=1}\left(c^{(0)}_{n1m}\right)^2. \tag{4.29}$$

The derivatives of $n(r)$ become

$$\begin{aligned} n'(r) =& 2Zn(0)[Zr-1] + n(0)[Z^3+B]r^2 + 2\zeta r \\ & -5Z\zeta r^2 + 2\xi r - 3Z\xi r^2, \end{aligned} \tag{4.30}$$

$$n''(r) = 2Z^2n(0) + 2n(0)[Z^3+B]r + 2\zeta - 10Z\zeta r + 2\xi - 6Z\xi r, \tag{4.31}$$

$$n'''(r) = 2n(0)[Z^3+B] - 10Z\zeta - 6Z\xi. \tag{4.32}$$

At $r = 0$ the derivatives have the values

$$n'(0) = -2Zn(0), \tag{4.33}$$

$$n''(0) = 2Z^2n(0) + 2\zeta + 2\xi, \tag{4.34}$$

$$n''(0) = 2n(0)[Z^3+B] - 10Z\zeta - 6Z\xi. \tag{4.35}$$

By inserting Eqs. (4.26), (4.30) and (4.31) into the kinetic energy term $\nabla^2\sqrt{n}/(2\sqrt{n})$ of Eq. (4.14) and expanding it as a power series we get

$$\begin{aligned}\frac{1}{2}\frac{\nabla^2\sqrt{n}}{\sqrt{n}} &= \frac{1}{4}\frac{n''}{n} - \frac{1}{8}\left(\frac{n'}{n}\right)^2 + \frac{n'}{2rn} \\ &= -\frac{Z}{r} - Z^2 + \frac{3}{2}\frac{\zeta+\xi}{n(0)} + \left(B + \frac{2Z\xi}{n(0)}\right)r + \mathcal{O}(r^2). \end{aligned} \tag{4.36}$$

When Eq. (4.36) is inserted into Eq. (4.14) V_{P} takes the form

$$V_{\text{P}} = \mu - Z^2 - V_{\text{H}}(0) - V_{\text{XC}}(0) + \frac{3}{2}\frac{\zeta+\xi}{n(0)} + \frac{2Z\xi}{n(0)}r + \mathcal{O}(r^2), \tag{4.37}$$

where we have utilized the fact that $A = V_{\text{H}}(0) + V_{\text{XC}}(0)$. It is readily seen that V_{P} and its derivative at the nucleus are

$$V_{\text{P}}(0) = \mu - Z^2 - V_{\text{H}}(0) - V_{\text{XC}}(0) + \frac{3}{2}\frac{\zeta+\xi}{n(0)} \tag{4.38}$$

and

$$V'_{\text{P}}(0) = \frac{2Z\xi}{n(0)}. \tag{4.39}$$

When ζ and ξ are solved from Eqs. (4.33)–(4.35) and inserted into Eqs. (4.38) and (4.39) we arrive at the final result

$$V_{\text{P}}(0) = \mu - \frac{5}{2}Z^2 - V_{\text{H}}(0) - V_{\text{XC}}(0) + \frac{3}{4}\frac{n''(0)}{n(0)} \tag{4.40}$$

and

$$V'_{\text{P}}(0) = -6Z^3 - V'_{\text{H}}(0) - V'_{\text{XC}}(0) + \frac{5Zn''(0) + n'''(0)}{2n(0)}. \tag{4.41}$$

The above cusp equations afford us to make some interesting observations, which are similar to the ones drawn in Ref. [110]:

- The chemical potential μ is present in the expression of $V_{\text{P}}(0)$, which according to Eq. (4.3) reflects the difficult non-local character of V_{P}.
- In addition to s-type electrons, p-type electrons (specifically) make significant contributions to $V_{\text{P}}(0)$ and $V'_{\text{P}}(0)$. For example, Be atom only has s-type electrons and so it can be shown that for Be $V'_{\text{P}}(0) \equiv 0$ (see paper III for details).

Our cusp conditions are related to the well-known Kato cusp condition [116], which states

$$n'(0) = -2Zn(0). \tag{4.42}$$

The importance of the Kato cusp condition was allegedly first pointed out by E. B. Wilson [34, 114] at a conference in 1965: If the density is known, the cusps and their positions can be computed, which thanks to the Kato cusp condition will reveal the atomic numbers and the locations of the nuclei. Kato cusp condition demonstrates that the electron density does indeed contain all the information about the system. Equations (4.40) and (4.41) require the knowledge of $V_{\mathrm{H}}(0)$, $V_{\mathrm{XC}}(0)$, and their derivatives, but fortunately a lot about them is already known [114, 115, 117]. Therefore, our cusp conditions can be useful for assessing the accuracy of V_{P} approximations; if any approximation is to replicate the behavior of the exact V_{P} near the nucleus, it needs to be able respect the above cusp conditions.

4.3 Pauli Potential Differential Equation

From a practical viewpoint OF-DFT will remain mostly a curiosity for as long as V_{P} cannot be approximated adequately. Kohn and Sham conjured orbitals, which are able to give V_{P} (of the KS-system) exactly, but the speed benefit will be lost. Recently Nagy has developed a novel orbital-free approach, which can be used, in principle, to calculate the exact V_{P} without solving the set of KS equations [118–120]. This new approach is valid for spherically symmetric systems, and produces a differential equation for V_{P}, from which it can be solved. The OF-DFT problem is therefore now described by a set of two differential equations: the Euler equation (4.12) and the Pauli potential differential equation (PPDE). Much like the KS system, we avoid approximating V_{P}, but the cardinal distinction between the KS method and the PPDE method is that in the PPDE method the number of equations will always be two[4], regardless of the number of electrons the system consists of. The two-equation problem is more complicated than the standard one-equation OF-DFT formulation, but the hope is that an efficient way of solving the additional PPDE either exactly or approximately can be learned. If an efficient solution is possible, the PPDE method would place itself somewhere between OF-DFT and KS-DFT in terms of computational speed, but the accuracy of the PPDE method could be expected to be much greater than that of regular OF-DFT. As is the case with the Pauli potential itself, understanding the PPDE is in its early stages, and in this

[4]Which is in keeping with the OF-DFT philosophy of ∂(Number of equations) / ∂(Number of electrons) $\equiv 0$.

thesis we present an exact numerical solution of the PPDE for one simple model system, the Be atom (see paper IV and section 5.2).

The PPDE is derived using ensemble densities formalism of Nagy [118–120]. We will also need the so-called ensemble differential virial theorem of Ref. [119]. Virial theorem is a well-known concept in physics, which relates the (time-averaged) kinetic energy to the total potential energy of a system. Differential virial theorem (DVT), which was first developed by March and Young in 1959 [121], can be seen as a considerable generalization[5] of the customary virial theorem, as it provides a differential form of it, and as a generalization is more powerful. More specifically speaking, the DVT provides an exact relation between the Kohn-Sham effective potential, the electron density, and the kinetic energy density [122]. Applications of the DVT include recovering KS potentials from input densities [123] and derivation of exact constraints to be exploited in XC functional development [124]. The original DVT of March and Young is valid in one dimension. The March-Young version was first generalized to spherically symmetric systems by Nagy and March [125] and then to three dimensions by Holas and March [126]. The spherically symmetric Nagy-March DVT was generalized for spherically symmetric ensemble densities by Nagy [119].

Since we are dealing with spherically symmetric systems, it is convenient to introduce a one-dimentional radial electron density

$$\rho(r) = 4\pi r^2 n(r). \tag{4.43}$$

Inserting ρ into the Euler equation (4.12) turns it after some algebra into

$$-\frac{1}{2}\varphi'' + [V_{\text{KS}} + V_{\text{P}}]\,\varphi = \mu\varphi, \quad \varphi^2 = \rho. \tag{4.44}$$

The ensemble densities formalism replaces the usual ground-state density ρ by a more general quantity

$$\rho(\beta, \gamma, r) = \sum_i \lambda_i \omega_i(\beta, \gamma)\rho_i(r), \tag{4.45}$$

where $\rho_i(r) = P_i(r)^2$ is the amplitude of the spherically symmetric KS orbital i. The orbitals P_i are the solutions of the radial KS equations

$$-\frac{1}{2}P_i'' + \left[\frac{l_i(l_i+1)}{2r^2} + V_{\text{KS}}\right] P_i = \epsilon_i P_i, \tag{4.46}$$

[5] When integrated, the DVT gives back the usual integral virial theorem.

where l_i is the azimuthal quantum number of orbital i. λ_i is the occupation number of the KS orbital i and ω_i is a so-called weighting factor of ensemble member i. The ensemble density is therefore a linear combination of the occupied KS orbitals, but weighted with certain weight factors w_i. The extra dimensions β and γ are only present in the weight factors and they will be defined as

$$\omega_i(\beta,\gamma) = e^{\beta\epsilon_i - \gamma l_i(l_i+1)}. \tag{4.47}$$

Note that if all $\omega_i \equiv 0$, $\rho(\beta,\gamma,r)$ reduces to the usual KS ground state density. The ground state density can therefore be accessed through the special case $\beta = \gamma = 0$.

The ensemble densities presented here are connected to the concept of *ensemble density functional theory* [127, 128], which is one of the many ways of calculating excited states [55]. We use them as an auxiliary quantity in the derivation of the PPDE. Since the PPDE is to produce the exact V_{P} the orbital information of KS orbitals is encoded in the extra β and γ dimensions of $\rho(\beta,\gamma,r)$.

We follow Ref. [119] in order to obtain the PPDE. First it is important to notice that the KS density ($\beta = \gamma = 0$) and the generalized ensemble density are both solutions to the same Euler equation. This means that V_{KS} and μ have no β or γ dependence and in the equation pair

$$\frac{\delta T_{\text{S}}(0,0,r)}{\delta n(0,0,r)} + V_{\text{KS}} = \mu, \tag{4.48}$$

$$\frac{\delta T_{\text{S}}(\beta,\gamma,r)}{\delta n(\beta,\gamma,r)} + V_{\text{KS}} = \mu \tag{4.49}$$

V_{KS} and μ are the same in both equations. For V_{KS} the "sameness" can be shown by refering to the generalized Rayleigh-Ritz variational principle [127, 129]. For μ an argument can be made by writing Eq. (4.3) in the form

$$|\mu| = \frac{1}{8}\lim_{r\to\infty}\left[\frac{2}{r} - \frac{\rho'(\beta,\gamma,r)}{\rho(\beta,\gamma,r)}\right]^2. \tag{4.50}$$

Assuming the highest occupied KS orbital (HOMO) has no nodal plane and $V_{\text{KS}} + V_{\text{P}} \to 0$ when $r \to \infty$ (HOMO nodal planes make things more complicated [130]) Eq. (4.50) can be written in terms of the HOMO as

$$|\mu| \to \frac{1}{8}\lim_{r\to\infty}\left[\frac{2}{r} - \frac{\cancel{\lambda_{\text{HOMO}}\omega_{\text{HOMO}}(\beta,\gamma)}\rho'_{\text{HOMO}}(r)}{\cancel{\lambda_{\text{HOMO}}\omega_{\text{HOMO}}(\beta,\gamma)}\rho_{\text{HOMO}}(r)}\right]^2, \tag{4.51}$$

where β and γ dependencies cancel out.

The ensemble DVT states

$$\begin{aligned}\tau'(\beta,\gamma,r) = &-\frac{1}{8}\rho'''(\beta,\gamma,r) - \frac{1}{2}\rho(\beta,\gamma,r)V'_{\text{KS}}(r)\\ &-\frac{1}{2r^2}\frac{\partial\rho'(\beta,\gamma,r)}{\partial\gamma} + \frac{1}{2r^3}\frac{\partial\rho(\beta,\gamma,r)}{\partial\gamma},\end{aligned} \tag{4.52}$$

where $\tau = 4\pi r^2 t = 4\pi r^2(t_{\text{W}} + t_{\text{P}})$ is the radial kinetic energy density. Equations (4.45) and (4.47) reveal that

$$\frac{\partial\rho(\beta,\gamma,r)}{\partial\gamma} \equiv \sum_i \lambda_i l_i(l_i+1)\omega_i(\beta,\gamma)\rho_i(r) \tag{4.53}$$

Combining KS Eqs. (2.6) with the Euler equation yields, after some algebra,

$$\tau(\beta,\gamma,r) = \rho(\beta,\gamma,r)\frac{\delta T_{\text{S}}(\beta,\gamma,r)}{\delta n(\beta,\gamma,r)} - \mu\rho(\beta,\gamma,r) + \frac{\partial\rho(\beta,\gamma,r)}{\partial\beta}. \tag{4.54}$$

From Eqs. (4.45) and (4.47) it immediately follows that

$$\frac{\partial\rho(\beta,\gamma,r)}{\partial\beta} \equiv \sum_i \lambda_i\epsilon_i\omega_i(\beta,\gamma)\rho_i(r). \tag{4.55}$$

When Eq. (4.54) is differentiated w.r.t. r and inserted into the ensemble DVT, we obtain

$$\frac{1}{2}\rho(\beta,\gamma,r)\left(\frac{\delta T_{\text{S}}(\beta,\gamma,r)}{\delta n(\beta,\gamma,r)}\right)' + \rho'(\beta,\gamma,r)\frac{\delta T_{\text{S}}(\beta,\gamma,r)}{\delta n(\beta,\gamma,r)} = \tilde{f}(\beta,\gamma,r), \tag{4.56}$$

where

$$\begin{aligned}\tilde{f}(\beta,\gamma,r) = &-\frac{1}{8}\rho'''(\beta,\gamma,r) - \frac{\partial\rho'(\beta,\gamma,r)}{\partial\beta} + \mu\rho(\beta,\gamma,r)\\ &-\frac{1}{2r^2}\frac{\partial\rho'(\beta,\gamma,r)}{\partial\gamma} + \frac{1}{2r^3}\frac{\partial\rho(\beta,\gamma,r)}{\partial\gamma}.\end{aligned} \tag{4.57}$$

By substituting Eqs. (4.5), (4.6), (4.10) and (4.11) into Eq. (4.56) we finally arrive, after some algebra, at the PPDE:

$$\begin{aligned}&\frac{1}{2}\rho(\beta,\gamma,r)V'_{\text{P}}(\beta,\gamma,r) + \rho'(\beta,\gamma,r)V_{\text{P}}(\beta,\gamma,r) =\\ &\mu\rho'(\beta,\gamma,r) - \frac{\partial\rho'(\beta,\gamma,r)}{\partial\beta} - \frac{1}{2r^2}\frac{\partial\rho'(\beta,\gamma,r)}{\partial\gamma} + \frac{1}{2r^3}\frac{\partial\rho(\beta,\gamma,r)}{\partial\gamma},\end{aligned} \tag{4.58}$$

where we have exploited

$$\frac{1}{2}\rho(\beta,\gamma,r)\left(\frac{\delta T_{\mathrm{W}}(\beta,\gamma,r)}{\delta n(\beta,\gamma,r)}\right)' + \rho'(\beta,\gamma,r)\frac{\delta T_{\mathrm{W}}(\beta,\gamma,r)}{\partial n(\beta,\gamma,r)} = -\frac{1}{8}\rho'''(\beta,\gamma,r). \tag{4.59}$$

The OF-DFT problem is now described by Eqs. (4.12) and (4.58). Since V_{P} is a functional of the density and conversely the density depends on V_{P} in the Euler equation, the two equations form a system of two coupled differential equations. Due to their coupled nature they have to be integrated simultaneously and the self-consistent ground state ρ, V_{KS}, and V_{P} are found using the familiar iterative scheme.

Figure 4.3 displays Xe atom $\rho(\beta,\gamma,r)$, $\partial\rho/\partial\beta(\beta,\gamma,r)$ and $\partial\rho/\partial\gamma(\beta,\gamma,r)$ for different values of β and γ. We notice that $\rho(\beta,\gamma,r)$ changes very rapidly as a function of β near the nucleus, because the eigenvalues ϵ_i are the largest for the innermost orbitals. Note that in the figure $\partial\rho/\partial\beta(\beta,\gamma,r)$ are drawn on a logarithmic y-axis. The change as a function of γ shows the opposite trend of strongest change located closer to the tail region, because the outermost orbitals tend to have larger azimuthal quantum numbers than the inner orbitals. It is these complex behaviors of $\rho(\beta,\gamma,r)$ as a function of β and γ that give rise to the exact V_{P} when it is solved from the PPDE.

The β dependence of V_{P} itself is shown in Fig. 4.4 for Be atom. The peak in V_{P} increases and is shifted towards the nucleus as a function of β. This behavior agrees with the top left panel of Fig. 4.3, where the nuclear region becomes increasingly evacuated as a function of β.

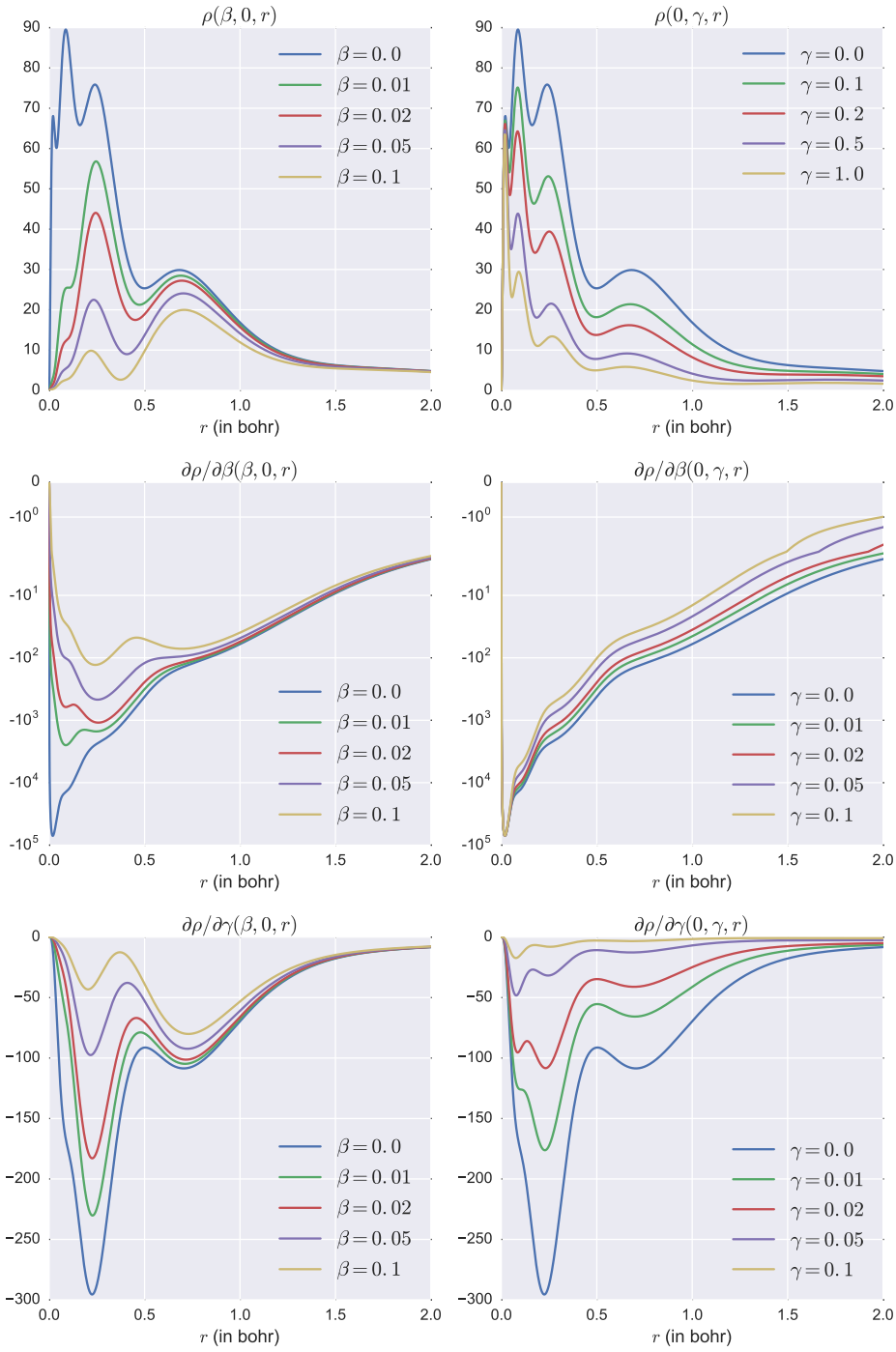

FIGURE 4.3: Xe atom $\rho(\beta, \gamma, r)$, $\partial\rho/\partial\beta(\beta, \gamma, r)$ and $\partial\rho/\partial\gamma(\beta, \gamma, r)$ for different values of β and γ.

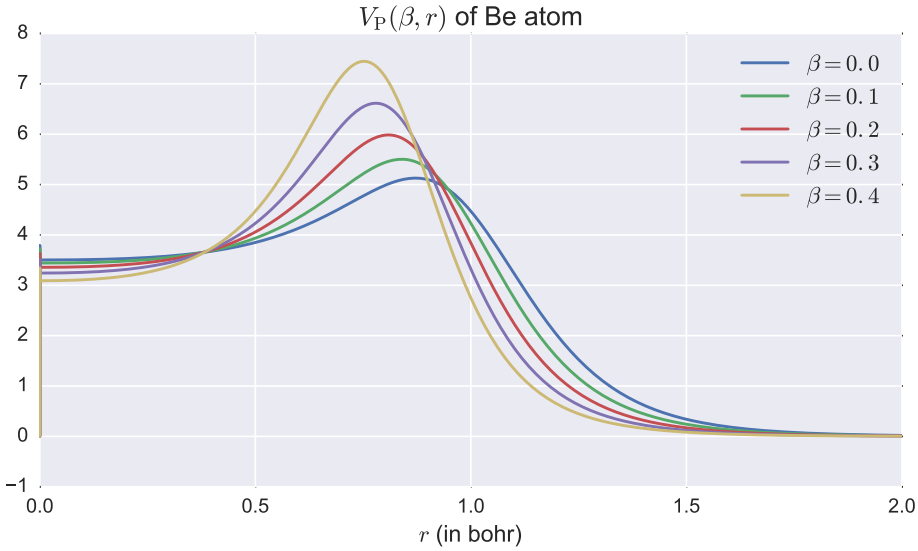

FIGURE 4.4: Pauli potential of Be atom as a function of β.

5 Practical Applications

5.1 Quasi-non-uniform Exchange-Correlation Approximation

QNA can trivially yield accurate results for pure elements, thanks to the optimal subsystem functionals. A much more interesting question is how and how much QNA might improve the description of compounds. In this section we will explore one very interesting application, which is metallic binary alloy formation energies.

Formation energy

$$\Delta H = E[\mathrm{A}_x\mathrm{B}_{1-x}] - xE[\mathrm{A}] - (1-x)E[\mathrm{B}] \tag{5.1}$$

is a key concept in alloy theory and it is, among other things, used in understanding stability and phase diagrams of alloys. The binary Cu-Au alloy [131] is one of the most important binary alloys due to its quintessence, and as such is often used as a benchmark for the accuracy of theoretical alloy theory techniques.

Recently, Zhang *et al*. have argued that semilocal DFT is incapable of accurately describing Cu-Au and similar binary alloys [88]. The most prominent failure of the semilocal level happens with the formation energies of the Cu-Au system; both LDA and PBE yield a considerable error of $\sim 50\,\%$ w.r.t. experiments. Zhang *et al*. also performed HSE hybrid functional [132] calculations and concluded that hybrid functionals are necessary for accurate binary alloy formation energies. While hybrids are shown to greatly improve over semilocal formation energies, not only quantitatively but also qualitatively, they still have to be employed rather sparingly due to their computational heaviness. Below we show that QNA principle can be used to greatly extend the applicability of GGA level in binary alloy formation energy calculations. We argue that it is not necessary to abandon the GGA level in order to calculate accurate binary alloy formation energies.

A very interesting and not yet fully understood question is how the nonlocal exact exchange of a hybrid functional improves formation energies. In the work of Zhang *et al*. it is shown how nonlocal exchange lowers

the d state energies, ergo spatially contracting the orbitals. Pauli repulsion between d states is reduced, which results in decreased LCs. For Cu and Au the HSE functional therefore gives more accurate LCs than PBE, which overestimates them for both elements. This is evidence that there exists some connection between the accuracy of the alloy components' LCs and the accuracy of the alloy formation energy. It should be noted that the above reasoning does not readily explain why LDA gives even worse formation energies than PBE, despite the fact that it also yields smaller LCs than PBE.

This connection between the accuracy of LCs and formation energies is investigated in detail in paper V. The source of error in semilocal DFT formation energies is identified to be similar in nature to the one causing inaccurate equilibrium volumes (and equations of state in general). Consequently, we arrive at the following conjecture: *accurate semilocal formation energy of a binary alloy requires from a semilocal XC functional that it is capable of producing accurate volumes for both alloy components simultaneously*. This is a physically motivated but not a "strict" condition; in some situations fortuitous cancellation of errors can also lead to an accurate formation energy.

It is important to note that we are not dealing with a simple "volume effect", which would mean that if e.g. PBE calculations were repeated using equilibrium QNA LCs, the so-obtained PBE formation energies would be noticeably more accurate. This, in fact, does not happen: PBE formation energies at QNA LCs are practically unchanged from regular PBE results. Conversely, calculating QNA formation energies with PBE LCs does not change QNA results.

Our insight can explain why both LDA and PBE give bad formation energies for Cu-Au. Neither of these functionals fulfills the above conjecture; LDA is accurate for Au, but inaccurate for Cu, while PBE follows the converse trend of accurate Cu and inaccurate Au. Both functionals therefore fail, albeit for slightly different reasons: LDA formation energy error originates from Cu inaccuracy and for PBE from Au inaccuracy. In more specific terms, the inaccuracy stems from an improper change in XC energy, when an alloy component is taken from its pure bulk phase and put in the alloy matrix. An XC functional that gives inaccurate LCs either over- or underestimates the "true" XC energy change, which results in inaccurate formation energies. In paper V we probe this effect for Cu_3Au by defining an "XC formation energy"

$$\Delta H_{\text{XC}} = \Delta H_{\text{total}} - \Delta H_{\text{other}} = \frac{3 \cdot \Delta H_{\text{XC}}[\text{Cu}] + 1 \cdot \Delta H_{\text{XC}}[\text{Au}]}{3+1}, \qquad (5.2)$$

TABLE 5.1: Alloy component resolved XC formation energies (meV/atom) for Cu3Au calculated with LDA, PBE, and QNA.

Cu_3Au	$\Delta H_{\text{XC}}[\text{Cu}]$	$\Delta H_{\text{XC}}[\text{Au}]$	ΔH_{XC}	ΔH_{other}	ΔH_{total}
LDA	-1574	4468	-64	18	-46
PBE	-1623	4617	-63	18	-46
QNA	-1612	4490	-87	18	-69

where "other" includes all energy contributions other than XC, and $H_{\text{XC}}[\text{Cu}]$ and $H_{\text{XC}}[\text{Au}]$ are the component-resolved changes that occur when Cu_3Au alloy is formed. Table 5.1 shows how alloy component-resolved XC formation energies are different between LDA, PBE, and QNA, and how these differences lead to an underestimated formation energy with LDA and PBE. For simplicity, all functionals in Table 5.1 use QNA LCs[1] and the total energy was evaluated non self-consistently. This way ΔH_{other} remains a constant and the trends in the formation energy can be explained solely based on the XC effects. We notice that $\Delta H_{\text{XC}}[\text{Cu}]$ are similar for PBE and QNA, while it is not low enough for LDA. The discrepancy in LDA $\Delta H_{\text{XC}}[\text{Cu}]$ is caused by same mechanism as the discrepancy in LDA Cu LC: Cu requires gradient enhancements for an accurate LC, but since these are absent in LDA the magnitude of $\Delta H_{\text{XC}}[\text{Cu}]$, as well as Cu LC, is underestimated. While LDA $\Delta H_{\text{XC}}[\text{Au}]$ is very close to that of QNA and therefore "correct", the underestimated LDA $\Delta H_{\text{XC}}[\text{Cu}]$ makes the total LDA formation energy also underestimated. Converse conclusions apply to PBE to explain its similarly underestimated total formation energy.

Further analysis can be carried out in the spirit of Section 3.6 and Eq. (3.32). The integral form of ΔH_{XC} is

$$\Delta H_{\text{XC}} = \Delta \int h_{\text{XC}}(\mathbf{r})\, d\mathbf{r}, \quad h_{\text{XC}}(\mathbf{r}) = n(\mathbf{r})\varepsilon_{\text{X}}^{\text{LDA}}([n],\mathbf{r})F_{\text{XC}}(r_s,s,t). \tag{5.3}$$

Δh_{XC} can be cast into the same form as Eq. (3.32) to get

$$\Delta h_{\text{XC}} = \frac{d(n\varepsilon^{\text{LDA}})}{dr_s} F_{\text{XC}} \Delta r_s + (n\varepsilon^{\text{LDA}}) \left[\frac{\partial F_{\text{XC}}}{\partial r_s} \Delta r_s + \frac{\partial F_{\text{XC}}}{\partial s} \Delta s \right]. \tag{5.4}$$

The first two terms in Eq. (5.4) are very similar for different functionals,

[1] As was mentioned earlier, using QNA LCs does not appreciably change the LDA and PBE predictions.

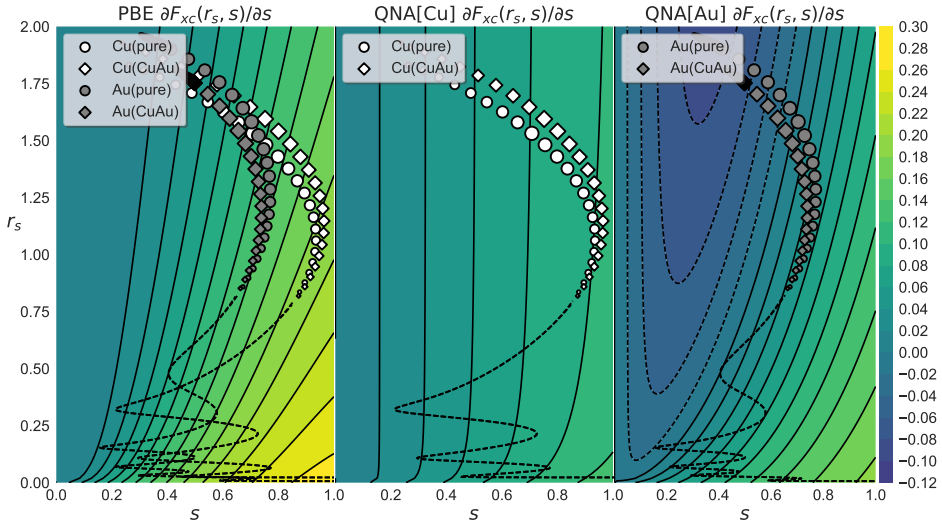

FIGURE 5.1: Enhancement function s-derivatives for PBE, QNA[Cu], and QNA[Au]. Round symbols indicate spherically averaged s vs. r_s curves of pure bulk and diamond symbols are for the alloy. Dashed contour lines indicate negative values.

so it is enough to consider the last term, which is characterized by the s-derivative of the XC enhancement function $\partial F_{\rm XC}/\partial s$. Fig. 5.1 shows these derivatives for PBE, QNA[Cu], and QNA[Au]. The pure bulk and alloy s versus r_s curves of Cu and Au, as well as the important CVORs, are also shown. The figure reveals that within the CVOR[Cu] $\Delta s > 0$ and $\partial F_{\rm XC}^{\rm QNA[Cu]}/\partial s \approx \partial F_{\rm XC}^{\rm PBE}/\partial s > 0$. From this results $\Delta H_{\rm XC}^{\rm QNA}[{\rm Cu}] \approx \Delta H_{\rm XC}^{\rm PBE}[{\rm Cu}] < \Delta H_{\rm XC}^{\rm LDA}[{\rm Cu}]$, because for LDA $\partial F_{\rm XC}^{\rm LDA}/\partial s \equiv 0$. For Au the situation is opposite and within the CVOR[Au] $\Delta s < 0$ and $F_{\rm XC}^{\rm PBE}/\partial s > F_{\rm XC}^{\rm QNA[Au]}/\partial s \approx 0 \equiv \partial F_{\rm XC}^{\rm LDA}/\partial s$. Thus it follows that $\Delta H_{\rm XC}^{\rm PBE}[{\rm Au}] > \Delta H_{\rm XC}^{\rm QNA}[{\rm Au}] \approx \Delta H_{\rm XC}^{\rm LDA}[{\rm Au}]$. The above observations nicely explain the trends found in Table 5.1.

Section 3.6 presented evidence that "conventional" GGA approximations do not have enough information available to them to be able to describe all elements accurately, and possibly the only way to introduce more flexibility is the subsystem functional approach. QNA was designed to yield accurate volumes for all elements, so presumably it should be able to produce better formation energies than other semilocal approximations. In paper V we show that this is indeed the case.

Table 5.2, which is adapter from paper V, shows results for nine binary

TABLE 5.2: Binary alloy formation energies (meV/atom) calculated with semilocal LDA, PBE, QNA, and SCAN approximations, as well as the nonlocal HSE approximation. The last column shows experimental values, where available uncertainties are inside parentheses. The most accurate semilocal values are in boldface (for CuAg with respect to the HSE result). The bottom row shows the mean absolute relative error (MARE).

	LDA	**PBE**	**PBE(FHI)**	**QNA**	**SCAN(FHI)**	**HSE**	**Exp.**
Cu_3Au	−39	−45	−38	**−70**	−64	−71	−74
CuAu	−54	−57	−47	**−87**	−78	−91	−93
$CuAu_3$	−18	−24	−20	**−41**	**−37**	−53	−39
CuPd	−138	−143	−120	**−141**	−126	−170	−140(21)
CuAg	103	93	103	**76**	124	74	···
CuPt	−119	−145	**−154**	**−154**	**−193**	···	−174
AgPd	−39	−42	−46	**−27**	−56	···	−23(3)
AgAu	−64	−59	−60	**−46**	−83	−52	−48
NiAl	−731	**−678**	−655	−689	−783	···	−680
MARE	36	30	38	**7**	36	···	···

alloys. In the table "(FHI)" refers to the numeric atom-centered orbitals DFT code FHI-aims [133, 134], which was used to perform the SCAN and the other set of PBE calculations. SCAN [135] is a recently developed non-empirical meta-GGA functional, which satisfies all known constraints of the meta-GGA level. HSE results are from Ref. [88] and references of experimental values can be seen in Table II of paper V. QNA uses optimal parameters from paper II. LDA and PBE are seen to produce relatively large mean absolute relative errors (MARE). Interestingly SCAN shows a nice improvement for the Cu-Au system, but for some reason seems to take its predictions in the wrong direction for CuAg, AgPd, AgAu, and NiAl. The MARE of SCAN ends up being on level with LDA and PBE, and so SCAN does not appear to be an improvement for the type of metallic binary alloys considered here. The HSE hybrid always corrects LDA/PBE predictions towards experimental values with some overcorrecting happening with CuPd. QNA shows excellent performance and in all but one cases its prediction is closest to the experimental value. For NiAl PBE is the most accurate, but it is important to note that the QNA scheme does not "break down" and that the QNA prediction is still very close to the experimental

value.

Table 5.2 shows a considerable amount of quantitative improvement in semilocal formation energies when they are calculated with QNA. The work of Zhang *et al*. concludes that the nonlocality of hybrids can also lead to qualitatively correct predictions conserning binary alloy phase stabilities. Therefore a very interesting question is whether or not QNA is capable of similar qualitative improvements on semilocal level. Below we will consider two examples, which offer qualitative challenges and they are the Cu-Au and Co-Pt systems.

For both binary alloy systems we calculate the formation energy of four ordered phases in $L1_2$, $L1_0$, and β_2 structures and then analyze their relative phase stability. $L1_2$ and $L1_0$ are fcc-type structures with alternating layers of A and B atoms in $[111]$ and $[001]$ directions, respectively. $L1_2$ does not require any geometry optimization, but $L1_0$ requires unit cell relaxation along the $[001]$ direction. The β_2 structure is fcc-type with a repeating sequence of ABB layers in $[001]$ direction. When its tetragonal 12-atom cell[2] is used, atomic positions and unit cell have to be relaxed along the $[001]$ direction. Relaxations are most conveniently taken into account by calculating forces and the stress tensor. However, the fact that QNA uses atom-centered space partitioning generates an extra challenge for geometrical relaxation calculations. The sizes and locations of the space partitions depend on the atomic positions, which means that the partitions will move and change as a function of atomic positions and stress. The partitions therefore induce extra terms in the analytical expressions of the forces and the stress tensor, which should be taken into account. In Appendix B we derive these extra expressions and they have been implemented in GPAW DFT code [92, 93].

Fig. 5.2 shows the formation energies of the ordered phases of Cu-Au. Not only are LDA and PBE formation energies highly underestimated, but the Au-rich side also contains qualitative phase stability problems. Both functionals predict $CuAu_2$ in β_2 structure to be stable, which is not the case experimentally. Furthermore, they also predict experimentally stable $CuAu_3$ in $L1_2$ structure to be unstable, because its formation energy lies above the CuAu-Au and $CuAu_2$-Au tie lines marked by dashed lines in Fig. 5.2.

The HSE hybrid is able to recover qualitatively correct phase stability by shifting the formation energy of $CuAu_2$ β_2 up and $CuAu_3$ $L1_2$ down. As a result, the β_2 phase moves above the tie line connecting CuAu and

[2] β_2 primitive unit cell is only three atoms.

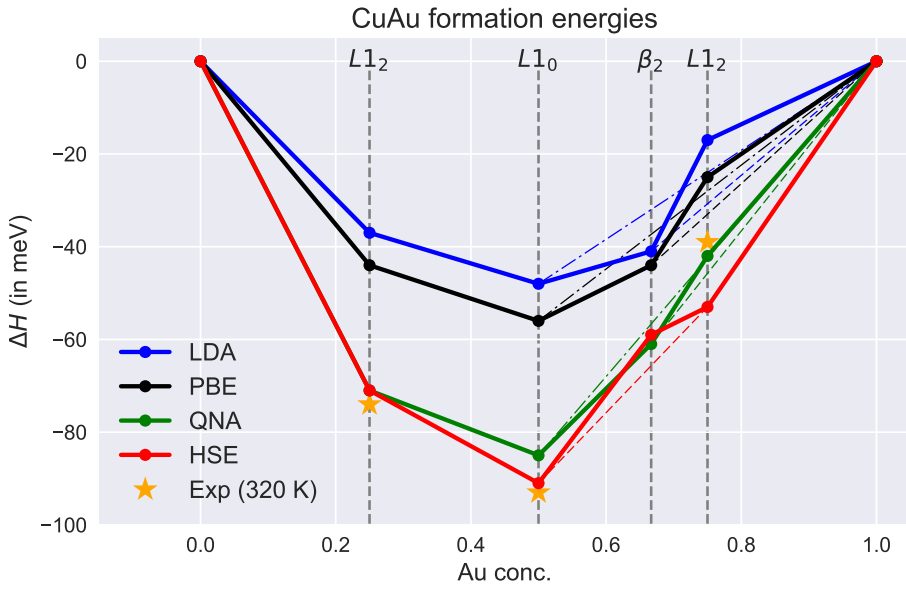

FIGURE 5.2: Formation energies of Cu-Au system. Dashed lines indicate phase stability tie lines.

$CuAu_3$, and $CuAu_3$ becomes a part of the convex hull, which corresponds to the experimental sequence of unstable β_2 and stable $L1_2$.

Starting from the Cu rich side, QNA results show excellent agreement with HSE and experimental values all the way up to β_2 $CuAu_2$. For $CuAu_3$ there is a key difference between QNA and HSE formation energies. QNA is seen to be very close to the reported experimental value. However, the veracity of the reported experimental value was questioned by Zhang *et al.* in the sense that the experimental sample might lack complete order, which would raise the formation energy (compared to the perfectly ordered DFT calculation). The HSE $CuAu_3$ formation energy is noticeably lower in comparison and thanks to this difference HSE is able destabilize the β_2 structure. The anomalous difference between HSE and QNA $CuAu_3$ formation energies means that QNA is unfortunately not quite capable of fixing the qualitative phase stability issue of the semilocal level.

The second example is the Co-Pt system, which has similar qualitative stability problems to Cu-Au. Here we illustrate a less empirical QNA where Co uses PBE and Pt uses LDA. The reason for this is twofold: it is

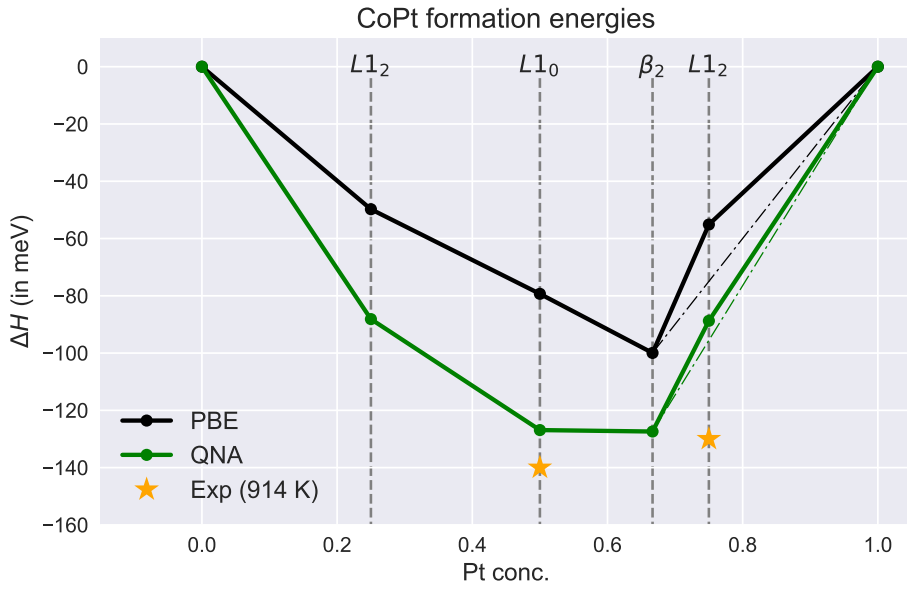

FIGURE 5.3: Formation energies of Co-Pt system.

important to demostrate that "non-empirical" QNA still offers great performance and, secondly, it is more difficult to obtain optimal μ and β parameters for Co because of its two-degrees-of-freedom hcp ground state.

Fig. 5.3 shows the computed formation energies with available experimental values taken from [89]. We notice that the PBE β_2 formation energy is very low, which is, at least partly, due to the large size mismatch of Co and Pt atoms; the PBE relaxation effect is strong, which lowers the formation energy. This results in a stable β_2 structure and unstable $L1_2$ structure, which is in conflict with experimental findings [89].

With QNA Pt uses LDA, which lessens the degree of size mismatch in the alloy. Atomic relaxation effects should therefore be smaller, and the QNA β_2 formation energy is shifted up noticeably, which is needed to make $L1_2$ $CoPt_3$ a stable structure. However, similarly to the case of Cu-Au, the QNA $L1_2$ $CoPt_3$ formation energy is still anomalously too high and quite far from the experimental value. Consequently, QNA still narrowly predicts $CoPt_3$ to be an unstable structure despite the improvement in the β_2 formation energy.

Qualitative trends are partially corrected by non-local treatment. It has been shown that HSE06 hybrid functional is able to make $L1_2$ $CoPt_3$ stable by reproducing the experimental trend of $L1_0$ $L1_2$ formation energies being

almost on the same level, but even then the β_2 remains incorrectly a stable structure [89].

In this section we have seen that accurate description of phase stability eludes the semilocal level of XC. The anomalously high semilocal formation energies of the $L1_2$ $CuAu_3$ and $CoPt_3$ phases suggest that there is some truly nonlocal effect which needs to be taken into account in order to correct the formation energy at this particular concentration.

5.2 Pauli Potential Differential Equation

In paper IV we demonstrate PPDE in practice by solving the electronic structure of a spherically symmetric Be atom. A Fortran program was developed for this purpose. For Be $\lambda_{1s} = \lambda_{2s} = 2$ and $l_{1s} = l_{2s} = 0$, which means that γ dependence vanishes because $\partial\rho/\partial\gamma \equiv 0$. For Be the system of equations is then

$$\begin{cases} -\frac{1}{2}\varphi''(\beta,r) + [V_{\text{KS}}(r) + V_{\text{P}}(\beta,r)]\,\phi(\beta,r) = \mu\phi(\beta,r), & (5.5) \\ V'_{\text{P}}(\beta,r) = \frac{2}{\rho(\beta,r)}\left\{[\mu - V_{\text{P}}(\beta,r)]\rho'(\beta,r) - \frac{\partial\rho'(\beta,r)}{\partial\beta}\right\}, & (5.6) \\ \varphi = \sqrt{\rho}. & (5.7) \end{cases}$$

In order to integrate them numerically we define $P(\beta,r) = \varphi(\beta,r)$ and $Q(\beta,r) = P'(\beta,r)$, which turns the second-order one-orbital Euler equation (5.5) into two coupled first-order differential equations:

$$\begin{cases} P'(\beta,r) = Q(\beta,r), & (5.8) \\ Q'(\beta,r) = 2\,[V_{\text{KS}}(r) + V_{\text{P}} - \mu]\,P(\beta,r), & (5.9) \\ V'_{\text{P}}(\beta,r) = 4\dfrac{[\mu - V_{\text{P}}(\beta,r)]\,P(\beta,r)Q(\beta,r) - \frac{\partial P(\beta,r)}{\partial\beta}Q(\beta,r)}{P^2(\beta,r)} \\ \qquad\qquad - 4\dfrac{P(\beta,r)\frac{\partial Q(\beta,r)}{\partial\beta}}{P^2(\beta,r)}. & (5.10) \end{cases}$$

When the problem is cast in the first-order form of Eqs. (5.8)–(5.10) standard integration schemes, such as Runge-Kutta and Adams methods, can be employed in the integration of the r dimension [16, 136]. Since the equations are coupled they need to be converged using a so-called predictor-corrector technique. In predictor-corrector methods, first a prediction is computed for the current point by extrapolating the known past points.

Then a correction is computed by using the prediction and an interpolation technique to refine the solution at the current point. It is a good idea to use a logarithmic radial mesh [136], which places more mesh points near the nucleus for higher accuracy. The β dimension can be handled by taking a linear mesh, for example $\{\beta_1, \beta_2\} = \{0.0, 0.1\}$. The needed β derivatives can be computed by solving Eqs. (5.8)–(5.10) for different values of β, and then evaluating the derivatives using finite-difference schemes. A more accurate way of getting the derivatives is to rely on their definition in Eq. (4.55). For Be a β mesh of two points is enough and we can write the β dependent total ensemble densities in the following form:

$$\begin{cases} \lambda_{1s} e^{\beta_1 b_1} a_1(r) + \lambda_{2s} e^{\beta_1 b_2} a_2(r) = \rho(\beta_1, r), & (5.11) \\ \lambda_{1s} e^{\beta_2 b_1} a_1(r) + \lambda_{2s} e^{\beta_2 b_2} a_2(r) = \rho(\beta_2, r). & (5.12) \end{cases}$$

The β derivatives can then be obtained analytically as

$$\begin{cases} b_1 \lambda_{1s} e^{\beta_1 b_1} a_1(r) + b_2 \lambda_{2s} e^{\beta_1 b_2} a_2(r) = \dfrac{\partial \rho}{\partial \beta}(\beta_1, r), & (5.13) \\ b_1 \lambda_{1s} e^{\beta_2 b_1} a_1(r) + b_2 \lambda_{2s} e^{\beta_2 b_2} a_2(r) = \dfrac{\partial \rho}{\partial \beta}(\beta_2, r). & (5.14) \end{cases}$$

Eqs. (5.11) and (5.12) is a linear system, which is a well-understood problem and thus it can be routinely solved in order to obtain $a_1(r)$ and $a_2(r)$. It should be noted that parameters b_1 and b_2 are also unknown, but they can be solved using a so-called shooting method [16, 136]. In the shooting method Eqs. (5.8)–(5.10) are integrated both inwards and outwards, and the two solutions meet at some radial point $\tilde{r}$ in the middle of the radial mesh. The inward and outward solutions are then compared in order to determine the correct b_1 and b_2. Correct b_2 is fixed by the condition that the derivatives $\rho'(\beta, \tilde{r})$ should be continuous for all β in the vicinity of $\tilde{r}$. The other parameter b_1 is determined by a continuity requirement of V_{P} at $\tilde{r}$.

It should be noted that when V_{P} is solved exactly from Eq. (5.10), $a_1(r)$ and $a_2(r)$ coincide with the KS orbital densities $\rho_{1s}(r)$ and $\rho_{2s}(r)$. Additionally, when exact analytical derivatives of Eqs. (5.13) and (5.14) are used, the parameters b_1 and b_2 are the same as the KS orbital eigenvalues, so $b_1 \to \epsilon_{1s}$ and $b_2 \to \epsilon_{2s} = \mu$. The exact solution scheme therefore produces the KS quantities as a "by-product".

The outline of the solution scheme is as follows:

- First construct some initial guess for V_{KS}. One option is to compute it initially from the density of hydrogen-like orbitals.

1. Choose some initial values for b_1 and b_2.
2. Construct initial values $P(\beta, r_0)$, $Q(\beta, r_0)$, and $V_{\text{P}}(\beta, r_0)$ for the first radial mesh point for each β. For P and Q initial values can be generated using techniques and asymptotic behaviors described in Ref. [136]. For V_{P} cusp conditions of paper III can be used for outward integration. Generating good initial values for V_{P} for inward integration is hard because in the tail region the non-trivial ($V_{\text{P}} \neq 0$) asymptotic behavior of V_{P} is a function of the spatial overlap of the two outermost KS orbitals and is not known.
3. Perform inward and outward integration of Eqs. (5.8)–(5.10) for each value of β. At each radial point r_n:
   (a) Compute initial solutions $P(\beta, r_{n+1})$, $Q(\beta, r_{n+1})$, and $V_{\text{P}}(\beta, r_{n+1})$ using Adams method predictor part.
   (b) Compute initial β derivatives from Eqs. (5.13) and (5.14) using predictor P and Q values from step (a).
   (c) Iterate the following steps of the corrector loop until $P(\beta, r_{n+1})$, $Q(\beta, r_{n+1})$, and $V_{\text{P}}(\beta, r_{n+1})$ converge:
      i. Compute $P(\beta, r_{n+1})$, $Q(\beta, r_{n+1})$, and $V_{\text{P}}(\beta, r_{n+1})$ with the corrector formula.
      ii. Calculate new β derivatives.
      iii. Insert the β derivatives into the differential equations.
4. Join the inward and outward solutions at $\tilde{r}$. If $\rho'(\beta, \tilde{r})$ and $V_{\text{P}}(\beta, \tilde{r})$ are not continuous, compute new guesses for b_1 and b_2 and repeat steps 2-3.
5. When b_1 and b_2 have converged, the correct solution of a given iteration has been found. Perform density mixing and recalculate V_{KS}.

- Steps 1-5 are repeated until ρ and V_{KS} are converged.

PPDE results for Be atom are shown in Table 5.3 and Fig. 5.4. To describe XC effects Vosko-Wilk-Nusair LDA [37] was used. We compare the PPDE solution to a reference KS-DFT calculation computed with dftatom atomic solver [136]. The dftatom solution agrees to at least six decimal places with the benchmark data of Refs. [137, 138]. Since we are solving the PPDE exactly, we are able to recover the KS-DFT solution. Table 5.3 confirms that the agreement is to a high degree, up to three decimal places. Also the convergence behavior is almost identical to that of KS-DFT. PPDE calculations converged in 18 iterations, which is very similar to KS-DFT.

TABLE 5.3: Energy components and orbital eigenvalues of the Be atom calculated with the PPDE scheme. Reference KS-DFT values are also displayed.

	PPDE	**KS-DFT**
E_{Total}	$-14.447\,227$	$-14.447\,209$
E_{Kin}	$14.309\,407$	$14.309\,424$
E_{Hartree}	$7.115\,258$	$7.115\,257$
$E_{\text{Elec-Nuc}}$	$-33.357\,033$	$-33.357\,034$
E_{XC}	$-2.514\,860$	$-2.514\,856$
b_1, ϵ_{1s}	$-3.856\,414$	$-3.856\,411$
b_2, ϵ_{2s}	$-0.205\,779$	$-0.205\,744$

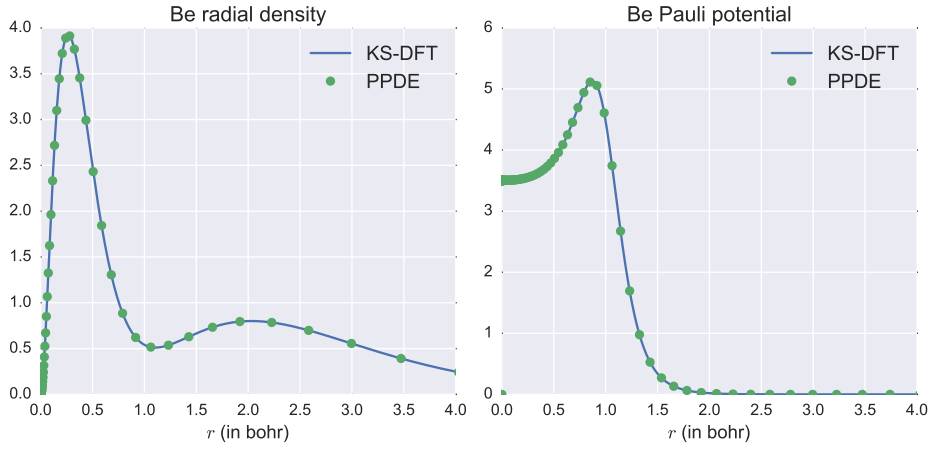

FIGURE 5.4: Radial density and Pauli potential of Be atom calculated with normal KS-DFT and the PPDE scheme.

It is clear that solving the PPDE exactly is quite complicated and so far only Be has been solved succesfully. There are certain issues which prohibit solving more complicated systems:

- The existence of p, d, and f orbitals of heavier atoms has been found to cause numerical stability problems.
- There is difficulty in describing the asymptotic behavior of the Pauli potential in the tail part of the density, where only the two outermost

KS orbitals are left.

- When P and Q are integrated, their absolute scale does not matter, because the solutions will be normalized to the electron number afterwards. This property makes it easy to generate good enough initial values for the integration, because only the relation of the points to each other matters, not their absolute scale. V_{P} does not have this prorerty; the initial values of V_{P} have to be "just right".
- Some of these problems could be solved by developing some approximate solution scheme for the PPDE. However, it is currently not clear how this should be done.

Real practical value of the PPDE method is currently nonexistent, but it is still very interesting that calculations at the KS level of accuracy can be performed without explicitly solving the KS equations.

6 Concluding remarks

In this thesis I have studied and developed two different types of approximations, which are those whose job it is to turn the two branches of DFT, Kohn-Sham and orbital-free, into powerful practical tools. The first one is the new GGA XC approximation, named QNA, whose roots are in the contemplation of the limits of GGA level and how to get around those limits. Said limits are circumvented in QNA with the use of subsystem functional approach and element-specific, optimal subsystem functionals. QNA has shown its practical usefulness, especially in the realm of alloy formation energies. But this is achieved with the price of QNA being semi-empirical at best, which is a strategy not advocated by some of the most influential people in DFT [139, 140].

The second one, called PPDE, is a way of obtaining the kinetic energy without using KS orbitals. Performing calculations without KS orbitals is of great interest, because dispensing with the KS orbitals makes DFT very fast and able to handle very big systems. The PPDE framework allows the orbital-free kinetic energy to be calculated exactly (for spherically symmetric systems) and an exact solution is presented for the Be atom. OF-DFT research is orders of magnitude less popular than KS-DFT research due to the sheer difficulty of approximating the kinetic energy and the Be solution can shed light on the nature of these difficulties. However, solving the PPDE exactly is at its current state so difficult that the speed advantage of OF-DFT is lost. It should also be noted that the exact solution of the PPDE does not scale linearly like the "simpler" OF-DFT models do, because the complexity of the exact PPDE scales superlinearly. For linear scaling some kind of approximation for the PPDE would be needed, and the approximate PPDE should ideally be able to combine much of the good accuracy of the exact PPDE with the blazing speed for which OF-DFT is known.

A Derivatives of GGA enhancement factor maps

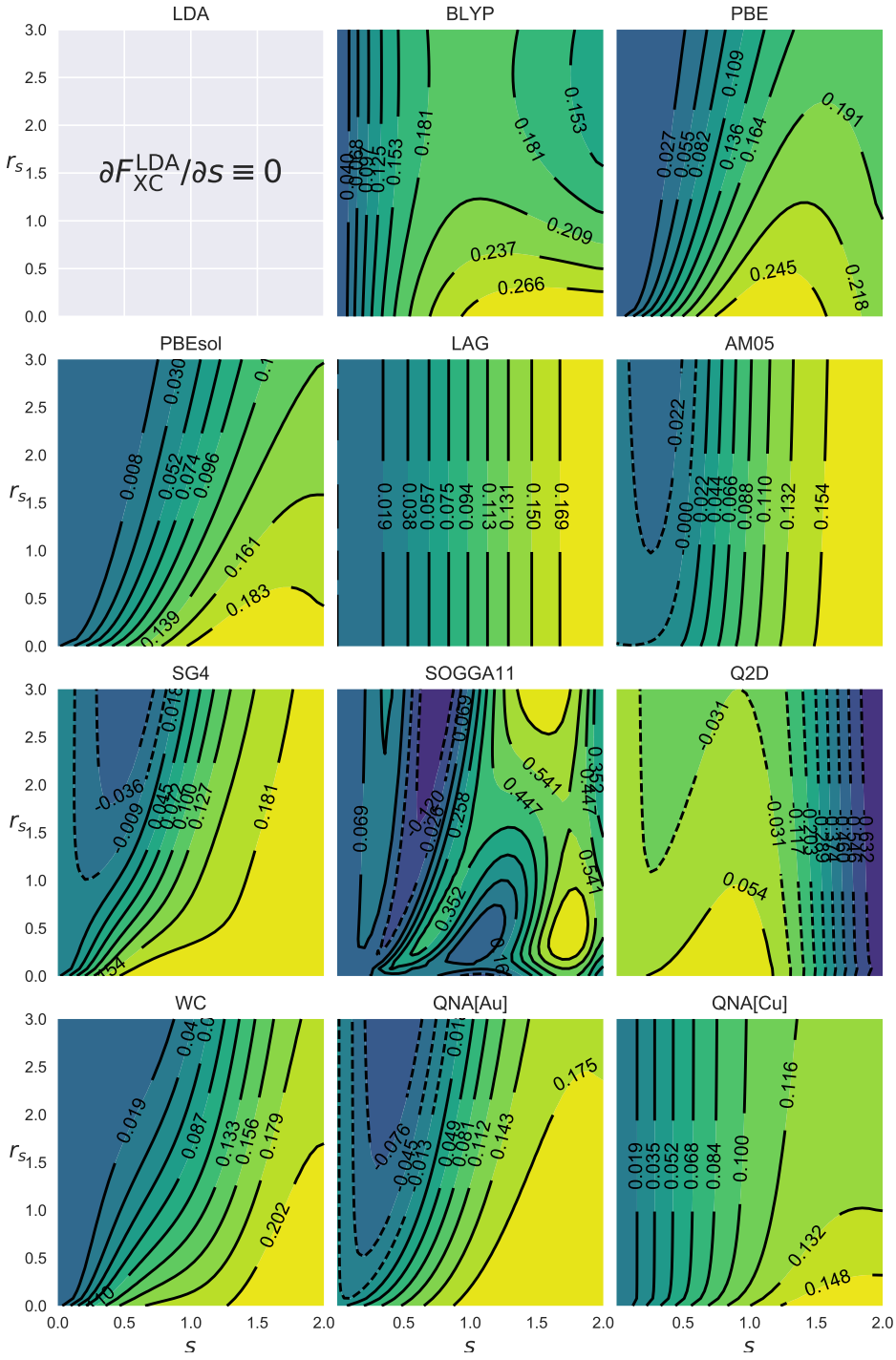

FIGURE A.1: $\partial F_{XC}/\partial s$ derivative maps of various GGA XC functionals.

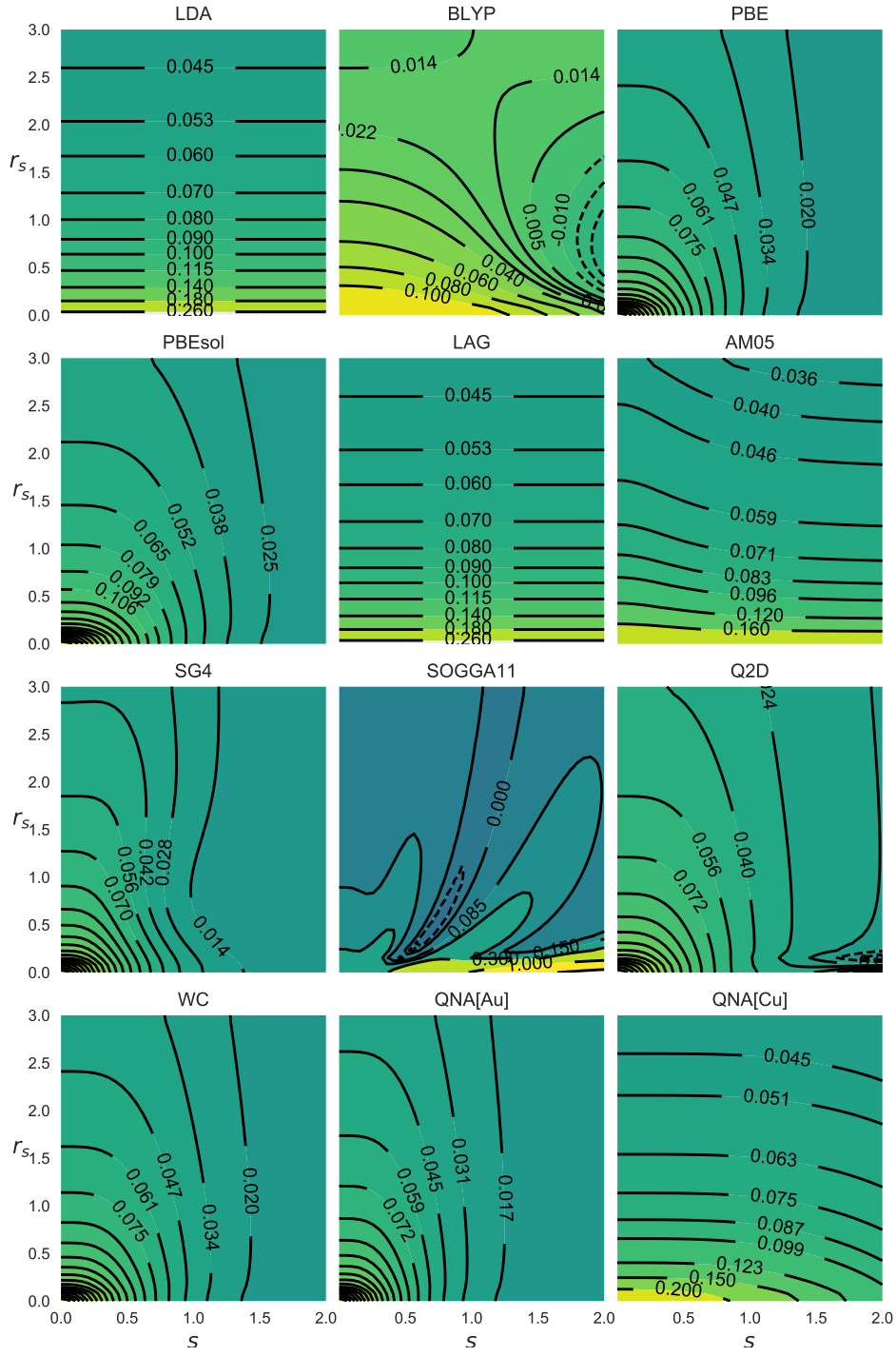

FIGURE A.2: $\partial F_{\mathrm{XC}}/\partial r_s$ derivative maps of various GGA XC functionals.

B Implementation of QNA in GPAW DFT code

B.1 Energy expression

QNA essentially generalizes the μ and β parameters of PBE XC functional into space dependent $\mu(\mathbf{r})$ and $\beta(\mathbf{r})$ fields

$$\beta(\mathbf{r}) = \sum_a w_a(\mathbf{r})\beta^a, \tag{B.1}$$

$$\mu(\mathbf{r}) = \sum_a w_a(\mathbf{r})\mu^a, \tag{B.2}$$

where μ^a and β^a are optimized parameters corresponding to a given element occupying atomic site a. Consequently the QNA XC energy can be written in the form

$$E_{\mathrm{XC}}^{\mathrm{QNA}}[n, |\nabla n|^2] = \int n(\mathbf{r})\varepsilon_{\mathrm{XC}}^{\mathrm{PBE}}[n(\mathbf{r}), |\nabla n(\mathbf{r})|^2, \mu(\mathbf{r}), \beta(\mathbf{r})]\,\mathrm{d}\mathbf{r}, \tag{B.3}$$

where, in practical calculations, $\mu(\mathbf{r})$ and $\beta(\mathbf{r})$ fields are simply fed into the usual PBE subroutines/functions rather than being constants defined inside the PBE subroutines/functions.

We want the $\mu(\mathbf{r})$ and $\beta(\mathbf{r})$ fields to interpolate sharply between atoms and in practice this creates the need to divide space into Voronoi-type atomic site centered regions. Space division can be accomplished by appropriate weight fields $w_a(\mathbf{r})$. Weight field $w_a(\mathbf{r})$ ought to attain unity, when we are close to atomic site a, and decay smoothly to zero, when we move away from site a. Additionally it must always hold that $\sum_a w_a(\mathbf{r}) = 1$. Here we define the weights as

$$w_a(\mathbf{r}) = \frac{P_a(\mathbf{r})}{\sum_{a'} P_{a'}(\mathbf{r})}, \tag{B.4}$$

where $P_a(\mathbf{r})$ are atomic site centered partial weights. Eq. (B.4) is actually a well-known concept in chemistry where partitioning schemes for the

atoms in molecules are routinely used [141–143]. $P_a(\mathbf{r})$ could be defined many different ways, but here we will use

$$P_a(\mathbf{r}) = f(|\mathbf{r} - \mathbf{R}^a|) = \exp\left[-\left(\frac{|\mathbf{r} - \mathbf{R}^a|}{\lambda}\right)^{2\alpha}\right], \tag{B.5}$$

which is very similar to the expression invented in Ref. [142]. Fig. B.1 illustrates the shape of $P_a(\mathbf{r})$ when defined by Eq. (B.5). The parameter λ

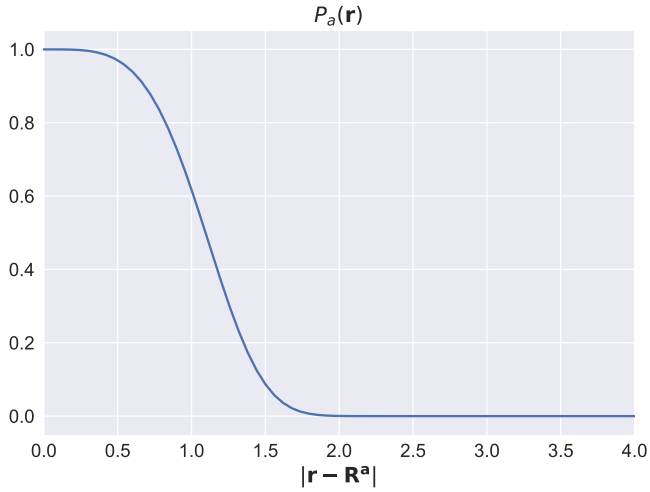

FIGURE B.1: Illustration of partial weights $P_a(\mathbf{r})$.

controls the location of the transition from 1 to 0 and α controls its sharpness. We have found that values $\lambda = 1.2$ and $\alpha = 2.0$ give partitioning that is very close to exact Voronoi cells.

The XC potential is evaluated in the usual fashion as

$$v_{\mathrm{xc}}(\mathbf{r}) = \frac{\delta E_{\mathrm{XC}}^{\mathrm{PBE}}[n, |\nabla n|^2, \mu(\mathbf{r}), \beta(\mathbf{r})]}{\delta n(\mathbf{r})}, \tag{B.6}$$

where the dependence on $\mu(\mathbf{r})$ and $\beta(\mathbf{r})$ is purely parametric as they are not explicit functions of density.

B.2 Forces

The evaluation of a force affecting atomic site a requires computing $\partial/\partial\mathbf{R}^a$ partial derivatives. The QNA XC force contribution is of the form

$$\begin{aligned}\mathbf{F}^a_{\mathrm{XC}} = &-\frac{\partial E^{\mathrm{PBE}}_{\mathrm{XC}}}{\partial \mathbf{R}^a} = -\frac{\partial E^{\mathrm{PBE}}_{\mathrm{XC}}}{\partial n(\mathbf{r})}\frac{\partial n(\mathbf{r})}{\partial \mathbf{R}^a} \\ &-\frac{\partial E^{\mathrm{PBE}}_{\mathrm{XC}}}{\partial \mu(\mathbf{r})}\frac{\partial \mu(\mathbf{r})}{\partial \mathbf{R}^a} - \frac{\partial E^{\mathrm{PBE}}_{\mathrm{XC}}}{\partial \beta(\mathbf{r})}\frac{\partial \beta(\mathbf{r})}{\partial \mathbf{R}^a}.\end{aligned} \tag{B.7}$$

$E^{\mathrm{PBE}}_{\mathrm{XC}}$ depends on the density, as all XC functionals do, and the first term on the right hand side in Eq. (B.7) is already handled by GPAW code. However, due to the atomic site centered $\mu(\mathbf{r})$ and $\beta(\mathbf{r})$ fields $E^{\mathrm{QNA}}_{\mathrm{XC}}$ has an additional dependency on the positions of the nuclei, which creates the extra second and third terms in Eq. (B.7). The extra terms can be written as

$$\begin{aligned}&\frac{\partial E^{\mathrm{PBE}}_{\mathrm{XC}}}{\partial \mu(\mathbf{r})}\frac{\partial \mu(\mathbf{r})}{\partial \mathbf{R}^a} = \\ &= \int \frac{\partial\left\{n(\mathbf{r})\varepsilon^{\mathrm{PBE}}_{\mathrm{XC}}[n(\mathbf{r}), |\nabla n(\mathbf{r})|^2, \mu(\mathbf{r}), \beta(\mathbf{r})]\right\}}{\partial \mu(\mathbf{r})} \sum_{a'} \frac{\partial w_{a'}(\mathbf{r})}{\partial \mathbf{R}^a}\mu^{a'}\,\mathrm{d}\mathbf{r},\end{aligned} \tag{B.8}$$

$$\begin{aligned}&\frac{\partial E^{\mathrm{PBE}}_{\mathrm{XC}}}{\partial \beta(\mathbf{r})}\frac{\partial \beta(\mathbf{r})}{\partial \mathbf{R}^a} = \\ &= \int \frac{\partial\left\{n(\mathbf{r})\varepsilon^{\mathrm{PBE}}_{\mathrm{XC}}[n(\mathbf{r}), |\nabla n(\mathbf{r})|^2, \mu(\mathbf{r}), \beta(\mathbf{r})]\right\}}{\partial \beta(\mathbf{r})} \sum_{a'} \frac{\partial w_{a'}(\mathbf{r})}{\partial \mathbf{R}^a}\beta^{a'}\,\mathrm{d}\mathbf{r}.\end{aligned} \tag{B.9}$$

The μ derivative is

$$\begin{aligned}&\frac{\partial\left\{n(\mathbf{r})\varepsilon^{\mathrm{PBE}}_{\mathrm{XC}}[n(\mathbf{r}), |\nabla n(\mathbf{r})|^2, \mu(\mathbf{r}), \beta(\mathbf{r})]\right\}}{\partial \mu(\mathbf{r})} = \\ &\frac{\partial\left[n(\mathbf{r})\varepsilon^{\mathrm{LDA}}_{\mathrm{X}}\left(F^{\mathrm{PBE}}_{\mathrm{X}}[n(\mathbf{r}), |\nabla n(\mathbf{r})|^2, \mu(\mathbf{r})] + \left\{\frac{\varepsilon^{\mathrm{LDA}}_{\mathrm{C}}}{\varepsilon^{\mathrm{LDA}}_{\mathrm{X}}} + \frac{H[n(\mathbf{r}), |\nabla n(\mathbf{r})|^2, \beta(\mathbf{r})]}{\varepsilon^{\mathrm{LDA}}_{\mathrm{X}}}\right\}\right)\right]}{\partial \mu(\mathbf{r})} \\ &= n(\mathbf{r})\varepsilon^{\mathrm{LDA}}_{\mathrm{X}}\frac{\partial F^{\mathrm{PBE}}_{\mathrm{X}}}{\partial \mu} = n(\mathbf{r})\varepsilon^{\mathrm{LDA}}_{\mathrm{X}}\left[\frac{s^2}{(1+\mu s^2/\kappa)^2}\right].\end{aligned} \tag{B.10}$$

The β derivative is

$$\begin{aligned}
&\frac{\partial\left\{n(\mathbf{r})\varepsilon_{\mathrm{XC}}^{\mathrm{PBE}}[n(\mathbf{r}),|\nabla n(\mathbf{r})|^2,\mu(\mathbf{r}),\beta(\mathbf{r})]\right\}}{\partial\beta(\mathbf{r})} = \\
&\frac{\partial\left[n(\mathbf{r})\varepsilon_{\mathrm{X}}^{\mathrm{LDA}}\left(F_{\mathrm{X}}^{\mathrm{PBE}}[n(\mathbf{r}),|\nabla n(\mathbf{r})|^2,\mu(\mathbf{r})]+\left\{\frac{\varepsilon_{\mathrm{C}}^{\mathrm{LDA}}}{\varepsilon_{\mathrm{X}}^{\mathrm{LDA}}}+\frac{H[n(\mathbf{r}),|\nabla n(\mathbf{r})|^2,\beta(\mathbf{r})]}{\varepsilon_{\mathrm{X}}^{\mathrm{LDA}}}\right\}\right)\right]}{\partial\beta(\mathbf{r})} \\
=&n(\mathbf{r})\frac{\partial H}{\partial\beta} \\
=&\frac{Yt^2}{X\gamma}\left[\frac{1+2At^2}{1+At^2+A^2t^4}-\frac{(1+At^2)(At^2+2A^2t^4)}{(1+At^2+A^2t^4)^2}\right],
\end{aligned} \tag{B.11}$$

where

$$Y = \frac{e^2}{a_0}\gamma\phi^3, \tag{B.12}$$

$$H = Y\times\ln\left\{1+\frac{\beta}{\gamma}t^2\left[\frac{1+At^2}{1+At^2+A^2t^4}\right]\right\}, \tag{B.13}$$

$$X = 1+\frac{\beta}{\gamma}t^2\left[\frac{1+At^2}{1+At^2+A^2t^4}\right], \tag{B.14}$$

$$A = \frac{\beta}{\gamma}\left[\exp\left\{-\varepsilon_{\mathrm{c}}^{\mathrm{LDA}}/Y\right\}-1\right]^{-1}, \tag{B.15}$$

$$\frac{\delta A}{\delta\beta} = \frac{A}{\beta}. \tag{B.16}$$

Above e is the elementary charge, a_0 is the Bohr radius, $\gamma=(1-\ln 2)/\pi^2$, and $\phi=[(1+\zeta)^{2/3}+(1-\zeta)^{2/3}]/2$, where $\zeta=(n_\uparrow-n_\downarrow)/n$.

In order to get the $\delta w_{a'}(\mathbf{r})/\delta\mathbf{R}^a$ derivatives we notice that

$$P_{a'}(\mathbf{r}) = f\left(\sqrt{(r_x-R_x^{a'})^2+(r_y-R_y^{a'})^2+(r_z-R_z^{a'})^2}\right) \tag{B.17}$$

and so e.g.

$$\frac{\partial P_{a'}(\mathbf{r})}{\partial R_x^a} = -\delta_{aa'}f'\left(\sqrt{\cdots}\right)\frac{(r_x-R_x^a)}{|\mathbf{r}-\mathbf{R}^a|} = -\delta_{aa'}\frac{\partial P_a(\mathbf{r})}{\partial r_x}. \tag{B.18}$$

The whole gradient w.r.t. $\mathbf{R}^a$ ($\nabla_{\mathbf{R}^a}$) is therefore easily obtained from the gradient of $\mathbf{r}$ (∇):

$$\frac{\partial P_{a'}(\mathbf{r})}{\partial\mathbf{R}^a} = \delta_{aa'}\nabla_{\mathbf{R}^a}P_a(\mathbf{r}) = -\delta_{aa'}\frac{\partial P_a(\mathbf{r})}{\partial\mathbf{r}} = -\delta_{aa'}\nabla P_a(\mathbf{r}). \tag{B.19}$$

With the help of Eq. (B.19) we obtain the following expression for the $\delta w_{a'}(\mathbf{r}) / \delta \mathbf{R}^a$ derivatives:

$$\frac{\partial w_{a'}(\mathbf{r})}{\partial \mathbf{R}^a} = \frac{\partial}{\partial \mathbf{R}^a} \frac{P_{a'}(\mathbf{r})}{\sum_{a''} P_{a''}(\mathbf{r})} = \frac{\frac{\partial P_{a'}(\mathbf{r})}{\partial \mathbf{R}^a} \sum_{a''} P_{a''}(\mathbf{r}) - P_{a'}(\mathbf{r}) \sum_{a''} \frac{\partial P_{a''}(\mathbf{r})}{\partial \mathbf{R}^a}}{\left[\sum_{a''} P_{a''}(\mathbf{r})\right]^2} = \frac{-\delta_{aa'} \nabla P_a(\mathbf{r}) \sum_{a''} P_{a''}(\mathbf{r}) + P_{a'}(\mathbf{r}) \nabla P_a(\mathbf{r})}{\left[\sum_{a''} P_{a''}(\mathbf{r})\right]^2}. \tag{B.20}$$

B.3 Stress tensor

Analogously to the case of forces additional terms manifest in the stress tensor formula, because the $\mu(\mathbf{r})$ and $\beta(\mathbf{r})$ fields change as a function of strain. The derivations below make use of Ref. [144] which studies the computation of various stress tensor contributions in great detail. Stress tensor σ is defined as a first order change under a strain ϵ as

$$\sigma_{\alpha\beta} = \frac{1}{V} \frac{\partial E_{\text{tot}}}{\partial \epsilon_{\alpha\beta}}. \tag{B.21}$$

Since XC energy is an integral in real space, it can be shown that the XC contribution to the total stress tensor can be written as

$$V \sigma^{\text{XC}}_{\alpha\beta} = \frac{\partial E_{\text{XC}}}{\partial \epsilon_{\alpha\beta}} = \delta_{\alpha\beta} E_{\text{XC}} + \int_V \frac{\partial [n(\mathbf{r}) \varepsilon_{\text{XC}}(\mathbf{r})]}{\partial \epsilon_{\alpha\beta}} \, \mathrm{d}\mathbf{r}. \tag{B.22}$$

For QNA the second term in Eq. (B.22) becomes, with the help of the chain rule,

$$\int_V \frac{\partial \{n(\mathbf{r}) \varepsilon^{\text{PBE}}_{\text{XC}}[n(\mathbf{r}), |\nabla n(\mathbf{r})|^2, \mu(\mathbf{r}), \beta(\mathbf{r})]\}}{\partial \epsilon_{\alpha\beta}} \, \mathrm{d}\mathbf{r} \tag{B.23}$$

$$= \int_V \frac{\partial \{n(\mathbf{r}) \varepsilon^{\text{PBE}}_{\text{XC}}[n(\mathbf{r}), |\nabla n(\mathbf{r})|^2, \mu(\mathbf{r}), \beta(\mathbf{r})]\}}{\partial n(\mathbf{r})} \frac{\partial n(\mathbf{r})}{\partial \epsilon_{\alpha\beta}} \, \mathrm{d}\mathbf{r} \tag{B.24}$$

$$+ \int_V \frac{\partial \{n(\mathbf{r}) \varepsilon^{\text{PBE}}_{\text{XC}}[n(\mathbf{r}), |\nabla n(\mathbf{r})|^2, \mu(\mathbf{r}), \beta(\mathbf{r})]\}}{\partial \nabla n(\mathbf{r})} \cdot \frac{\partial \nabla n(\mathbf{r})}{\partial \epsilon_{\alpha\beta}} \, \mathrm{d}\mathbf{r} \tag{B.25}$$

$$+ \int_V \frac{\partial \{n(\mathbf{r}) \varepsilon^{\text{PBE}}_{\text{XC}}[n(\mathbf{r}), |\nabla n(\mathbf{r})|^2, \mu(\mathbf{r}), \beta(\mathbf{r})]\}}{\partial \mu(\mathbf{r})} \frac{\partial \mu(\mathbf{r})}{\partial \epsilon_{\alpha\beta}} \, \mathrm{d}\mathbf{r} \tag{B.26}$$

$$+ \int_V \frac{\partial \{n(\mathbf{r}) \varepsilon^{\text{PBE}}_{\text{XC}}[n(\mathbf{r}), |\nabla n(\mathbf{r})|^2, \mu(\mathbf{r}), \beta(\mathbf{r})]\}}{\partial \beta(\mathbf{r})} \frac{\partial \beta(\mathbf{r})}{\partial \epsilon_{\alpha\beta}} \, \mathrm{d}\mathbf{r}. \tag{B.27}$$

Below we expand each term one at a time (function arguments are dropped for simplicity). Eq. (B.24) is the LDA-level term and it can be written as

$$\int_V \frac{\partial\{n\varepsilon_{\mathrm{XC}}^{\mathrm{PBE}}\}}{\partial n}\frac{\partial n}{\partial\epsilon_{\alpha\beta}}\,\mathrm{d}\mathbf{r} = \int_V \frac{\partial n}{\partial\epsilon_{\alpha\beta}}\left[\varepsilon_{\mathrm{XC}}^{\mathrm{PBE}} + n\frac{\partial\varepsilon_{\mathrm{XC}}^{\mathrm{PBE}}}{\partial n}\right]\mathrm{d}\mathbf{r}. \tag{B.28}$$

Eq. (B.25) is the GGA-level gradient term and it can be written as

$$\int_V \frac{\partial\{n\varepsilon_{\mathrm{XC}}^{\mathrm{PBE}}\}}{\partial\nabla n}\cdot\frac{\partial\nabla n}{\partial\epsilon_{\alpha\beta}}\,\mathrm{d}\mathbf{r} = \int_V n\frac{\partial\varepsilon_{\mathrm{XC}}^{\mathrm{PBE}}}{\partial\nabla n}\cdot\frac{\partial\nabla n}{\partial\epsilon_{\alpha\beta}}\,\mathrm{d}\mathbf{r} \tag{B.29}$$

$$= \int_V n\frac{\partial\varepsilon_{\mathrm{XC}}^{\mathrm{PBE}}}{\partial|\nabla n|^2}\left(\frac{\partial|\nabla n|^2}{\partial\nabla n}\right)\cdot\left(\frac{\partial\nabla n}{\partial\epsilon_{\alpha\beta}}\right)\mathrm{d}\mathbf{r} \tag{B.30}$$

$$= 2\int_V n\frac{\partial\varepsilon_{\mathrm{XC}}^{\mathrm{PBE}}}{\partial|\nabla n|^2}(\nabla n)\cdot\left(\frac{\partial\nabla n}{\partial\epsilon_{\alpha\beta}}\right)\mathrm{d}\mathbf{r}, \tag{B.31}$$

where we have used the fact that $\partial|\nabla n|^2/\partial\nabla n = 2\nabla n$. These LDA and GGA terms are already handled by GPAW. Eq. (B.26) arises from the fact that the $\mu(\mathbf{r})$ field changes as a function of strain and it can be written as

$$\int_V \frac{\partial\{n\varepsilon_{\mathrm{XC}}^{\mathrm{PBE}}\}}{\partial\mu}\frac{\partial\mu}{\partial\epsilon_{\alpha\beta}}\,\mathrm{d}\mathbf{r} = \int_V n\frac{\partial\varepsilon_{\mathrm{XC}}^{\mathrm{PBE}}}{\partial\mu}\sum_a\frac{\partial w_a}{\partial\epsilon_{\alpha\beta}}\mu^a\,\mathrm{d}\mathbf{r} \tag{B.32}$$

$$= \int_V n\varepsilon_{\mathrm{X}}^{\mathrm{LDA}}\frac{\partial F_{\mathrm{X}}^{\mathrm{PBE}}}{\partial\mu}\sum_a\frac{\partial w_a}{\partial\epsilon_{\alpha\beta}}\mu^a\,\mathrm{d}\mathbf{r}. \tag{B.33}$$

Eq. (B.27) arises from the fact that the $\beta(\mathbf{r})$ field changes as a function of strain and it can be written as

$$\int_V \frac{\partial\{n\varepsilon_{\mathrm{XC}}^{\mathrm{PBE}}\}}{\partial\beta}\frac{\partial\beta}{\partial\epsilon_{\alpha\beta}}\,\mathrm{d}\mathbf{r} = \int_V n\frac{\partial\varepsilon_{\mathrm{XC}}^{\mathrm{PBE}}}{\partial\beta}\sum_a\frac{\partial w_a}{\partial\epsilon_{\alpha\beta}}\beta^a\,\mathrm{d}\mathbf{r} \tag{B.34}$$

$$= \int_V n\frac{\partial H}{\partial\beta}\sum_a\frac{\partial w_a}{\partial\epsilon_{\alpha\beta}}\beta^a\,\mathrm{d}\mathbf{r}. \tag{B.35}$$

$\partial F_{\mathrm{X}}^{\mathrm{PBE}}/\partial\mu$ and $\partial H/\partial\beta$ terms were already derived in the Forces section. The $\partial w_a/\epsilon_{\alpha\beta}$ derivative can be written as

$$\frac{\partial w_{a'}}{\partial\epsilon_{\alpha\beta}} = \frac{\partial}{\partial\epsilon_{\alpha\beta}}\frac{P_a}{\sum_{a'}P_{a'}} = \frac{\frac{\partial P_a}{\partial\epsilon_{\alpha\beta}}\sum_{a'}P_{a'} - P_a\sum_{a'}\frac{\partial P_{a'}}{\partial\epsilon_{\alpha\beta}}}{\left[\sum_{a'}P_{a'}\right]^2}. \tag{B.36}$$

To get the $\partial P_a/\epsilon_{\alpha\beta}$ derivative we use Eq. (15) of Ref. [144]:

$$\frac{\partial P_a}{\partial \epsilon_{\alpha\beta}} = \frac{\partial f(|\mathbf{r}-\mathbf{R}^a|)}{\partial \epsilon_{\alpha\beta}} = \frac{\partial f(|\mathbf{r}-\mathbf{R}^a|)}{\partial r_\alpha}(r_\beta - R^a_\beta) \tag{B.37}$$

$$= f'(|\mathbf{r}-\mathbf{R}^a|)\frac{r_\alpha - R^a_\alpha}{|\mathbf{r}-\mathbf{R}^a|}(r_\beta - R^a_\beta) = \frac{\partial P_a}{\partial r_\alpha}(r_\beta - R^a_\beta). \tag{B.38}$$

At the time of writing these correction terms for stress have not yet been implemented into GPAW, but it has been shown that terms like those of Eqs. (B.26) and (B.27), ones that are a consequence of the fact that the space has been partitioned, seem to be so small that they fall below the general numerical accuracy of DFT codes [144].

Bibliography

[1] Schwarz, K., Sham, L., Mattsson, A., Scheffler, M., "Obituary for Walter Kohn (1923–2016)", Computation **4**, 40 (2016), DOI: 10.3390/computation4040040 (See pp. 1, 6).

[2] Kohn, W., "Nobel Lecture: Electronic structure of matter—wave functions and density functionals", Reviews of Modern Physics **71**, 1253–1266 (1999), DOI: 10.1103/RevModPhys.71.1253 (See pp. 1, 5).

[3] Burke, K., *Viewpoint: Improving Electronic Structure Calculations*, (2016 [accessed November 29, 2017]) http://physics.aps.org/articles/v9/108#c3 (See p. 1).

[4] Anderson, A., *Uncertainty gives scientists new confidence in search for novel materials*, (2014 [accessed February 16, 2017]) http://web.ornl.gov/info/news/pulse/no422/story2.shtml (See p. 1).

[5] Pribram-Jones, A., Gross, D. A., Burke, K., "DFT: A Theory Full of Holes?", Annual review of physical chemistry **66**, 283–304 (2015), DOI: 10.1146/annurev-physchem-040214-121420 (See pp. 1, 5, 6, 14).

[6] Smith, J. C., Sagredo, F., Burke, K., "Warming Up Density Functional Theory", arXiv:1701.00873v1 (2017) (See p. 1).

[7] Brockherde, F., Vogt, L., Li, L., Tuckerman, M. E., Burke, K., Müller, K.-R., "Bypassing the Kohn-Sham equations with machine learning", Nature Communications **8**, 872 (2017), DOI: 10.1038/s41467-017-00839-3 (See p. 1).

[8] Wasserman, A., Nafziger, J., Jiang, K., Kim, M.-C., Sim, E., Burke, K., "The Importance of Being Inconsistent", Annual Review of Physical Chemistry **68**, 555–581 (2017), DOI: 10.1146/annurev-physchem-052516-044957 (See p. 1).

[9] Mattsson, A. E., "DENSITY FUNCTIONAL THEORY: In Pursuit of the "Divine" Functional", Science **298**, 759–760 (2002), DOI: 10.1126/science.1077710 (See pp. 2, 11).

[10] Booth, G. H., Grüneis, A., Kresse, G., Alavi, A., "Towards an exact description of electronic wavefunctions in real solids.", Nature **493**, 365–70 (2013), DOI: 10.1038/nature11770 (See p. 2).

[11] Van Noorden, R., Maher, B., Nuzzo, R., "The top 100 papers", Nature **514**, 550–553 (2014), DOI: 10.1038/514550a (See p. 2).

[12] Schrödinger, E., "An undulatory theory of the mechanics of atoms and molecules", Physical Review **28**, 1049–1070 (1926), DOI: 10.1103/PhysRev.28.1049 (See p. 5).

[13] Ribeiro, R. F., Lee, D., Cangi, A., Elliott, P., Burke, K., "Corrections to Thomas-Fermi Densities at Turning Points and Beyond", Physical Review Letters **114**, 050401 (2015), DOI: 10.1103/PhysRevLett.114.050401 (See pp. 5, 14).

[14] Ribeiro, R. F., Burke, K., "Uniform semiclassical approximations for one-dimensional fermionic systems", arXiv:1510.05676 (2015) (See pp. 5, 14).

[15] Ribeiro, R. F., Burke, K., "Leading corrections to local approximations. II. The case with turning points", Physical Review B **95**, 115115 (2017), DOI: 10.1103/PhysRevB.95.115115 (See pp. 5, 14).

[16] Johnson, W. R., *Atomic Structure Theory* (Springer-Verlag Berlin Heidelberg, Berlin, Heidelberg : 2007), p. 317, DOI: 10.1007/978-3-540-68013-0 (See pp. 6, 59, 60).

[17] Thomas, L. H., "The calculation of atomic fields", Mathematical Proceedings of the Cambridge Philosophical Society **23**, 542–548 (1927), DOI: 10.1017/S0305004100011683 (See p. 6).

[18] Fermi, E., "Un metodo statistico per la determinazione di alcune priorieta dellatomo", Atti Acad.Naz.Lincei, Rend. **6**, 602–607 (1927) (See p. 6).

[19] Dirac, P. A. M., "Note on Exchange Phenomena in the Thomas Atom", Mathematical Proceedings of the Cambridge Philosophical Society **26**, 376 (1930), DOI: 10.1017/S0305004100016108 (See pp. 6, 14).

[20] Becke, A. D., "Perspective: Fifty years of density-functional theory in chemical physics", The Journal of Chemical Physics **140**, 18A301 (2014), DOI: 10.1063/1.4869598 (See pp. 6, 18).

[21] Hohenberg, P., Kohn, W., "Inhomogeneous Electron Gas", Physical Review **136**, B864–B871 (1964), DOI: 10.1103/PhysRev.136.B864 (See p. 6).

[22] Fiolhais, C., Nogueira, F., Marques, M., Engel, E., "A Primer in Density Functional Theory", Materials Today **6**, 59 (2003), DOI: 10.1016/S1369-7021(03)01229-X (See pp. 6, 12, 16, 17, 20).

[23] R. M. Martin, *Electronic Structure: Basic Theory and Practical Methods* (Cambridge University Press, 2005) (See pp. 6–8, 12, 14, 16).

[24] Burke, K., *The ABC of DFT*, (2007 [accessed February 21, 2017]) http://dft.uci.edu/doc/g1.pdf (See pp. 6, 9, 12, 16, 17, 19, 29).

[25] R. M. Dreizler, Gross, E. K. U., *Density Functional Theory* (Springer-Verlag, Berlin Heidelberg, 1990) (See pp. 6, 8, 16).

[26] Engel, E., Dreizler, R. M., *Density Functional Theory: An advanced Course*, Theoretical and Mathematical Physics (Springer Berlin Heidelberg, Berlin, Heidelberg, 2011), pp. 255–368, DOI: 10.1007/978-3-642-14090-7 (See p. 6).

[27] Kohn, W., Sham, L. J., "Self-Consistent Equations Including Exchange and Correlation Effects", Physical Review **140**, A1133–A1138 (1965), DOI: 10.1103/PhysRev.140.A1133 (See pp. 8, 13, 15).

[28] Wagner, L. O., Stoudenmire, E. M., Burke, K., White, S. R., "Guaranteed Convergence of the Kohn-Sham Equations", Physical Review Letters **111**, 093003 (2013), DOI: 10.1103/PhysRevLett.111.093003 (See p. 10).

[29] Hartree, D. R., "The Wave Mechanics of an Atom with a Non-Coulomb Central Field. Part I. Theory and Methods", Mathematical Proceedings of the Cambridge Philosophical Society **24**, 89 (1928), DOI: 10.1017/S0305004100011919 (See p. 11).

[30] Hartree, D. R., "The Wave Mechanics of an Atom with a Non-Coulomb Central Field. Part II. Some Results and Discussion", Mathematical Proceedings of the Cambridge Philosophical Society **24**, 111 (1928), DOI: 10.1017/S0305004100011920 (See p. 11).

[31] Hartree, D. R., "The Wave Mechanics of an Atom with a non-Coulomb Central Field. Part III. Term Values and Intensities in Series in Optical Spectra", Mathematical Proceedings of the Cambridge Philosophical Society **24**, 426 (1928), DOI: 10.1017/S030500410001595 4 (See p. 11).

[32] Kurth, S., Perdew, J. P., "Role of the exchange-correlation energy: Nature's glue", International Journal of Quantum Chemistry **77**, 814–818 (2000), DOI: 10.1002/(SICI)1097-461X(2000)77:5<814::AID-QUA3>3.0.CO;2-F (See p. 11).

[33] Lejaeghere, K., Bihlmayer, G., Bjorkman, T., Blaha, P., Blugel, S., Blum, V., Caliste, D., Castelli, I. E., Clark, S. J., Dal Corso, A., Gironcoli, S., Deutsch, T., Dewhurst, J. K., Di Marco, I., Draxl, C., Du ak, M., Eriksson, O., Flores-Livas, J. A., Garrity, K. F., Genovese, L., Giannozzi, P., Giantomassi, M., Goedecker, S., Gonze, X., Granas, O., Gross, E. K. U., Gulans, A., Gygi, F., Hamann, D. R., Hasnip, P. J., Holzwarth, N. A. W., Iu an, D., Jochym, D. B., Jollet, F., Jones, D., Kresse, G., Koepernik, K., Kucukbenli, E., Kvashnin, Y. O., Locht, I. L. M., Lubeck, S., Marsman, M., Marzari, N., Nitzsche, U., Nordstrom, L., Ozaki, T., Paulatto, L., Pickard, C. J., Poelmans, W., Probert, M. I. J., Refson, K., Richter, M., Rignanese, G.-M., Saha, S., Scheffler, M., Schlipf, M., Schwarz, K., Sharma, S., Tavazza, F., Thunstrom, P., Tkatchenko, A., Torrent, M., Vanderbilt, D., Setten, M. J., Van Speybroeck, V., Wills, J. M., Yates, J. R., Zhang, G.-X., Cottenier, S., "Reproducibility in density functional theory calculations of solids", Science **351**, aad3000 (2016), DOI: 10.1126/science.aad3000 (See p. 11).

[34] Jones, R. O., "Density functional theory: Its origins, rise to prominence, and future", Reviews of Modern Physics **87** (2015), DOI: 10.1103/RevModPhys.87.897 (See pp. 12, 18, 44).

[35] Fock, V., "Näherungsmethode zur Lösung des quantenmechanischen Mehrkörperproblems", Zeitschrift für Physik **61**, 126–148 (1930), DOI: 10.1007/BF01340294 (See p. 14).

[36] Ceperley, D. M., Alder, B. J., "Ground State of the Electron Gas by a Stochastic Method", Physical Review Letters **45**, 566–569 (1980), DOI: 10.1103/PhysRevLett.45.566 (See p. 15).

[37] Vosko, S. H., Wilk, L., Nusair, M., "Accurate spin-dependent electron liquid correlation energies for local spin density calculations: a critical analysis", Canadian Journal of Physics **58**, 1200–1211 (1980), DOI: 10.1139/p80-159 (See pp. 15, 61).

[38] Perdew, J. P., Zunger, A., "Self-interaction correction to density-functional approximations for many-electron systems", Physical Review B **23**, 5048–5079 (1981), DOI: 10.1103/PhysRevB.23.5048 (See p. 15).

[39] Perdew, J. P., Wang, Y., "Accurate and simple analytic representation of the electron-gas correlation energy", Physical Review B **45**, 13244–13249 (1992), DOI: 10.1103/PhysRevB.45.13244 (See p. 15).

[40] Levy, M., Perdew, J. P., "Hellmann-Feynman, virial, and scaling requisites for the exact universal density functionals. Shape of the correlation potential and diamagnetic susceptibility for atoms", Physical

Review A **32**, 2010–2021 (1985), DOI: 10.1103/PhysRevA.32.2010 (See pp. 16, 17).

[41] Burke, K., Perdew, J. P., Ernzerhof, M., "Why the generalized gradient approximation works and how to go beyond it", International Journal of Quantum Chemistry **61**, 287–293 (1997), DOI: 10.1002/(SICI)1097-461X(1997)61:2<287::AID-QUA11>3.0.CO;2-9 (See p. 16).

[42] Perdew, J. P., Ruzsinszky, A., "Fourteen easy lessons in density functional theory", International Journal of Quantum Chemistry **110**, 2801–2807 (2010), DOI: 10.1002/qua.22829 (See p. 16).

[43] Cohen, A. J., Mori-Sánchez, P., Yang, W., "Challenges for Density Functional Theory", Chemical Reviews **112**, 289–320 (2012), DOI: 10.1021/cr200107z (See pp. 16, 18).

[44] Perdew, J. P., "Density-functional approximation for the correlation energy of the inhomogeneous electron gas", Physical Review B **33**, 8822–8824 (1986), DOI: 10.1103/PhysRevB.33.8822 (See p. 16).

[45] Langreth, D. C., Mehl, M. J., "Beyond the local-density approximation in calculations of ground-state electronic properties", Physical Review B **28**, 1809–1834 (1983), DOI: 10.1103/PhysRevB.28.1809 (See p. 16).

[46] Perdew, J. P., "Accurate Density Functional for the Energy: Real-Space Cutoff of the Gradient Expansion for the Exchange Hole", Physical Review Letters **55**, 1665–1668 (1985), DOI: 10.1103/PhysRevLett.55.1665 (See p. 16).

[47] Perdew, J. P., Yue, W., "Accurate and simple density functional for the electronic exchange energy: Generalized gradient approximation", Physical Review B **33**, 8800–8802 (1986), DOI: 10.1103/PhysRevB.33.8800 (See p. 16).

[48] Perdew, J. P., Chevary, J. A., Vosko, S. H., Jackson, K. A., Pederson, M. R., Singh, D. J., Fiolhais, C., "Atoms, molecules, solids, and surfaces: Applications of the generalized gradient approximation for exchange and correlation", Physical Review B **46**, 6671–6687 (1992), DOI: 10.1103/PhysRevB.46.6671 (See p. 16).

[49] Perdew, J. P., Schmidt, K., "Jacob's ladder of density functional approximations for the exchange-correlation energy", AIP Conference Proceedings **577**, edited by V. V. VanDoren C Geerlings,P., 1–20 (2001), DOI: 10.1063/1.1390175 (See pp. 16, 21).

[50] Della Sala, F., Fabiano, E., Constantin, L. A., "Kinetic-energy-density dependent semilocal exchange-correlation functionals", International Journal of Quantum Chemistry **116**, 1641–1694 (2016), DOI: 10.1002/qua.25224 (See p. 16).

[51] Perdew, J. P., Constantin, L. a., Sagvolden, E., Burke, K., "Relevance of the slowly varying electron gas to atoms, molecules, and solids", Physical Review Letters **97**, 1–4 (2006), DOI: 10.1103/PhysRevLett.97.223002 (See p. 17).

[52] Ma, S.-K., Brueckner, K. A., "Correlation Energy of an Electron Gas with a Slowly Varying High Density", Physical Review **165**, 18–31 (1968), DOI: 10.1103/PhysRev.165.18 (See p. 17).

[53] Marques, M. A., Oliveira, M. J., Burnus, T., "Libxc: A library of exchange and correlation functionals for density functional theory", Computer Physics Communications **183**, 2272–2281 (2012), DOI: 10.1016/j.cpc.2012.05.007 (See p. 18).

[54] Wu, Z., Cohen, R. E., "More accurate generalized gradient approximation for solids", Physical Review B **73**, 235116 (2006), DOI: 10.1103/PhysRevB.73.235116 (See pp. 18, 21, 23).

[55] Burke, K., "Perspective on density functional theory", The Journal of Chemical Physics **136**, 150901 (2012), DOI: 10.1063/1.4704546 (See pp. 18, 46).

[56] Su, N. Q., Xu, X., "Development of New Density Functional Approximations", Annual Review of Physical Chemistry **68**, 8.1–8.28 (2017), DOI: 10.1146/annurev-physchem-052516-044835 (See p. 18).

[57] Perdew, J. P., Burke, K., Ernzerhof, M., "Generalized Gradient Approximation Made Simple", Physical Review Letters **77**, 3865–3868 (1996), DOI: 10.1103/PhysRevLett.77.3865 (See pp. 18–20).

[58] Lieb, E. H., Oxford, S., "Improved lower bound on the indirect Coulomb energy", International Journal of Quantum Chemistry **19**, 427–439 (1981), DOI: 10.1002/qua.560190306 (See p. 20).

[59] Mattsson, A. E., Armiento, R., Schultz, P. A., Mattsson, T. R., "Nonequivalence of the generalized gradient approximations PBE and PW91", Physical Review B **73**, 195123 (2006), DOI: 10.1103/PhysRevB.73.195123 (See p. 20).

[60] Perdew, J. P., Ruzsinszky, A., Csonka, G. I., Vydrov, O. A., Scuseria, G. E., Constantin, L. A., Zhou, X., Burke, K., "Restoring the Density-Gradient Expansion for Exchange in Solids and Surfaces", Physical Review Letters **100**, 136406 (2008), DOI: 10.1103/PhysRevLett.100.136406 (See pp. 20, 23).

[61] Tao, J., Perdew, J. P., Staroverov, V. N., Scuseria, G. E., "Climbing the Density Functional Ladder: Non-Empirical Meta-Generalized Gradient Approximation Designed for Molecules and Solids", Physical Review Letters **91**, 146401 (2003), DOI: 10.1103/PhysRevLett.91.146401 (See p. 21).

[62] Ropo, M., Kokko, K., Vitos, L., "Assessing the Perdew-Burke-Ernzerhof exchange-correlation density functional revised for metallic bulk and surface systems", Physical Review B **77**, 195445 (2008), DOI: 10.1103/PhysRevB.77.195445 (See p. 21).

[63] Haas, P., Tran, F., Blaha, P., "Calculation of the lattice constant of solids with semilocal functionals", Physical Review B **79**, 85104 (2009), DOI: 10.1103/PhysRevB.79.085104 (See p. 21).

[64] Csonka, G. I., Perdew, J. P., Ruzsinszky, A., Philipsen, P. H. T., Lebègue, S., Paier, J., Vydrov, O. a., Ángyán, J. G., "Assessing the performance of recent density functionals for bulk solids", Physical Review B **79**, 155107 (2009), DOI: 10.1103/PhysRevB.79.155107 (See pp. 21, 25).

[65] Haas, P., Tran, F., Blaha, P., Pedroza, L. S., Da Silva, A. J. R., Odashima, M. M., Capelle, K., "Systematic investigation of a family of gradient-dependent functionals for solids", Physical Review B **81**, 125136 (2010), DOI: 10.1103/PhysRevB.81.125136 (See p. 21).

[66] Armiento, R., Mattsson, a. E., "Functional designed to include surface effects in self-consistent density functional theory", Physical Review B **72**, 1–5 (2005), DOI: 10.1103/PhysRevB.72.085108 (See p. 21).

[67] Mattsson, A. E., Armiento, R., Paier, J., Kresse, G., Wills, J. M., Mattsson, T. R., "The AM05 density functional applied to solids", The Journal of Chemical Physics **128**, 084714 (2008), DOI: 10.1063/1.2835596 (See p. 21).

[68] Mattsson, A. E., Armiento, R., "Implementing and testing the AM05 spin density functional", Physical Review B **79**, 155101 (2009), DOI: 10.1103/PhysRevB.79.155101 (See p. 21).

[69] Haas, P., Tran, F., Blaha, P., Schwarz, K., "Construction of an optimal GGA functional for molecules and solids", Physical Review B **83**, 205117 (2011), DOI: 10.1103/PhysRevB.83.205117 (See p. 21).

[70] Constantin, L. A., Terentjevs, A., Della Sala, F., Cortona, P., Fabiano, E., "Semiclassical atom theory applied to solid-state physics", Physical Review B **93**, 045126 (2016), DOI: 10.1103/PhysRevB.93.045126 (See pp. 21, 33).

[71] Perdew, J. P., Ruzsinszky, A., Tao, J., Staroverov, V. N., Scuseria, G. E., Csonka, G. I., "Prescription for the design and selection of density functional approximations: More constraint satisfaction with fewer fits", The Journal of Chemical Physics **123**, 062201 (2005), DOI: 10.1063/1.1904565 (See p. 21).

[72] Perdew, J. P., Ruzsinszky, A., Constantin, L. A., Sun, J., Csonka, G. I., "Some Fundamental Issues in Ground-State Density Functional Theory: A Guide for the Perplexed", Journal of Chemical Theory and Computation **5**, 902–908 (2009), DOI: 10.1021/ct800531s (See p. 21).

[73] Tran, F., Stelzl, J., Blaha, P., "Rungs 1 to 4 of DFT Jacob's ladder: extensive test on the lattice constant, bulk modulus, and cohesive energy of solids", The Journal of Chemical Physics **144**, 1–20 (2016), DOI: 10.1063/1.4948636 (See p. 21).

[74] Kohn, W., Mattsson, A. E., "Edge Electron Gas", Physical Review Letters **81**, 3487–3490 (1998), DOI: 10.1103/PhysRevLett.81.3487 (See pp. 21, 22).

[75] Mattsson, A. E., Kohn, W., "An energy functional for surfaces", Journal of Chemical Physics **115**, 3441–3443 (2001), DOI: 10.1063/1.1396649 (See pp. 21, 22).

[76] Armiento, R., Mattsson, A., "Subsystem functionals in density-functional theory: Investigating the exchange energy per particle", Physical Review B **66**, 1–17 (2002), DOI: 10.1103/PhysRevB.66.165117 (See pp. 21, 22).

[77] Mattsson, A. E., Armiento, R., "The subsystem functional scheme: The Armiento-Mattsson 2005 (AM05) functional and beyond", International Journal of Quantum Chemistry **110**, 2274–2282 (2010), DOI: 10.1002/qua.22601 (See p. 21).

[78] Hao, F., Armiento, R., Mattsson, A. E., "Subsystem functionals and the missing ingredient of confinement physics in density functionals", Physical Review B **82**, 115103 (2010), DOI: 10.1103/PhysRevB.82.115103 (See p. 21).

[79] Kohn, W., "Density Functional and Density Matrix Method Scaling Linearly with the Number of Atoms", Physical Review Letters **76**, 3168–3171 (1996), DOI: 10.1103/PhysRevLett.76.3168 (See p. 21).

[80] Vitos, L., *Computational Quantum Mechanics for Materials Engineers*, Engineering Materials and Processes (Springer-Verlag, London, 2007), DOI: 10.1007/978-1-84628-951-4 (See pp. 22, 32).

[81] Fabiano, E., Constantin, L. A., Della Sala, F., "Two-Dimensional Scan of the Performance of Generalized Gradient Approximations with Perdew–Burke–Ernzerhof-Like Enhancement Factor", Journal of Chemical Theory and Computation **7**, 3548–3559 (2011), DOI: 10.1021/ct200510s (See pp. 23, 24).

[82] Yao, Y., Kanai, Y., "Plane-wave pseudopotential implementation and performance of SCAN meta-GGA exchange-correlation functional for extended systems", The Journal of Chemical Physics **146**, 224105 (2017), DOI: 10.1063/1.4984939 (See p. 23).

[83] Powell, M., "Least Frobenius norm updating of quadratic models that satisfy interpolation conditions", Mathematical Programming **100**, 183–215 (2004), DOI: 10.1007/s10107-003-0490-7 (See p. 24).

[84] Fuchs, M., Bockstedte, M., Pehlke, E., Scheffler, M., "Pseudopotential study of binding properties of solids within generalized gradient approximations: The role of core-valence exchange correlation", Physical Review B **57**, 2134–2145 (1998), DOI: 10.1103/PhysRevB.57.2134 (See p. 25).

[85] Zupan, A., Blaha, P., Schwarz, K., Perdew, J., "Pressure-induced phase transitions in solid Si, SiO2, and Fe: Performance of local-spin-density and generalized-gradient-approximation density functionals", Physical Review B **58**, 11266–11272 (1998), DOI: 10.1103/PhysRevB.58.11266 (See p. 25).

[86] Ruban, a. V., Abrikosov, I. a., "Configurational thermodynamics of alloys from first principles: effective cluster interactions", Reports on Progress in Physics **71**, 046501 (2008), DOI: 10.1088/0034-4885/71/4/046501 (See p. 25).

[87] Haas, P., Tran, F., Blaha, P., Schwarz, K., Laskowski, R., "Insight into the performance of GGA functionals for solid-state calculations", Physical Review B - Condensed Matter and Materials Physics **80**, 195109 (2009), DOI: 10.1103/PhysRevB.80.195109 (See pp. 25, 26, 29).

[88] Zhang, Y., Kresse, G., Wolverton, C., "Nonlocal First-Principles Calculations in Cu-Au and Other Intermetallic Alloys", Physical Review Letters **112**, 075502 (2014), DOI: 10.1103/PhysRevLett.112.075502 (See pp. 30, 51, 55).

[89] Decolvenaere, E., Gordon, M. J., Van der Ven, A., "Testing Predictions from Density Functional Theory at Finite Temperatures: β_2-Like Ground States in Co-Pt", Physical Rewiev B **085119**, 1–8 (2015), DOI: 10.1103/PhysRevB.92.085119 (See pp. 30, 58, 59).

[90] Hutchinson, M., Widom, M., "VASP on a GPU: Application to exact-exchange calculations of the stability of elemental boron", Computer Physics Communications **183**, 1422–1426 (2012), DOI: 10.1016/j.cpc.2012.02.017 (See p. 30).

[91] Hacene, M., Anciaux-Sedrakian, A., Rozanska, X., Klahr, D., Guignon, T., Fleurat-Lessard, P., "Accelerating VASP electronic structure calculations using graphic processing units", Journal of Computational Chemistry **33**, 2581–2589 (2012), DOI: 10.1002/jcc.23096 (See p. 30).

[92] Mortensen, J. J., Hansen, L. B., Jacobsen, K. W., "Real-space grid implementation of the projector augmented wave method", Physical Review B **71**, 035109 (2005), DOI: 10.1103/PhysRevB.71.035109 (See pp. 32, 56).

[93] Enkovaara, J., Rostgaard, C., Mortensen, J. J., Chen, J., Dułak, M., Ferrighi, L., Gavnholt, J., Glinsvad, C., Haikola, V., Hansen, H. A., Kristoffersen, H. H., Kuisma, M., Larsen, A. H., Lehtovaara, L., Ljungberg, M., Lopez-Acevedo, O., Moses, P. G., Ojanen, J., Olsen, T., Petzold, V., Romero, N. A., Stausholm-Møller, J., Strange, M., Tritsaris, G. A., Vanin, M., Walter, M., Hammer, B., Häkkinen, H., Madsen, G. K. H., Nieminen, R. M., Nørskov, J. K., Puska, M., Rantala, T. T., Schiøtz, J., Thygesen, K. S., Jacobsen, K. W., "Electronic structure calculations with GPAW: a real-space implementation of the projector augmented-wave method", Journal of Physics: Condensed Matter **22**, 253202 (2010), DOI: 10.1088/0953-8984/22/25/253202 (See pp. 32, 56).

[94] Constantin, L. a., Fabiano, E., Laricchia, S., Della Sala, F., "Semiclassical Neutral Atom as a Reference System in Density Functional Theory", Physical Review Letters **106**, 186406 (2011), DOI: 10.1103/PhysRevLett.106.186406 (See p. 33).

[95] Karasiev, V. V., Chakraborty, D., Trickey, S. B., "Progress on New Approaches to Old Ideas: Orbital-Free Density Functionals", in *Many-Electron Approaches in Physics, Chemistry and Mathematics*, May (2014), pp. 113–134, DOI: 10.1007/978-3-319-06379-9_6 (See pp. 35–37).

[96] White, T. G., Richardson, S., Crowley, B. J. B., Pattison, L. K., Harris, J. W. O., Gregori, G., "Orbital-Free Density-Functional Theory Simulations of the Dynamic Structure Factor of Warm Dense Aluminum", Physical Review Letters **111**, 175002 (2013), DOI: 10.1103/PhysRevLett.111.175002 (See p. 35).

[97] Wang, Y. A., Carter, E. A., "Orbital-Free Kinetic-Energy Density Functional Theory", in *Theoretical Methods in Condensed Phase Chemistry*, Vol. 184 (Kluwer Academic Publishers, Dordrecht, 2000), pp. 117–184, DOI: 10.1007/0-306-46949-9_5 (See p. 35).

[98] Chen, M., Jiang, X. W., Zhuang, H., Wang, L. W., Carter, E. A., "Petascale Orbital-Free Density Functional Theory Enabled by Small-Box Algorithms", Journal of Chemical Theory and Computation **12**, 2950–2963 (2016), DOI: 10.1021/acs.jctc.6b00326 (See p. 36).

[99] Karasiev, V. V., Trickey, S. B., "Frank Discussion of the Status of Ground-State Orbital-Free DFT", in *Advances in Quantum Chemistry*, Vol. 71, edited by J. Sabin and R. Cabrera-Trujillo (Elsevier, 2015) Chap. 9, pp. 221–245, DOI: 10.1016/bs.aiq.2015.02.004 (See p. 36).

[100] Levy, M., Perdew, J. P., Sahni, V., "Exact differential equation for the density and ionization energy of a many-particle system", Physical Review A **30**, 2745–2748 (1984), DOI: 10.1103/PhysRevA.30.2745 (See p. 37).

[101] Weizsäcker, C. F. v., "Zur Theorie der Kernmassen", Zeitschrift für Physik **96**, 431–458 (1935), DOI: 10.1007/BF01337700 (See p. 37).

[102] Karasiev, V. V., Trickey, S. B., "Issues and challenges in orbital-free density functional calculations", Computer Physics Communications **183**, 2519–2527 (2012), DOI: 10.1016/j.cpc.2012.06.016 (See pp. 38, 40).

[103] Lehtomäki, J., Makkonen, I., Caro, M. A., Harju, A., Lopez-Acevedo, O., "Orbital-free density functional theory implementation with the projector augmented-wave method", Journal of Chemical Physics **141**, 234102 (2014), DOI: 10.1063/1.4903450 (See p. 38).

[104] Tran, F., Wesolowski, T. A., "Semilocal Approximations for the Kinetic Energy", in *Recent Progress in Orbital-free Density Functional Theory*, edited by T. A. Wesolowski and Y. A. Wang (World Scientific, 2013) Chap. 16, pp. 429–442, DOI: 10.1142/9789814436731_0016 (See p. 38).

[105] March, N., "The local potential determining the square root of the ground-state electron density of atoms and molecules from the Schrödinger equation", Physics Letters A **113**, 476–478 (1986), DOI: 10.1016/0375-9601(86)90123-4 (See p. 38).

[106] Yonei, K., Tomishima, Y., "On the Weizsäcker Correction to the Thomas-Fermi Theory of the Atom", Journal of the Physical Society of Japan **20**, 1051–1057 (1965), DOI: 10.1143/JPSJ.20.1051 (See p. 39).

[107] Levy, M., Hui Ou-Yang, Ou-yang, H., "Exact properties of the Pauli potential for the square root of the electron density and the kinetic energy functional", Physical Review A **38**, 625–629 (1988), DOI: 10.1103/PhysRevA.38.625 (See pp. 39, 40).

[108] March, N. H., "Concept of the Pauli potential in density functional theory", Journal of Molecular Structure: THEOCHEM **943**, 77–82 (2010), DOI: 10.1016/j.theochem.2009.10.030 (See p. 40).

[109] Amovilli, C., March, N., "Bosonised DFT potential estimated from QMC calculations of the ground-state density for the inhomogeneous electron liquid in Be", Physics and Chemistry of Liquids, 1–6 (2015), DOI: 10.1080/00319104.2015.1020806 (See p. 40).

[110] Della Sala, F., Fabiano, E., Constantin, L. A., "Kohn-Sham kinetic energy density in the nuclear and asymptotic regions: Deviations from the von Weizsäcker behavior and applications to density functionals", Physical Review B **91**, 035126 (2015), DOI: 10.1103/PhysRevB.91.035126 (See pp. 40, 43).

[111] Esquivel, R. O., Chen, J., Stott, M. J., Sagar, R. P., Smith, V. H., "Pseudoconvexity of the atomic electron density: Lower and upper bounds", Physical Review A **47**, 936–943 (1993), DOI: 10.1103/PhysRevA.47.936 (See p. 41).

[112] Nagy, Á., Sen, K., "Exact results on the curvature of the electron density at the cusp in certain highly excited states of atoms", Chemical Physics Letters **332**, 154–158 (2000), DOI: 10.1016/S0009-2614(00)01250-1 (See p. 41).

[113] Nagy, Á., Sen, K. D., "Higher-order cusp of the density in certain highly excited states of atoms and molecules", Journal of Physics B: Atomic, Molecular and Optical Physics **33**, 1745–1751 (2000), DOI: 10.1088/0953-4075/33/9/306 (See p. 41).

[114] Nagy, Á., Sen, K. D., "Ground- and excited-state cusp conditions for the electron density", The Journal of Chemical Physics **115**, 6300 (2001), DOI: 10.1063/1.1402165 (See pp. 41, 42, 44).

[115] Qian, Z., "Exchange and correlation near the nucleus in density functional theory", Physical Review B **75**, 193104 (2007), DOI: 10.1103/PhysRevB.75.193104 (See pp. 41, 42, 44).

[116] Kato, T., "On the eigenfunctions of many-particle systems in quantum mechanics", Communications on Pure and Applied Mathematics **10**, 151–177 (1957), DOI: 10.1002/cpa.3160100201 (See p. 44).

[117] Constantin, L., Fabiano, E., Della Sala, F., "Kinetic and Exchange Energy Densities near the Nucleus", Computation **4**, 19 (2016), DOI: 10.3390/computation4020019 (See p. 44).

[118] Nagy, Á., "Alternative descriptors of Coulomb systems and their relationship to the kinetic energy", Chemical Physics Letters **460**, 343–346 (2008), DOI: 10.1016/j.cplett.2008.05.077 (See pp. 44, 45).

[119] Nagy, Á., "Functional derivative of the kinetic energy functional for spherically symmetric systems", Journal of Chemical Physics **135**, 44106 (2011), DOI: 10.1063/1.3607313 (See pp. 44–46).

[120] Nagy, Á., "Kinetic Energy and Fisher Information", in *Recent Progress in Orbital-free Density Functional Theory*, edited by T. A. Wesolowski and Y. A. Wang (World Scientific, May 2013), pp. 387–400, DOI: 10.1142/9789814436731_0014 (See pp. 44, 45).

[121] March, N., Young, W., "Approximate solutions of the density matrix equation for a local average field", Nuclear Physics **12**, 237–240 (1959), DOI: 10.1016/0029-5582(59)90169-5 (See p. 45).

[122] Ryabinkin, I. G., Staroverov, V. N., "Determination of Kohn–Sham effective potentials from electron densities using the differential virial theorem", The Journal of Chemical Physics **137**, 164113 (2012), DOI: 10.1063/1.4763481 (See p. 45).

[123] Ryabinkin, I. G., Staroverov, V. N., "Exact relations between the electron density and external potential for systems of interacting and noninteracting electrons", International Journal of Quantum Chemistry **113**, 1626–1632 (2013), DOI: 10.1002/qua.24374 (See p. 45).

[124] Holas, A., March, N. H., Rubio, A., "Differential virial theorem in relation to a sum rule for the exchange-correlation force in density-functional theory", The Journal of Chemical Physics **123**, 194104 (2005), DOI: 10.1063/1.2114848 (See p. 45).

[125] Nagy, A., March, N. H., Nagy, Á., March, N. H., "Exact potential-phase relation for the ground state of the C atom", Physical Review A **40**, 554–557 (1989), DOI: 10.1103/PhysRevA.40.554 (See p. 45).

[126] Holas, A., March, N. H., "Exact exchange-correlation potential and approximate exchange potential in terms of density matrices", Physical Review A **51**, 2040–2048 (1995), DOI: 10.1103/PhysRevA.51.2040 (See p. 45).

[127] Gross, E. K. U., Oliveira, L. N., Kohn, W., "Density-functional theory for ensembles of fractionally occupied states. I. Basic formalism", Physical Review A **37**, 2809–2820 (1988), DOI: 10.1103/PhysRevA.37.2809 (See p. 46).

[128] Oliveira, L. N., Gross, E. K. U., Kohn, W., "Density-functional theory for ensembles of fractionally occupied states. II. Application to the He atom", Physical Review A **37**, 2821–2833 (1988), DOI: 10.1103/PhysRevA.37.2821 (See p. 46).

[129] Theophilou, A. K., "The energy density functional formalism for excited states", Journal of Physics C: Solid State Physics **12**, 5419–5430 (1979), DOI: 10.1088/0022-3719/12/24/013 (See p. 46).

[130] Gori-Giorgi, P., Gál, T., Baerends, E. J., "Asymptotic behaviour of the electron density and the Kohn–Sham potential in case of a Kohn–Sham HOMO nodal plane", Molecular Physics **114**, 1086–1097 (2016), DOI: 10.1080/00268976.2015.1137643 (See p. 46).

[131] Hultgren, R., Desai, P., Hawkins, D., Gleiser, M., Kelley, K., *Selected Values of the Thermodynamic Properties of Binary Alloys* (American Society for Metals, Metals Park (OH), 1973) (See p. 51).

[132] Heyd, J., Scuseria, G. E., Ernzerhof, M., "Hybrid functionals based on a screened Coulomb potential", Journal of Chemical Physics **118**, 8207–8215 (2003), DOI: 10.1063/1.1564060 (See p. 51).

[133] Blum, V., Gehrke, R., Hanke, F., Havu, P., Havu, V., Ren, X., Reuter, K., Scheffler, M., "Ab initio molecular simulations with numeric atom-centered orbitals", Computer Physics Communications **180**, 2175–2196 (2009), DOI: 10.1016/j.cpc.2009.06.022 (See p. 55).

[134] Havu, V., Blum, V., Havu, P., Scheffler, M., "Efficient O(N) integration for all-electron electronic structure calculation using numeric basis functions", Journal of Computational Physics **228**, 8367–8379 (2009), DOI: 10.1016/j.jcp.2009.08.008 (See p. 55).

[135] Sun, J., Ruzsinszky, A., Perdew, J. P. J., "Strongly Constrained and Appropriately Normed Semilocal Density Functional", Physical Review Letters **115**, 036402 (2015), DOI: 10.1103/PhysRevLett.115.036402 (See p. 55).

[136] Čertík, O., Pask, J. E., Vackář, J., "Dftatom: A robust and general Schrödinger and Dirac solver for atomic structure calculations", Computer Physics Communications **184**, 1777–1791 (2013), DOI: 10.1016/j.cpc.2013.02.014 (See pp. 59–61).

[137] Kotochigova, S., Levine, Z. H., Shirley, E. L., Stiles, M. D., Clark, C. W., "Local-density-functional calculations of the energy of atoms", Physical Review A **55**, 191–199 (1997), DOI: 10.1103/PhysRevA.56.5191.2 (See p. 61).

[138] NIST, N. I. o. S., Technology, U. D. o. C., *Atomic Reference Data for Electronic Structure Calculations, Atomic Total Energies and Eigenvalues (HTML)*, (2015 [accessed May 6, 2017]) https://www.nist.gov/pml/data/atomic-total-energies-and-eigenvalues-html (See p. 61).

[139] Hammes-Schiffer, S., "A conundrum for density functional theory", Science **355**, 28–29 (2017), DOI: 10.1126/science.aal3442 (See p. 65).

[140] Medvedev, M. G., Bushmarinov, I. S., Sun, J., Perdew, J. P., Lyssenko, K. A., "Density functional theory is straying from the path toward the exact functional", Science **355**, 49–52 (2017), DOI: 10.1126/science.aah5975 (See p. 65).

[141] Becke, A. D., "A multicenter numerical integration scheme for polyatomic molecules", The Journal of Chemical Physics **88**, 2547–2553 (1988), DOI: 10.1063/1.454033 (See p. 72).

[142] Franchini, M., Philipsen, P. H. T., Visscher, L., "The Becke Fuzzy Cells Integration Scheme in the Amsterdam Density Functional Program Suite", Journal of Computational Chemistry **34**, 1819–1827 (2013), DOI: 10.1002/jcc.23323 (See p. 72).

[143] Salvador, P., Ramos-Cordoba, E., "Communication: An approximation to Bader's topological atom", The Journal of Chemical Physics **139**, 071103 (2013), DOI: 10.1063/1.4818751 (See p. 72).

[144] Knuth, F., Carbogno, C., Atalla, V., Blum, V., Scheffler, M., "All-electron formalism for total energy strain derivatives and stress tensor components for numeric atom-centered orbitals", Computer Physics Communications **190**, 33–50 (2015), DOI: 10.1016/j.cpc.2015.01.003 (See pp. 75, 77).

Annales Universitatis Turkuensis

Turun yliopisto
University of Turku

Painosalama Oy, Turku, Finland 2017

ISBN 978-951-29-7099-5 (PRINT)
ISBN 978-951-29-7100-8 (PDF)
ISSN 0082-7002 (PRINT) | ISSN 2343-3175 (PDF)